Development of New Silicon Quantum Dots–Polymer Composite Nanoparticles *via* Miniemulsion Polymerization: Synthesis and Characterizations

Noor Aniza Harun

A thesis submitted for the degree of

Doctor of Philosophy in Chemistry

School of Chemistry

Newcastle University

Newcastle upon Tyne, UK

September 2013

ABSTRACT OF THE DISSERTATION

Development of New Silicon Quantum Dots–Polymer Composite Nanoparticles *via* Miniemulsion Polymerization: Synthesis and Characterizations

by

Noor Aniza Harun

The research presented throughout this dissertation demonstrates the potential of miniemulsion polymerization to co-encapsulate silicon quantum dots (SiQDs) within polymeric nanoparticles and shows that the optical properties of SiQDs can be manipulated by their co-encapsulation with metal nanoparticles. In Chapter 1, the current state of the art in the preparation of inorganic/polymer composite nanoparticles *via* miniemulsion polymerization, utilizing inorganic species ranging from semiconductor nanocrystal quantum dots, metal nanoparticles, magnetic and oxide nanoparticles, is reviewed. A brief discussion on the properties of SiQDs, which are the inorganic entities of interest in this work, is presented. Chapter 2 describes the synthesis and characterization of encapsulated alkylated SiQDs within polymer nanoparticles composed of the monomers styrene and 4-vinylbenzaldehyde *via* miniemulsion polymerization. It was shown that the polymer nanoparticle surfaces, which display aldehyde groups, can be further decorated with organic molecules through the formation of imine, oxime or hydrazone bonds. The preparation of two-component polymer composite nanoparticles encapsulating both SiQDs and gold nanoparticles (AuNPs) is presented in Chapter 3. These Au-Si polymer composite nanoparticles display plasmon-enhanced fluorescence of the SiQDs attributable to the localized surfaced plasmon resonance of AuNPs co-encapsulated within the polymer nanoparticles. A preliminary study of Au-Si polymer composite nanoparticles in inkjet printing is also discussed. Chapter 4 presents the development of multicomponent polymer composite nanoparticles which co-encapsulate SiQDs and Au-Ag alloys NPs encoded with Raman-active molecules within polymer nanoparticles. The multicomponent polymer composite nanoparticles exhibit the simultaneous effects of surface-enhanced Raman scattering and metal-enhanced fluorescence as a consequence of the close proximity of the co-encapsulated SiQDs and Raman-active Au-Ag NPs. In Chapter 5, the conclusions and future directions of this study are discussed. This research moves

towards the development of novel inorganic/polymer composite nanoparticles which may offer potential as new chemical probes with applications in biology, sensing and anti-counterfeiting.

DEDICATION

To the most precious man and woman in my life, Harun Muhammad and Gayah Mamat. Your spirit, strength and soul bring me here. Thanks mom and dad!

Noor Aniza Harun

September 2013

ACKNOWLEDGEMENTS

First and foremost, I praise Allah, the Almighty for providing me this opportunity and granting me the capabilities and guidance to successfully complete this study.

My deepest and sincere gratitude is to my supervisor Dr David A Fulton for his thoughtful guidance, motivation and encouragement during the whole period of the study. I have been amazingly fortunate to have a supervisor who has given me freedom to explore my research whilst providing an excellent learning atmosphere. He has inspired me to become an independent researcher, helped me to comprehend the power of critical thinking and has also demonstrated what a brilliant and excellent scientist can accomplish. It is a matter of utmost pleasure for me to also extend my gratitude to my co-supervisor Dr Benjamin R Horrocks, who never failed to help me with his insightful discussion and valuable scientific advice during the whole period of this study. I am infinitely grateful for his enthusiasm, patience and guidance whilst holding me to very high standards in research.

My sincere thanks also goes to Prof J Robin Harris for his help and advice in Transmission Electron Microscopy (TEM), especially in sample preparation and characterization. Dr Matthew J Benning and Dr Scott Watson are also thanked for their help with inkjet printing and AFM, respectively.

It is my pleasure to acknowledge the Ministry of Higher Education, Malaysia and University Malaysia Terengganu for financial support and the opportunity to pursue my doctorate study at Newcastle University. My sincere gratitude also to all staff in the School of Chemistry who have always given excellent service and support during my study, and also to Newcastle University, for a great learning environment and facilities.

Special thanks to all my friends (too many to list here but you know who you are) especially to Fulton group members and Chemical Nanoscience Laboratory colleagues for always being supportive throughout my time here.

Most importantly, I express my deepest gratitude to my parents, for their unconditional love, support and encouragement throughout this endeavour. I love them so much and I would not have made it this far without them. Lastly, I also would like to thank all members of my family for providing endless support and motivation during my “up and down” moments throughout this journey. I am incredibly grateful to have such lovely family.

TABLE OF CONTENTS

Chapter 1: Miniemulsion Polymerization as an Encapsulation Technique for Inorganic Nanoparticles

Chapter 2: A Miniemulsion Polymerization Technique for Encapsulation of Silicon Quantum Dots in Polymer Nanoparticles

Chapter 5: Conclusions and Future Work

LIST OF FIGURES

Chapter 1: Miniemulsion Polymerization as an Encapsulation Technique for Inorganic Nanoparticles

LIST OF TABLES

LIST OF SCHEMES

PUBLICATIONS

N.A. Harun, B.R. Horrocks and D.A. Fulton, "A Miniemulsion Polymerization Technique for Encapsulation of Silicon Quantum Dots in Polymer Nanoparticles", *Nanoscale*, 2011, 3, 4733 – 4741.

N.A. Harun, M.J. Benning, B.R. Horrocks and D.A. Fulton, "Gold Nanoparticle-Enhanced Luminescence of Silicon Quantum Dots Co-Encapsulated within Polymer Nanoparticles", *Nanoscale*, 2013, 5, 3817 – 3827.

Chapter 1

Miniemulsion Polymerization as an Encapsulation Technique for Inorganic Nanoparticles

1.1 Abstract

Tremendous growth in research of inorganic/polymer composite nanoparticles has allowed for the preparation of new materials with multifunctional properties. These polymer composite nanoparticles offer the advantages of the processability of a polymer matrix and numerous unique properties associated with inorganic species, and may find application in diverse fields. Miniemulsion polymerization is a powerful technique to encapsulate inorganic nanoparticles within a polymer shell, and thus provides a method to prepare inorganic/polymer composite nanoparticles. In this introductory chapter, a brief overview of semiconductor nanocrystal quantum dots and their optical properties, advantages and surface chemistry are presented. The principles of miniemulsion polymerization to encapsulate inorganic species are described. Additionally, the recent state of the art in the encapsulation of different types of inorganic nanoparticles by miniemulsion polymerization is highlighted.

1.2 Introduction

A key driver in the development of new and improved materials has been the ability to control structure at smaller length scales in order to create a range of materials with novel characteristics, functions and applications. There are two principal factors that differentiate the properties of materials in the "nano regime" over bulk materials. Firstly, nanomaterials have relatively larger surface area (per unit mass) compared to the same mass of material produced in bulk form, resulting in increased chemical reactivity and electrical properties.[1] As most functionalization processes and catalytic chemical reactions occur on surfaces, nanoscale materials therefore possess greater reactivity than the same mass of larger-scale materials. The second main reason is that quantum effects can begin to play a role in the behaviour of nanomaterials, especially within materials whose sizes are in the range of tens of nanometres or less, and these unique effects can significantly change the optical, electrical or magnetic properties of nanomaterials[1]

Inorganic nanostructures including semiconductor nanocrystals, often known as quantum dots, noble metallic nanoparticles and metal oxides have attracted particularly high interest from researchers, as these species are promising candidates in wide-ranging applications including optical physics and biomedical applications.[2, 3] On

account of their interesting and useful optical, magnetic, electronic and catalytic properties,[4-7] these materials also offer unique characteristics related to their particle sizes in nano-size regime, which often display a huge contrast with their corresponding bulk materials.[8]

1.3 Semiconductor Nanocrystals Quantum Dots – An Overview and History

Semiconductor nanocrystal quantum dots (QDs) are of interest on account of their unique photophysical properties which are useful in a diverse range of applications.[3, 6, 7] QDs are classified as zero-dimensional confined semiconductor nanocrystals possessing diameters in the range of 1 – 10 nm and have properties in-between bulk crystals and individual isolated atoms.[9] QDs typically consist of combinations of elements from groups II and VI (*e.g.* CdSe), groups IV and VI (*e.g.* PbS), or groups III and V (*e.g.* GaAs) of the periodic table.[10] Historically, the first published work in the field of QDs was reported in 1960 by the group of Lawson.[11] In this paper, however, the word QDs was not mentioned, but the crystal size of lead telluride (PbTe) measured was reported to be very small (~ 0.03 μm). In the early 1970s the first use of the term "quantum dot" was reported,[12] and by the late 1980s many impressive works investigating the properties of QDs were reported.[13, 14] The work presented[15] by Bawendi *et al.* in the early 1990s pioneered the synthesis of monodisperse highly crystalline cadmium selenide QDs in a single reaction. In 1998, the first synthetic approaches to water-disperse quantum dots were published,[16, 17] which opened the possibility of their application in biological imaging.

1.3.1 Optical Properties of Quantum Dots

In general, solid state physics classifies materials into three categories: insulators, semiconductors or conductors, depending on the band gap energy (E_g) (usually expressed in electron volts [eV]) between the valence and conduction bands. The top of valence band refers to the highest electronic energy level that is occupied with electrons at room temperature. The bottom of the conduction band is the lowest energy electronic state that is not occupied by electrons. The band gap energy is defined as the difference in energy between the top of the valence and the bottom of the conduction bands. The band gap energy determines the energy that must be gained to promote an electron from

the valence band to the conduction band.[9] The absence of the electron in the valence band is called a hole and behaves like a positive charge.

The unique optical characteristics of semiconductor nanocrystals are based on an effect known as quantum confinement (hence the name quantum dots), which is caused by the restricted movement of electrons and holes in all three dimensions.[18] In comparison to bulk semiconductors, quantum confinement describes an effect arising in QDs when the radii of the nanocrystals are smaller than the Bohr exciton radius. The Bohr exciton is the lowest excited state of a crystal. It consists of an electron in the conduction band orbiting the hole in the valence band in the same manner as an electron orbits a proton in the H atom.[19, 20] As a result the electron energy levels become discreet and the band gap increases as the confinement increases (Figure 1.1).

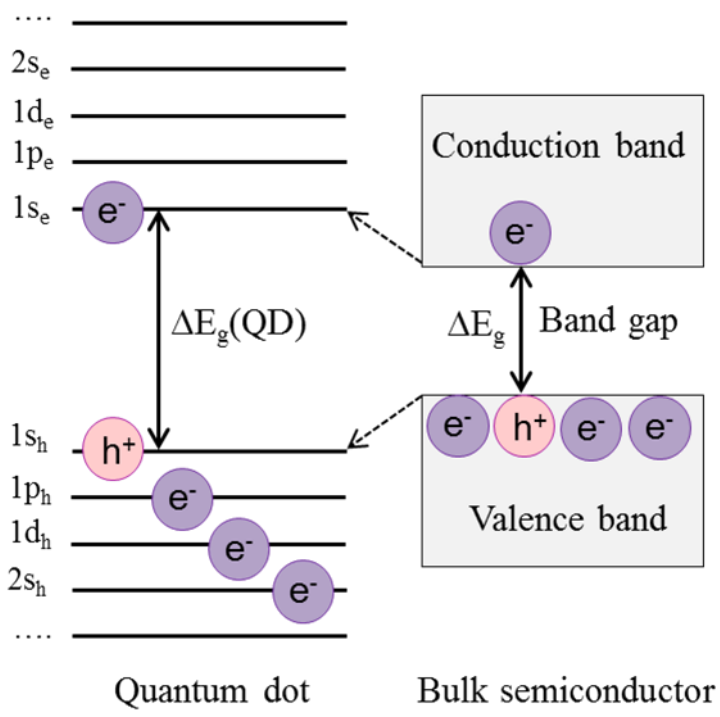

Figure 1.1 Schematic diagram illustrating energy levels of quantum dots compared to its bulk semiconductor material.[21] 1s, 1p and 1d are atomic-like notations which refer to the well-separated QDs energy.

The electrons in nanocrystal QDs are confined in a small space which can be assumed to be similar to the quantization arising from the "particle in a box" model.[22] QDs can be considered as a spherical box containing two particles, an electron and a hole, which together constitute a so-called 'exciton', which is formed when the electron is promoted from the valence band to the conduction band by energy absorption. The kinetic energies of these two carriers increases as the size of the nanocrystal QD

decreases, thus more energy is required to create excitons, and more energy is released upon recombination of the electron with its hole. As a consequence, the excitation and emission spectra shift to higher energies (shorter wavelengths) with decreasing QD size, presenting the opportunity to precisely tune the emission wavelengths of QDs simply by modulating their sizes.[9, 20]

1.3.2 Quantum Dots as Luminescent Labels – Comparison with Organic Dyes

QDs exhibit several fascinating characteristics compared to fluorescent organic molecules. QDs possess broad excitation profiles and narrow/symmetric emission spectra (in a range of 25 – 35 nm full width at half maximum), unlike common organic dyes, such as Rhodamine 6G, which can display asymmetric emission peaks with up to several 100 nm width (Figure 1.2).[23] Consequently, multi-coloured QDs can be simultaneously excited with a single light source and with minimal spectral overlap, features which are beneficial for multiplexed detection of molecular targets.

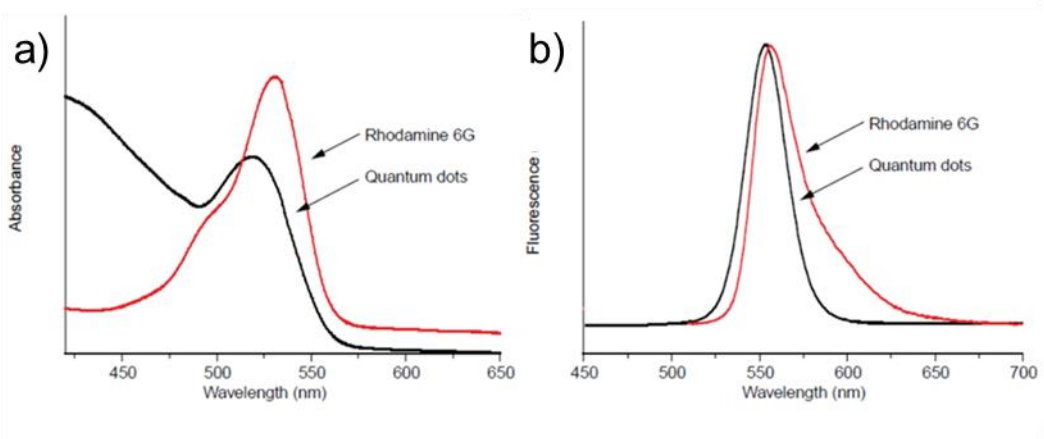

Figure 1.2 Comparison of (a) the excitation and **(**b**)** the emission profiles between rhodamine 6G (red) and CdSe QDs (black). The QD emission spectrum is nearly symmetric and much narrower in its peak width. Its excitation profile is broad and continuous. The QDs can be efficiently excited at any wavelength shorter than ~530 nm. By contrast, the organic dye rhodamine 6G has a broad and asymmetric emission peak and is excited only in a narrow wavelength range.[24]

Besides these spectral attributes, QDs show excellent photostability and remain brightly emissive after long periods of excitation, whereas organic dyes tend to photobleach quickly. This contrast has been demonstrated in several biological labelling experiments which showed the comparison between the photostability of QDs and organic fluorophores such as rhodamine and fluorescein.[16, 17] Because of these characteristics, the possibility of continuous, real-time imaging of single molecules over

long periods of time can be achieved using QDs. Furthermore, by changing the size and composition of QDs, the emission of QDs can be tuned to emit in the near infrared (NIR) spectrum, a desirable property for deep fluorescence imaging in living organisms.[25] In contrast, most organic dyes with NIR emission suffer from low quantum yields, rapid photobleaching and poor stabilities.[26] The unique properties of QDs give them undoubted advantages over common organic dyes and broaden the scope of potential applications of QDs from biological applications[27] into light emitting diodes,[28] lasers[29] and solar cell[30] applications.

1.4 Concerns about Toxicity of "Conventional" QDs

Most of the reported studies for biological applications of QDs involve the utilization of the QDs from the group of cadmium chalcogenide[31, 32] on account of their ease of synthesis and handling.[20] There are, however, some drawbacks associated with these probes in biological studies due to toxicity of the particles which arises as a consequence of leaching of Cd^{2+} at low concentrations of QDs,[33] and their potential to facilitate the production of reactive oxygen species (ROS) by photochemical processes.[34] ROS is a generic term used to describe a number of reactive molecules and free radicals derived from molecular oxygen (*e.g.* O_2^-, $HO^\bullet$, $HO_2^\bullet$, H_2O_2) which can cause unwanted damage to cells.[35]

QDs can be stabilized with a protecting shell in order to prevent the cells and tissues from exposure to cadmium. However, after prolonged circulation in the body the shell may depreciate resulting in "naked" QDs. This circumstance may induce damage to cellular plasma membranes, mitochondria and nuclei.[36] Shiohara and co-workers investigated[37] the cytotoxicity caused by mercapto-undeconoic acid (MUA) modified – CdSe QDs by performing cell viability assays to determine the difference in cell damage depending on the sizes and colours of MUA modified-QDs and the cell types. It was observed that by increasing the concentration of MUA-QDs, the cell viability decreased and resulted in cell death after 4 – 6 h incubation. Importantly, this study highlighted the need for "new safer QDs, such as silicon-QDs", as alternative QDs for research in the cells.

Amongst the alternative semiconductor QDs, silicon-based nanocrystals or silicon quantum dots (SiQDs) show very good biocompatibilities and low cytotoxicities.[38, 39] Chemically pure small SiQDs (less than 10 nm) are non-toxic and biodegradable to othosilicic acid, which can be excreted via the urine system in living

organisms.[40, 41] Erogbogbo and co-workers reported[42, 43] the syntheses of biocompatible SiQDs using PEGylated phospholipids micelles for targeting pancreatic cancer cells. Micelles encapsulating SiQDs were found to be robustly taken up by pancreatic cancer cells *in vitro* with no observable toxicity. In recent studies,[44] the same group also reported the first investigations of *in vivo* tumour targeting and multiplex imaging, together with *in vivo* and *in vitro* cytotoxicity studies. Results of this study showed that SiQDs can be used both *in vitro* and *in vivo* with minimal cytotoxicities. In contrast, *in vitro* studies using CdTe and CdHgTe QDs revealed toxicity effects are observed at much lower concentrations. Alsharif *et al.* investigated[39] intracellular internalization and toxicity of alkyl-capped SiQDs in human neoplastic and normal primary cells. It was found that neoplastic cell lines internalise the SiQDs faster than normal cell lines, and exposure of the cells to alkyl-capped SiQDs resulted in no evidence of *in vitro* cytotoxicity as assessed by cell morphology, apoptosis, and cell viability assays. This observation suggests the potential of alkyl-capped SiQDs in biological applications.

Additional advantages of SiQDs are their robust surface chemistry,[38, 45] (see page 10) and small SiQDs possess orange-red luminescence[32] which is of great utility in biological studies, where orange-red fluorescence is not strongly absorbed by cells and the fluorescence from cells themselves is at shorter wavelengths.[46]

1.4.1 Optical Properties of SiQDs

The SiQDs studied in this research work were prepared by electrochemical etching of porous silicon and exhibit an orange-red luminescence. Their general optical behaviour can be rationalised on the basis of bulk Si band structure, with some changes to take account of the quantum confinement effects in SiQDs.

1.4.1.1 Bulk Band Structure

Figure 1.3a represents the diagram of electron energy (E) against the electron wavenumber (k) for bulk Si. The valence orbitals of Si form two bands referred to as the valence band, which is filled with electrons, and the conduction band, which is completely empty of electrons. When light is absorbed by the solid, an electron is promoted from the valence band (occupied levels) across the gap to the conduction band (unoccupied level). The momentum carried by light is small compared to the momentum of the electron ($\hbar k$), thus the absorption of light can only produce a vertical

transition on the diagram. The smallest gap between the valence and conduction bands is known as the band gap.

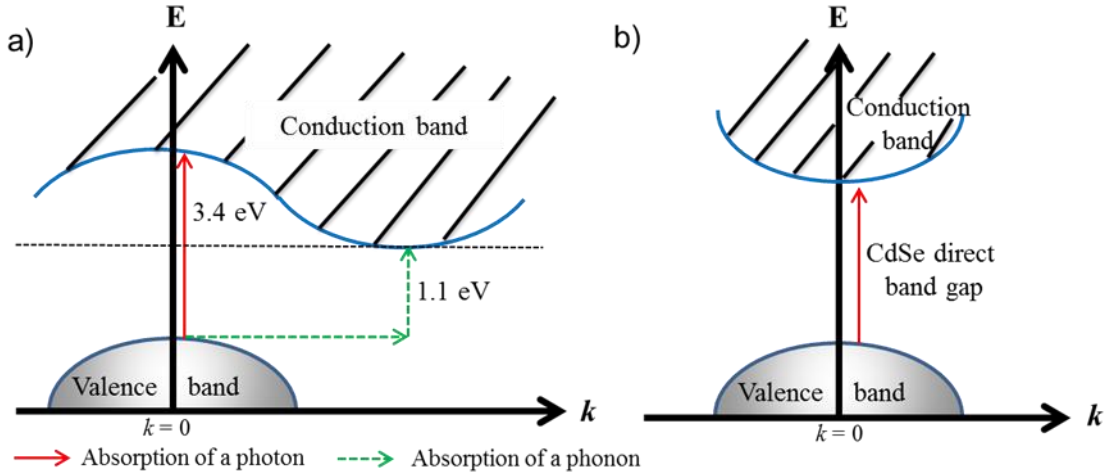

Figure 1.3 Diagrams showing electron energy (E) versus the electron wavenumber (*k*) for (a) bulk silicon and (b) cadmium selenide (CdSe) QDs. These diagrams show differences between the indirect band gap in Si band structure in comparison to direct band gap materials *e.g.* CdSe.

In bulk Si, the band gap is about 1.1 eV (~1230 nm in the near infrared) at room temperature. However, the band gap transition of an electron does not correspond to a vertical transition on the diagram; extra momentum where needed is supplied by the absorption of a lattice vibration (phonon), which is represented by the dotted horizontal arrow in Figure 1.3a. The 1.1 eV gap in Si is called an "indirect band gap", and the absorbance of Si depends on the possibility of both photon and phonon absorption and is therefore much less than a simple vertical transition which depends on only the absorption of a photon (a typical phenomenon of direct band gap materials *e.g.* CdSe) (Figure 1.3b). In addition to an indirect band gap, Si also has a direct gap, where an electron at the top of the valence band can be excited 3.4 eV across the gap to the conduction band levels directly above. Semiconductors for which the smallest gap (band gap) is direct are known as direct gap materials (*e.g.* CdSe, GaAs etc). The absorbance at the energy (wavelength) of the direct gap is much larger.

1.4.1.2 Quantum Confinement Effect of SiQDs

The optical properties of SiQDs are much less well understood than for particles possessing direct band gaps.[47] The explanation of the optical behaviour of quantum confinement in SiQDs is given in this section.

As the size of a Si particle is reduced, the electronic structure (Figure 1.3a) changes in several ways. The selection rule that requires a transition to be vertical is no longer such a constraint because in a finite particle the wavenumber of the electron (k) is not so well defined, resulting in a transition which can be referred to as quasi-direct. Also, the size of the indirect band gap increases because of the quantum confinement effect, which increases the energy of levels near a minimum and reduces the energy of levels near a maximum. This means that the size of the indirect band gap increases until it reaches the visible region (~ 2 eV for SiQDs prepared in our lab). However, the size of the direct band gap does not have a significant change because in Si, the valence band maximum locates below a maximum (strictly, a saddle point) in the conduction band. In contrast, for direct band gap materials such as CdSe, the minimum of the conduction band is above the maximum of the valence band at k = 0, which is also known as the Γ point in the solid state literature (Figure 1.3b). The direct gap in CdSe increases massively with reduction in particle size.

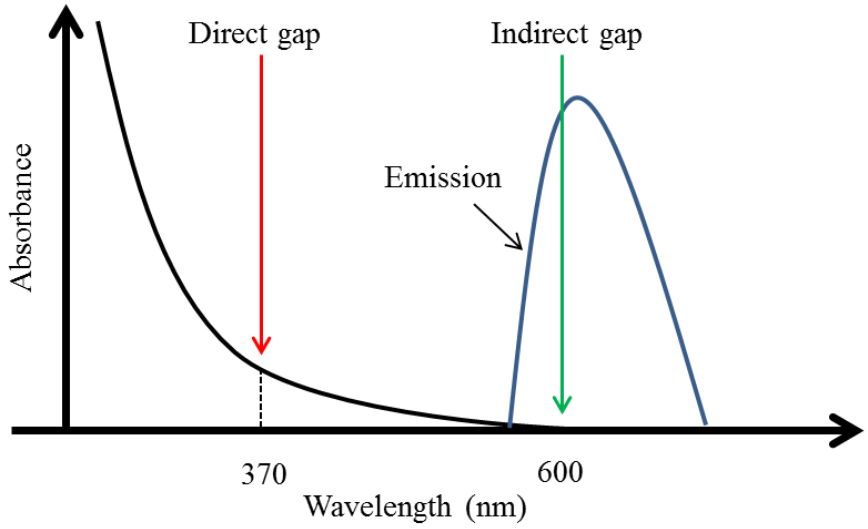

Figure 1.4 The illustration of absorption spectrum of SiQDs indicating the indirect and direct band gap.

Because the light absorption in SiQDs is strong at the direct band gap and weak at the indirect band gap, the absorption spectrum of SiQDs appears as illustrated in Figure 1.4. The emission of SiQDs occurs at the energy of the indirect band gap because an electron promoted to the conduction band at k = 0 will rapidly move down (*e.g.* by vibrational relaxation) to the conduction band minimum.

1.4.2 Surface Functionalization of SiQDs

Early work on SiQDs was performed mostly on porous silicon, which was discovered over 50 years ago.[48] Typically, porous silicon is obtained by electrochemical etching of bulk silicon with hydrofluoric acid (HF). In 1990, intense visible photoluminescence was observed from porous silicon[49] and the luminescence was attributed to quantum confinement effects.[50] Highly porous silicon offers an enormous surface area, which is available for functionalization either by chemical reactions or physisorption of molecules.[51] However, the main drawback of porous silicon is its chemical instability on account of the presence of reactive Si-H bonds, which makes porous silicon susceptible to oxidation and limits its usefulness.[52]

Consequently, surface modifications on SiQDs, including various functionalization with organic molecules (such as poly(acrylic acid), alkynes, allylamine, propionic acid or surfactants) have been reported. In this case, alkyl chains are good candidates for surface modification of SiQDs due to stability endowed by the formation of strong covalent Si-C bonds (Scheme 1.1), which prevents them from photo-oxidation.

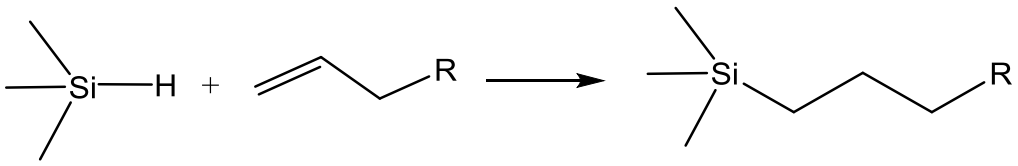

Scheme 1.1 Surface functionalization of porous silicon: hydrosilylation of Si through its reaction with an alkene to form a covalent Si-C bond.

Work performed at Newcastle resulted[45] in the formation of colloidal suspensions of luminescent SiQDs by refluxing porous Si prepared at high current densities in toluene solutions of alkenes. The porous silicon layer breaks up under the conditions of the reflux and hydrosilylation of alkene occurs at the particle surface to form a hydrocarbon monolayer. The alkyl monolayer on the surface of SiQDs rendered the colloid lyophilic and stable against flocculation over 14 days. Luminescent SiQDs were synthesized using 1-octene, 1-undecene, and difunctional unsaturated molecules such as dimethoxytrityl-protected undecenol and 1,9-decadiene. This method provides a simple route to synthesize stable dispersions of colloidal SiQDs with small particle sizes (~2.5 nm of the Si core)[53] which showed a peak of emission wavelength at 670 nm and emit bright red orange luminescence.[45]

1.5 Fabrication of Inorganic–Polymer Composite Nanoparticles

The encapsulation of various inorganic or organic species possessing different functionalities within a polymer matrix allows the preparation of new materials with multifunctional properties. Such polymer composite nanoparticles reflect the properties of its individual components and synergetic effects can arise on account of the interaction of different materials. Considerable efforts have been devoted towards the development of polymer encapsulation techniques to afford polymer composite nanoparticles possessing both processability and stability, together with the optical, magnetic, electronic or mechanical properties of inorganic materials.[54]

Encapsulation can be defined as a process of incorporating small solid nanoparticles, liquid nanodroplets or gas nanobubbles within a polymeric coating.[55] Compared with other organic nanoparticulate systems *e.g.* liposomes and micelles, polymer nanoparticles attain an increased colloidal stability, a better chemical resistance, and the formation of polymer nanoparticles is usually easier.[56]

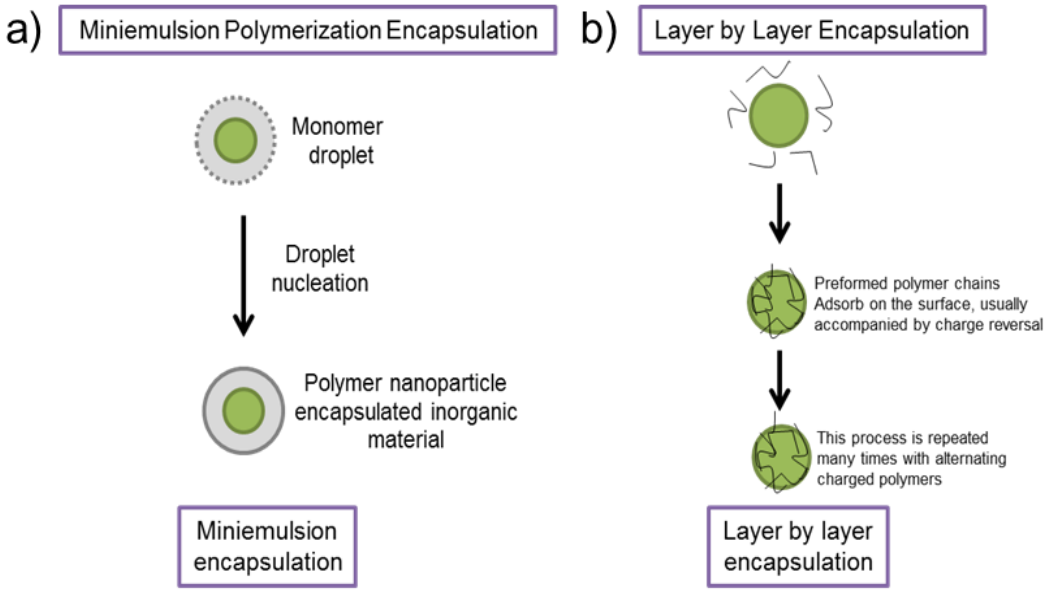

Figure 1.5 Representation of encapsulation of inorganic nanoparticles through (a) the chemical method using miniemulsion polymerization technique which is driven by monomer droplet nucleation (b) physical method *e.g.* the layer by layer approach. Green spheres represent the inorganic nanoparticles.

In general, the encapsulation of inorganic species can be achieved by either of two main approaches: i) a chemical method involving polymerization of monomer droplets containing inorganic nanoparticles, resulting in the encapsulation of the inorganic nanoparticles within polymer nanoparticle (Figure 1.5a), and ii) the physical

method in which the polymer nanoparticles are deposited onto the surface of inorganic nanoparticles by heterocoagulation, also known as 'layer by layer encapsulation' (Figure 1.5b). Heterocoagulation is a process where different types of particles, which often have different charges and different compositions and/ or sizes, coagulate in a controlled way to form hybrid polymer composite nanoparticles.[55]

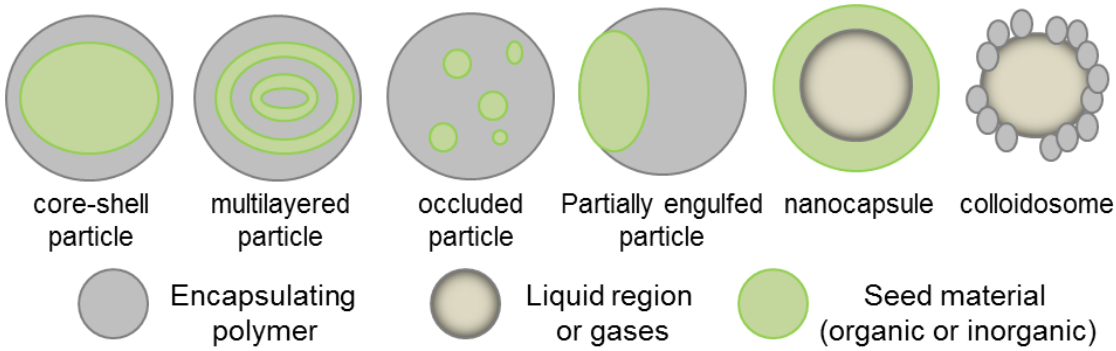

Figure 1.6 Possible morphologies obtained during the preparation of hybrid polymer composite nanoparticles.

The resulting hybrid polymer composite nanoparticles can be obtained in various types of morphologies (Figure 1.6). In the encapsulation of inorganic nanoparticles, polymer composite nanoparticles can form as core-shell particles. On the other hand, if more than one particle is encapsulated within the polymer nanoparticle; occluded polymer composite nanoparticles can be obtained. In addition, the combination between monomer or dissolved polymer molecules and inorganic nanoparticles may lead to the formation of either occluded or multi-layered particles. Partially engulfed particles can be produced if there are changes of surface tension between the seed material and the polymer. The formation of nanocapsules can be achieved by encapsulating a liquid inside a polymer particle. Depositing particles on a droplet leads to the production of colloidosome.[55]

1.5.1 Polymerization Techniques – Heterophase Polymerization

Polymerization techniques have attracted great attention for the encapsulation of inorganic species on account of their versatility, allowing control of the nature and the chemical composition of the polymer nanoparticles produced.[57] From a physical perspective, the polymerization process can be categorized into homogenous or heterogeneous according to the state of the reaction mixture. In a homogenous process, all the reactants including monomers, initiators and solvents are mutually soluble and

compatible with the resulting polymer.[58] Bulk polymerization and solution polymerization are the most typical examples of polymerization in homogenous systems. On the other hand, heterogeneous polymerization, more commonly known as heterophase polymerization, describes systems where more than one phase is present during polymerization and some of the reactants are mutually insoluble. Heterophase polymerization methods include suspension,[59] dispersion,[60] emulsion,[61] and miniemulsion[62, 63] polymerizations, which are the most convenient and widely used polymerization techniques to prepare polymer composite nanoparticles which encapsulate inorganic nanomaterials.

Nowadays, millions of tons of synthetic polymer dispersions are produced worldwide by heterophase polymerization techniques, the products of which have been utilized in a vast range of applications including adhesives, paints, coatings, flocculants in water treatment, and more recently, in drug delivery systems for biomedical and pharmaceutical applications.[64] Heterophase polymerizations describe polymerization techniques under nonhomogeneous conditions with respect to physical and chemical properties of the reaction mixture. Heterophase polymerization also typically defines a process resulting in polymer dispersion, a state of matter where polymers are finely dispersed in a continuous phase. Thus, this type of polymerization process is colloidal in nature and can bridge two important scientific areas: polymer science and colloid science. A significant driver of the massive on-going development of this polymerization method is its "green" and "environmentally friendly" credentials, which arise because most heterophase polymerizations are commonly performed in water as the continuous phase.[64] Furthermore, heterophase polymerization allows the formation of very high molecular weight polymers under reasonable conditions, offering a convenient and inexpensive method for the production of polymers.[54]

1.6 Limitation of Conventional Emulsion Polymerization as an Encapsulation Technique

Amongst the many techniques in heterophase polymerization, conventional emulsion polymerization was the most frequently employed method for the encapsulation of inorganic species.[55] However, many limitations have been discovered with this method, for instance, irregular structures of the encapsulating polymer layers[55, 65] and inhomogeneous distribution of inorganic species[66] within the polymer matrices. Emulsion systems contain the emulsified monomer droplets (~ 1 – 10 μm in diameter)

dispersed in a continuous aqueous phase with the presence of surfactant to stabilize the emulsion system from coalescence. In addition, monomer swollen micelles (5 – 10 nm in diameter) also exist in this system, but only if the concentration of surfactant in the aqueous phase is above the critical micelle concentrations (CMC). Most of the monomer molecules are present in the form of monomer droplets, which act as a reservoir of monomer during polymerization. The polymerization takes place when a water-soluble initiator is introduced into the emulsion system, and the final result is a stable colloidal dispersion (also known as latex) of polymer particles in an aqueous medium.

On account of the complex particle nucleation process in emulsion polymerization and the difficulties in controlling the dispersion stability of inorganic materials in the aqueous phase prior to or during polymerization, attempts to use conventional emulsion polymerization to encapsulate inorganic species may lead to unfavourable types of polymerization. Thus, emulsion polymerization is not a sufficiently versatile or robust technique for encapsulation. Other limitations of emulsion polymerization are its lack of versatility, where it is only successful for the radical polymerization of a set of barely water-soluble monomers. The principle reason for this limitation is that all the monomer has to be transported through the water phase by diffusion. As a result, a lack of homogeneity for example in particle sizes and encapsulation efficiency can occur. In order to overcome these limitations, other types of heterophase polymerizations can be applied where small, homogenous and stable droplets of monomer or polymer precursor preform polymer nanoparticles which maintain their identity as the encapsulation process unfolds. The technique known as miniemulsion polymerization can form stable, small and homogenous nanoparticles, and is a convenient alternative method over conventional emulsion polymerization.[67]

1.7 Miniemulsion Polymerization as an Alternative Encapsulation Technique

Miniemulsion polymerization offers several advantages over conventional emulsion polymerization,[67, 68] the most significant of which is the elimination of the need for the monomer to diffuse through the aqueous phase from the monomer droplets into the polymer particles. Instead, the polymerization occurs directly inside the monomer droplets.[69] Compared to polymerization processes in organic solvents, miniemulsion polymerization offers the benefits of an environmentally friendly method as it uses a water-based formulation as the polymerization medium. Numerous types of

polymerization can be obtained by the miniemulsion approach, for example, anionic, cationic, enzymatic, catalytic, ring-opening metathesis, oxidative, polyaddition and polycondensation processes.[56]

1.7.1 General Principle of Miniemulsion Polymerization

In general, miniemulsion is defined as a two-phase system consisting of an aqueous dispersion of relatively small, stable and narrowly distributed droplets within a size range of 50 – 500 nm.[67] The major factors which distinguish between conventional emulsion polymerization and miniemulsion polymerization are the use of a high shear device and a costabilizer. High shear is required to break-up the emulsion into submicron droplets, allowing for a stable miniemulsion to form, whilst the costabilizer acts as a component to retard monomer diffusion from the submicron monomer droplets. Both factors are essential requirements to ensure the polymerization nucleates predominantly in the droplets. The addition of costabilizer helps to stop the conversion of miniemulsion into conventional emulsion. However, in the absence of a high shear device, a miniemulsion system can convert to conventional emulsion polymerization, demonstrating that the presence of costabilizer alone is not enough to generate predominant droplet nucleation. The presence of surfactant in miniemulsion polymerization is to help prevent droplet coalescence by the action of Brownian motion or settling.[67]

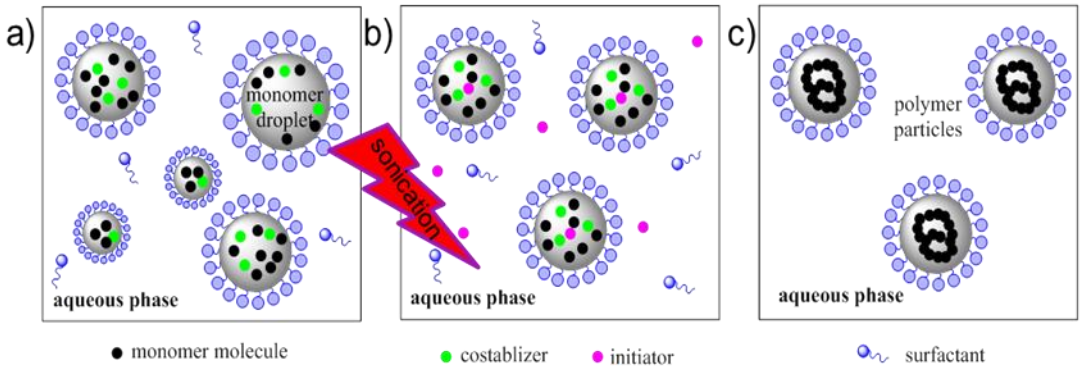

Figure 1.7 Minimulsion polymerisation processes: (a) initial coarse emulsion system containing dissolved surfactant and monomer droplets of different sizes; (b) application of high shear generates a more uniform distribution of monomer droplets; (c) aqueous phase radicals initiate polymerization within each droplet yielding a polymer particle.

When the emulsion is subjected to shear by a high-power homogenization device, the formation of small droplets is obtained in the continuous phase. As the

droplets have a distribution of sizes, the monomer tends to diffuse from small monomer droplets to larger monomer droplets if the monomer is even slightly soluble in the continuous phase (Figure 1.7a).[67, 70] The working principle in miniemulsion polymerization is based upon the nanoreactor concept, where the essential ingredients for the formation of the nanoparticles are present within the droplets,[67] which can be treated as individual entities.[71] The droplets obtained by high shear force in miniemulsion polymerization are small enough to result in a large droplet surface area, and these droplets can compete for radical capture in a very effective way (Figure 1.7b). Consequently, particle nucleation in miniemulsion polymerization is primarily via radical entry into monomer droplets, since the amount of surfactant present in the form of micelles, or involved in the stabilization of precipitated and growing oligomers in the continuous aqueous phase, is very small (Figure 1.7c).

Thus, in comparison to conventional emulsion polymerization, the particle size distribution and sizes of polymer particles prepared by miniemulsion polymerization can be controlled depending on the formulation *e.g.* choice and amount of surfactant and costabilizer used and the type and procedure of the homogenization process, since the polymerization of each small monomer droplet will lead to the formation of a single polymer nanoparticle.[72] On account of this unique feature of miniemulsion polymerization, high levels of encapsulation of inorganic species inside polymer nanoparticles can be obtained. Encapsulation will arise only when the hydrophobic inorganic species can be directly dispersed into the monomer phase, which is conventionally also hydrophobic, and encapsulated upon polymerization of miniemulsion droplets.[73]

1.7.2 Properties of Miniemulsion Polymerization

This section will discuss thoroughly the main mechanistic features involved in miniemulsion polymerization.

1.7.2.1 Shear or Homogenization Devices

A variety of instruments are available to apply mechanical shear in miniemulsion polymerization, for instance ultrasonication, rotor-stator type mechanical homogenizer and high-pressure homogenizers. Among them, ultrasonication is one of the most common methods for laboratory scale-batch miniemulsion polymerization due to its

simplicity of use and rapidity.[74] However, it may not be practical for large-scale application of miniemulsion polymerization in industry. Ultrasonication may produce monomer droplets dependent on the sonication time,[75] as it has been shown that emulsion droplet sizes decrease with increasing sonication time. In general, the emulsion is initially subjected to the miniemulsification process involving vigorous stirring before continuing with the sonication. This requirement arises because most high shear devices are usually poor mixers, and therefore the miniemulsification process may result in the monomer and water phase not being in close proximity when they enter the high shear field. The formation of a coarse emulsion during the miniemulsification process can be achieved by vigorous stirring of the monomer phase, which includes costabilizer, and aqueous surfactant phase together before subjecting to high shear emulsification devices.[68] In addition, it is worth mentioning that to prevent degradation of the newly formed droplets during the high shear of emulsion, the heat generated in the system needs to be avoided, typically using an ice bath.[74]

1.7.2.2 Continuous Phase

In oil-water miniemulsion polymerizations, water is used as a continuous phase medium for the monomer droplets and polymer nanoparticles which are formed. Water is cheap, inert and an environmentally friendly medium which can lead to the production of "green" products. It also acts as a medium for particle nucleation from droplets to particles, the medium of dynamic exchange of surfactant between the phases, and the solvent for surfactant, initiator and other ingredients. Furthermore, it provides excellent heat transfer and low viscosity.

1.7.2.3 Costabilizer

Good monomer droplet stability during storage or particle nucleation is key to obtaining a successful miniemulsion polymerization. When the emulsion system is subjected to high shear, the small droplets break up. Due to their surface energies, the chemical potential arising from a distribution of monomer droplet sizes will cause monomer molecules in the smaller droplets to dissolve in water, disperse through the aqueous phase and then enter the larger monomer droplets (Figure 1.8).[76] Consequently, monomer diffuses from small to larger droplets leading to diffusional degradation, a phenomenon known as Ostwald ripening which ultimately causes destabilization of the

emulsion system. The driving force for Ostwald ripening is the surface tension and the fact that larger droplet has less surface area than small droplets. If the Ostwald ripening process is allowed to happen continuously, 'creaming' of the monomer will occur in a matter of seconds to minutes on account of the formation of larger droplet sizes.[68, 70] As a result, the smaller the droplet, the more stable is the miniemulsion towards settling and creaming.

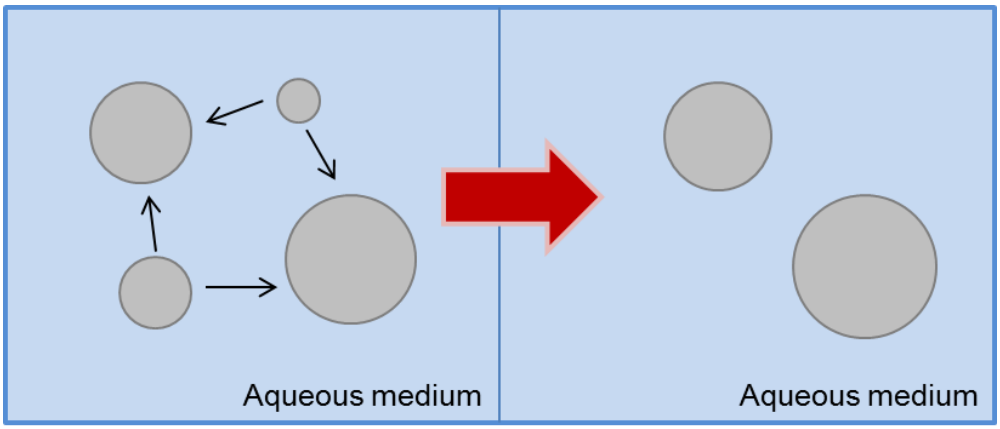

Figure 1.8 Schematic of the Ostwald ripening phenomenon whereby smaller droplets are lost when their contents disperses through the aqueous phase and enter the larger droplets.

Higuchi and Misra were the first to propose[77] that the presence of a small amount of costabilizer can retard emulsion degradation by molecular diffusion, because the slow rate of diffusion of the costabilizer allows the monomer to remain distributed among the droplets.[70] Thus, costabilizer is an important component in miniemulsion polymerization. This compound has also been called the 'hydrophobe', and typically refers to water-insoluble high molecular weight compounds (*e.g.* polymers) that can also reduce Ostwald ripening.[78] The terms 'costabilizer' or 'co-surfactant' are used to refer to low molecular weight water-insoluble compounds which efficiently stabilize monomer droplets against diffusional degradation.

In early studies of miniemulsion polymerization, cetyl alcohol (CA) or hexadecane (HD) were used as costabilizers to retard Oswald ripening in submicron monomer droplets.[68] In 1973, Ugelstad *et al*. prepared[79] a miniemulsion of styrene in the presence of cetyl alcohol (CA) and sodium lauryl sulphate in water. They found that the miniemulsions were stable for two weeks, and a large fraction of polymer nanoparticles were formed by droplet nucleation when surfactant was used. The use of the long chain hydrocarbon hexadecane as a costabilizer in miniemulsion polymerization was then explored. Hansen and Ugelstad observed[80] that as the intensity

of the homogenization increased, the number of particles initially decreased, but then gradually increased. At higher homogenization intensities, micelles tended to disappear and the formation of particles occurred by droplet nucleation. As a consequence, more droplets were produced and hence the number of particles also increased. Furthermore, polymers including polystyrene,[81] poly(methyl methacrylate)[81] or poly(vinyl acetate),[82] can be used as alternative hydrophobes to delay Ostwald ripening sufficiently by allowing nucleation of the monomer droplets by water-phase radicals.[68] Polymers have been shown to perform a similar role to hexadecane in stabilizing droplets for the short periods necessary to ensure nucleation. In addition, they also possess the advantage of reduced toxicity in the final products.[68]

1.7.2.4 Surfactant

Surfactants (also known as emulsifiers, soaps, dispersing agents or detergents) are surface-active agents which play two main roles in miniemulsion polymerization. Firstly, the surfactant molecules lower the interfacial tension during emulsification and facilitate droplet breakage.[83] The second role is to retard droplet coalescence caused by collisions between droplets which occur due to Brownian motion and van der Waals forces (Figure 1.9).[70]

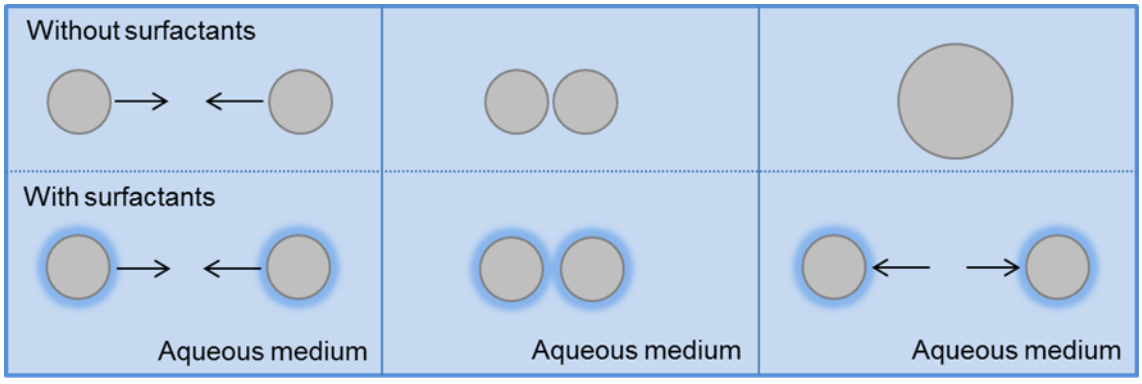

Figure 1.9 Droplets coalescing in the absence of surfactants due to attractive van der Waals forces. Droplets stabilised with surfactants repel each other due to the repulsive forces induced by surfactants.

Landfester *et al.* reported[84] that the particle size can be controlled by the ultrasonication time and the amount of surfactant used. At constant ultrasonication times, particle size will mainly depend upon the ability of the surfactant to increase and stabilize the interfacial areas of the new droplets. This circumstance depends solely on the amount of surfactant used, and hence the area of the droplet which will be covered

by surfactant chains becomes a significant parameter in particle size determination. Small droplets rely on a dense surfactant layer to stay stable whereas big droplets require less surfactant to be protected. It is worth pointing out that the surfactants for miniemulsion polymerization should meet the same criteria as in conventional emulsion polymerization: (1) they must have polar and non-polar groups; (2) they must be more soluble in the aqueous phase to ensure availability for adsorption on the oil droplet surface; (3) they must be adsorbed strongly by the droplet and not be easily displaced when two droplets collide; (4) they must perform these tasks when present in small concentrations; (5) they should be relatively inexpensive, non-toxic, and safe to handle.[70]

In general, surfactants contain long chain hydrophobic (oil-soluble) groups (*e.g.* dodecyl, hexadecyl or alkyl-benzene) and hydrophilic (water-soluble) head groups. They are normally classified according to the nature of this head group, which can be either anionic, cationic, non-ionic or zwitterionic.[85] Anionic surfactants possess negatively charged hydrophilic head groups, and usually comprise sodium, potassium and ammonium salts of higher fatty acids, or sulfonated derivatives of aliphatic, arylaliphatic or naphthenic compounds. The most commonly used anionic surfactants in miniemulsion polymerization are sodium lauryl (dodecyl) sulphate ($C_{12}H_{25}OSO_3^-Na^+$) and sodium dodecyl benzene sulfonate ($C_{12}H_{25}C_6H_4SO_3^-Na^+$). The vast majority of reported studies in miniemulsion polymerization have utilized anionic surfactants, on account of their compatibility with neutral or anionic monomers and anionic initiators, and also most likely because of the extensive historical application of anionic surfactants in conventional emulsion polymerization.

Cationic surfactants are compounds in which the hydrophilic end-group contains a positively-charged ion. Quaternary salts such as alkyltrimethylammonium salts, for example cetyl trimethylammonium bromide (CTAB) and cetyl trimethylammonium chloride (CTAC), are examples belonging to the family of cationic surfactants. Landfester and co-workers have reported[86, 87] the production of styrene miniemulsions using cationic surfactants of cetyltrimethyl ammonium bromide (CTAB) and cetyltrimethyl ammonium tartrate, observing that these surfactants show similar particles sizes when compared with anionic surfactants used in the similar amounts. Non-ionic surfactants do not carry any charge and usually consist of hydrophilic ethylene oxide units. Zwitterionic surfactants show cationic or anionic properties depending on the pH of the medium, and are based mainly upon alkylamino or alkylimino propionic acids.

1.7.2.5 Initiator

Most of the reported polymer syntheses by miniemulsion are performed *via* free radical polymerization. The role of the initiator is to generate free radicals, which then leads to the initiation of the monomers. Free radical initiators can be either water or oil soluble, but in the case of miniemulsion polymerization most of the polymerizations have been initiated using water-soluble initiators, although there is also reported[88] work which utilizes oil-soluble initiators in miniemulsion polymerization. In terms of water-soluble initiators, persulfates (or peroxodilsulfates) such as potassium-, sodium-, and ammonium persulfate, are most commonly used in miniemulsion polymerization. The persulfate ion decomposes thermally in the aqueous phase to afford two sulphate radical anions which can then initiate the polymerization system (Equation 1).

$$S_2O_8^{-2} \longrightarrow SO_4^{\bullet -1} + SO_4^{\bullet -1} \qquad \text{Equation 1}$$

Hydrogen peroxide and other peroxides also thermally decompose to afford radical initiators, for example benzoyl peroxide, which is an example of oil-soluble type initiator. Another type of initiation system consists of redox initiators (*e.g.* persulfate-bisulfite) that utilize free radicals obtained through an oxidation-reduction reaction at relatively low temperatures.

1.8 Miniemulsion Polymerization in the Presence of Inorganic Nanoparticles

Inorganic/polymer composite nanoparticles are excellent examples of nanocomposite materials that combine the unique features of inorganic nanoparticles with the ease of processing and handling associated with an organic polymeric matrix. Miniemulsion polymerization is a very versatile method which has been used for the formation of polymer nanoparticles encapsulating different types of inorganic materials. There is a large volume of published studies describing works involving the encapsulation of inorganic species within polymer nanoparticles. Landfester[66] reviewed miniemulsion methods as a technique to encapsulate a range of different materials, *e.g.* organic and inorganic pigments, magnetite or other solid nanoparticles, hydrophobic and hydrophilic liquids, and also the possibilities to utilize surface functionalization and modification of the resulting polymer latex particles. Recently, Hu *et al.* also reviewed[89] the development of miniemulsion polymerization for the syntheses of hybrid polymer-inorganic nanocomposites, focusing on a different selection of materials. This section

will discuss the key work describing the encapsulation of different inorganic nanoparticles by miniemulsion polymerization techniques.

1.8.1 Encapsulation of Semiconductor Nanocrystal Quantum Dots

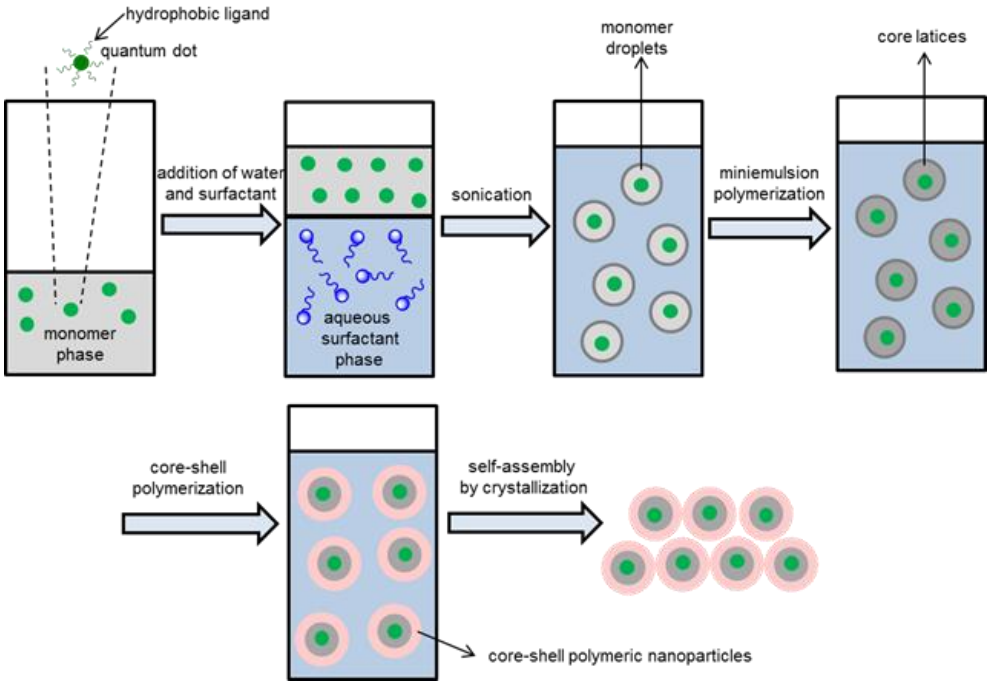

Figure 1.10 Schematic illustration of QD incorporation into the core of core-shell polymeric nanoparticles.[90]

Amongst the earliest work describing the encapsulation of semiconductor QDs into polymeric particles prepared by miniemulsion techniques is the example reported[90] by Fleischhaker and Zentel in 2005. They initially synthesized nanoparticles possessing PS cores using a modified miniemulsion polymerization method which allowed for the encapsulation of fluorescent CdS/ZnS-coated CdSe quantum dots (QDs). Then, the secondary polymeric shell of poly(methyl methacrylate) was prepared by seeded emulsion polymerization to afford PS/PMMA core-shell nanoparticles as depicted in Figure 1.10. This second shell is expected to further protect the QDs located in the outer part of the primary core shell particles. These multilayer hybrid nanoparticles, with diameters between 150 nm to 300 nm, could be self-assembled into photonic crystals (PCs) with stop bands covering the visible range of the electromagnetic spectrum.[90] The hybrid nanoparticles obtained also showed strong photoluminescence (PL) due to the embedded CdSe QDs present in the core of the nanoparticles, and this work presents a significant platform for the design of novel optoelectronic devices based on PCs.

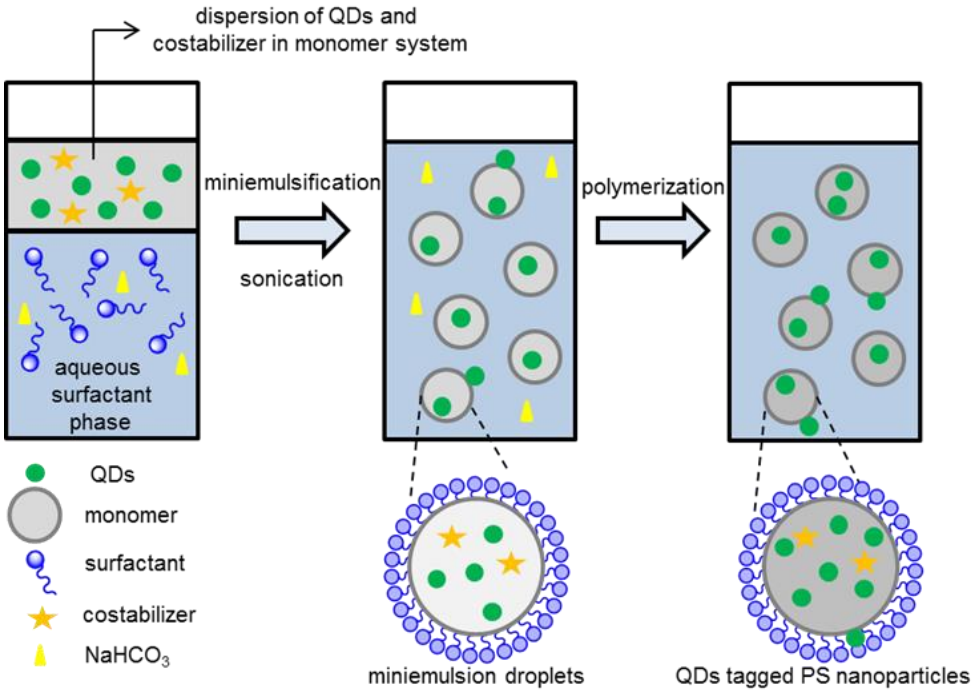

Figure 1.11 Schematic synthetic route of the miniemulsion polymerization of polystyrene nanoparticles incorporating CdSE/ZnS core-shell QDs.[63]

Lansalot *et al.* have developed[63] polystyrene nanoparticles incorporating luminescent CdSe/ZnS core-shell QDs prepared *via* miniemulsion polymerization (Figure 1.11). They investigated the encapsulation of two different types of modified QDs, either trioctylphosphine oxide (TOPO)-coated or vinyl-functionalized CdSe/ZnS QDs into polystyrene nanoparticles by emulsion and miniemulsion polymerizations. They showed that the encapsulation of TOPO-coated QDs inside PS nanoparticles by conventional emulsion polymerization was unsuccessful, an observation which confirms the limitations of this technique. In contrast, the incorporation of either TOPO-coated or vinyl functionalized QDs into polystyrene nanoparticles by miniemulsion polymerization resulted in submicrometer particle sizes and a narrow particle size distribution of polymer nanoparticles which encapsulate QDs. Different surface modifications employed on the encapsulated QDs do not change the polymerization kinetics, final diameters or particle size distributions of the polymer nanoparticles, which exhibit particles sizes between 100 nm and 300 nm. A slight red shift of the emission maximum was observed for polymer nanoparticles encapsulating both QDs as compared to the QDs alone. The incompatibility between PS nanoparticles and QDs of (TOPO)-coated or vinyl-functionalized CdSe/ZnS QDs was observed as evidenced by TEM imaging of ultrathin slices of polymer nanoparticles. These images suggest that as a consequence of phase separation occurring during polymerization, the QDs locate

themselves at the polymer nanoparticle/ water interface, instead of being homogenously dispersed within the polymer nanoparticles.

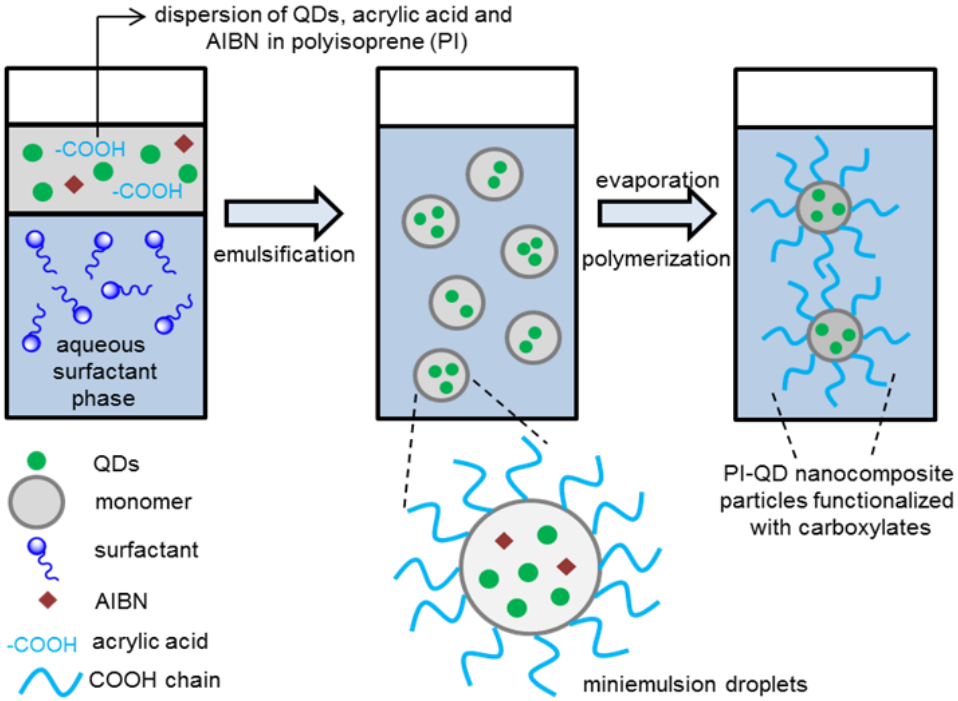

Figure 1.12 Schematic of the synthetic route to polymer composite nanoparticles by emulsification/solvent evaporation method.[91]

The encapsulation of fluorescent CdSe (ZnS) quantum dots into biocompatible polyisoprene (PI) nanoparticles through an emulsification/solvent evaporation method (Figure 1.12) was successfully employed[91] by Yin *et al*. This simple and facile method delivers QDs encapsulated inside polymer nanoparticles without requiring surface modification of the QDs. To increase the usefulness of the polymer composite nanoparticle, the surfaces of the PI nanoparticles were modified with carboxyl groups, and bioconjugation was demonstrated by conjugating streptavidin onto the surface of PI-QDs hybrid nanoparticles, and their subsequent binding to biotin-coated polystyrene was demonstrated. These fluorescent nanocomposites showed potential application in bio-labelling and other applications that could exploit the high-throughput afforded by multicolour coding.[91]

On account of the limitations of conventional radical polymerization in controlling polymer structure, such as its number-average molecular weight (M_n), polydispersity index (PDI) and composition of the final polymer composite nanoparticles, a new chemical functionalization method based upon controlled/living radical polymerization from the surface of QDs was developed[92] by Esteves *et al*. They

demonstrated an alternative to the miniemulsion technique for preparing QD-polymer composites by using a catalytic system termed “activator generated by electron transfer” (AGET) (Figure 1.13a).

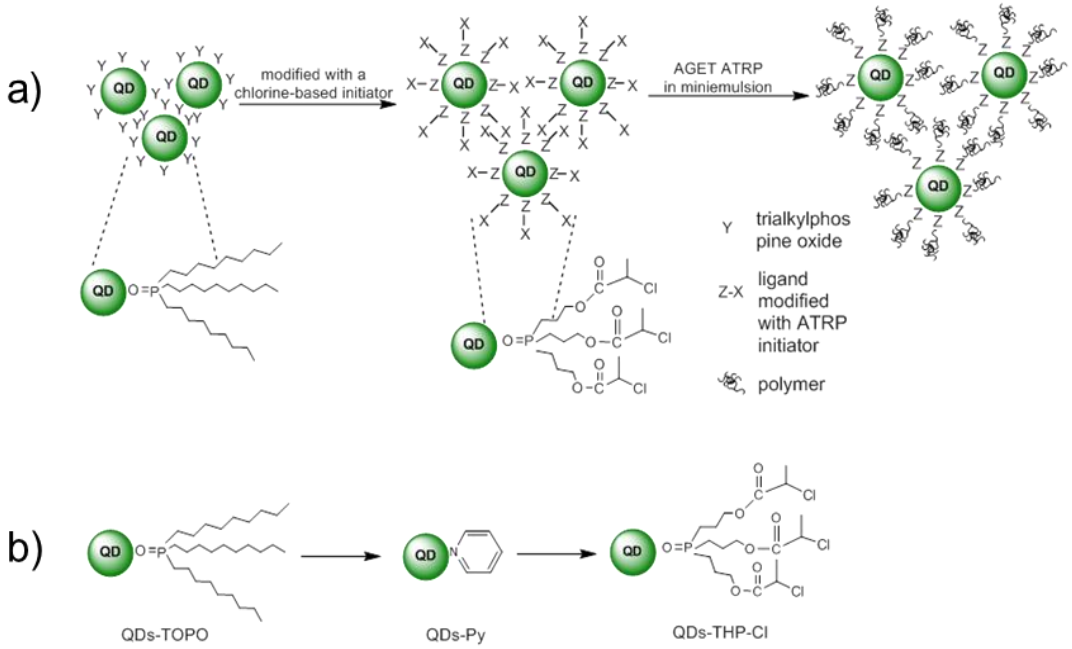

Figure 1.13 (a) Schematic of the synthetic route for the preparation of CdS–poly(acrylate) nanocomposite by AGET for atom transfer radical polymerization (ATRP) miniemulsion polymerization. (b) Schematic of ligand exchange on the surface of QDs. During the ligand-exchange process, as trioctylphosphine oxide (QDs-TOPO) is replaced by pyridine (QDs-Py), and finally by the ATRP macroinitiator ligand (QDs-THP-Cl).[92]

By coordinating a phospine-oxide-modified atom transfer radical polymerization (ATRP) macro-initiator onto the surfaces of CdS QDs, it was possible to produce poly(*n*-butyl acrylate) (PBA) shells around the CdS nanocrystals. They then investigated the use of AGET for atom transfer radical polymerization (ATRP) within a miniemulsion to synthesize CdS-QDs–poly(acrylate) nanocomposites. Firstly, TOPO molecules on the surface of QDs were exchanged with pyridine to minimize degradation. Then, to inhibit the surface oxidation of QDs, pyridine then was substituted by *tris*(alkyl) phosphines featuring (2-chloropropionyl) chloride as an initiating point for ATRP (Figure 1.13b). The polymerization of *n*-butyl acrylate was then initiated on the surface of modified QDs using a catalytic system of AGET ATRP in aqueous miniemulsion in the presence of Brij 98 as surfactant, hexadecane as co-surfactant and ascorbic acid as reducing agent to activate the catalyst complex. This technique was shown to control effectively the growth of poly(*n*-butyl acrylate) (P-*n*BA) chains from the modified surface of CdS-QDs to obtain polymer-encapsulated QD nanocomposites. This

synthetic approach also can be applied for growing or grafting other hydrophilic monomers in order to form versatile polymer composites which display tremendous potential in biological applications, especially as biomarkers. The same group expanded[93] their investigation on the synthesis of nanocomposite materials to include polymer chains grown upon the surface of QDs. In this work, they reported the use of reversible addition-fragmentation chain transfer (RAFT) polymerization in miniemulsion polymerization using a "grafting from" approach to grow polystyrene (PS) and P-*n*BA blocks from the surfaces of CdS and CdSe QDs.

Recent work on QD encapsulation performed[94] by Carpenter *et al.* involved the miniemulsion polymerization of styrene encapsulating CdSe utilizing cetyl trimethylammonium bromide (CTAB) as surfactant and 2,2-azobisisobutyronitrile (AIBN) as initiator. This work focused on the evaluation of the fluorescence of CdSe QDs/PS composite nanoparticles as the miniemulsion polymerization conditions were altered, including variations in the surfactant and initiator concentrations. They found that by increasing the surfactant concentration, the size of monomer droplet decreases but the number of droplets increases and thus the probability of droplet nucleation. Consequently, the rate of polymerization rises and produces smaller-sized polymer nanoparticles. Furthermore, the variation in the level of initiator significantly changed the polymerization kinetics, without changing the photoluminescence emission. The interesting finding from this research study was the observation that the emission intensity is strongly related to changes in polymer nanoparticle size, where polymer particles with larger sizes displaying higher fluorescence intensities on account of the large number of QDs per polymer nanoparticles. Interestingly, the particle size of the CdSe QD is maintained, even after encapsulation within the polymer nanoparticles, suggesting that miniemulsion polymerization technique does not affect the optical properties of QDs.

1.8.2 Encapsulation of Metallic Nanoparticles

Recently, Fuchs and Will developed[62] a new route for the synthesis of decanethiol-capped gold nanoparticles encapsulated within PMMA nanoparticles by photo-initiated miniemulsion polymerization. This simple and facile method conducts the polymerization under very mild conditions with reaction temperatures no higher than 40 $^{\circ}$C and a polymerization period of only 1 h. The concept of photo-initiated miniemulsion polymerization as an alternative technique to conventional miniemulsion has arisen

because some potential additivites are not sufficiently thermally stable to be incorporated inside latex particles. Previous efforts by this research group towards the encapsulation of thiol-capped AuNPs at elevated temperatures (~70 °C) caused AuNPs to degrade and precipitate from the miniemulsion droplets, without successful encapsulation into the polymer nanoparticles. The polymerization was conducted using the biologically compatible surfactant Tween80 and an organic-soluble UV initiator, benzoyl peroxide (BPO) which forms radicals under ultraviolet irradiation. The particle sizes of the PMMA latex particles were between 100 – 200 nm with narrow particle size distributions. The successful encapsulation of AuNPs into PMMA nanoparticles was observed by transmission electron microscopy (TEM), which also revealed excellent dispersion of AuNPs inside the polymer latex particles with no aggregation of the AuNPs.

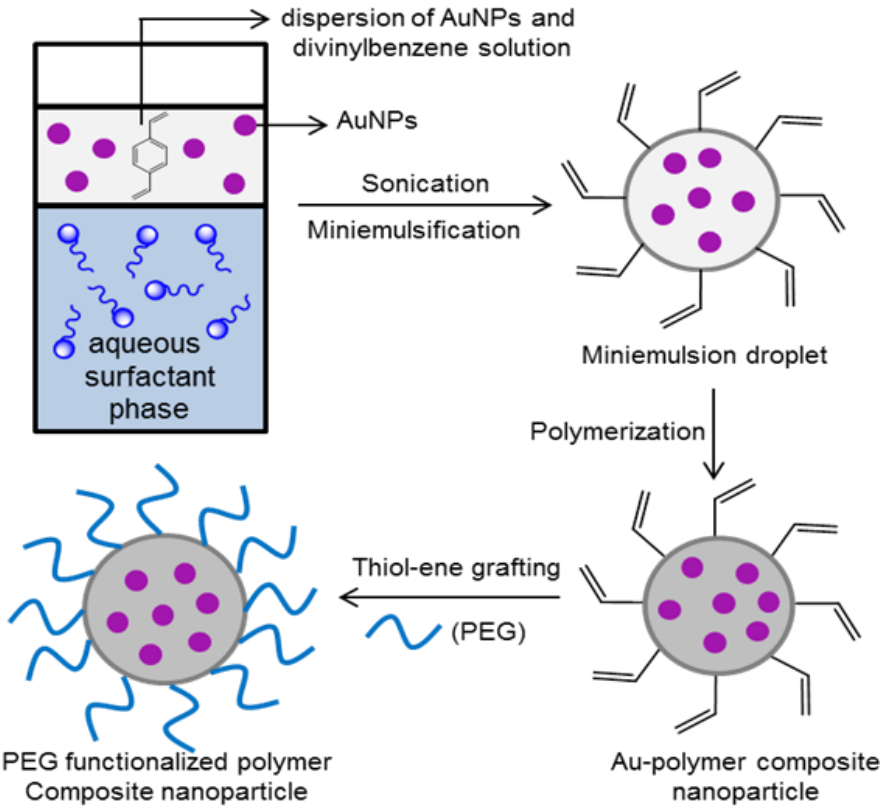

Figure 1.14 Schematic description of Au-composite nanoparticles synthesis.[95]

Hawker and co-workers have demonstrated[95] a robust, reliable, and scalable method for the preparation of composite polymer-inorganic nanoparticles based on miniemulsion polymerization, observing the incorporation of multiple inorganic materials within polymer nanoparticles. They investigated the miniemulsion polymerization of divinylbenzene using AuNPs as the inorganic cargo. To increase the

usefulness of the polymer composite nanoparticles in applications, the surface of the polymer nanoparticles were further functionalized through the conjugation of PEG chains by thiol-ene 'click' chemistry (Figure 1.14). This surface functionalization allows these materials to be successfully dispersed in a wide range of solvents and to be stable against aggregation. It should be noted that the surface of the inorganic materials must be hydrophobic enough to ensure a good dispersion of the inorganic materials in the monomer system. Initial attempts have been made by this research group to modify the AuNPs surfaces by using long alkyl amines (oleylamine), but this approach was unsuccessful in obtaining a good dispersion of AuNPs in the divinylbenzene monomer. They therefore utilized an alternative approach, using the so-called polymer "grafting-to" method to improve the dispersibility of AuNPs, whereby thiol-terminated PS chains are grafted onto AuNPs to form PS-grafted AuNPs. PS-grafted AuNPs disperse well in divinylbenzene, and their subsequent encapsulation into polymer latex particles was successfully achieved. They also explored[96] the encapsulation of a variety of inorganic materials of different shapes and natures (*e.g.* manganese ferrite ($MnFe_2O_4$) nanoparticles, AgNPs, and Au nanorods) into poly(divinylbenzene) nanoparticles, broadening the scope of the encapsulation methodology.

In recent work, the group of Betancourt-Galindo have investigated[97] the antimicrobial activity of Ag/PS composite nanoparticles prepared by miniemulsion polymerization techniques. The surfaces of Ag nanoparticles were modified with 3-aminopropyltrimethoxysilane (APTMS), which acts as a coupling agent and costabilizer in the miniemulsion polymerization reaction. They studied the effects of different concentrations of initiator used in Ag/PS composite nanoparticles and, as expected, increased initiator concentrations lead to higher monomer conversion, and encapsulation efficiencies. Moreover, the average particle sizes of the polymer composite nanoparticles also decreased at high concentrations of initiator. Importantly, in this work they showed that Ag/PS composite nanoparticles had excellent biocidal properties against *E.coli* and *S. aureus,* and it is expected that these particles will be utilized in different applications such as clinical paints and coatings for biomedical materials.

1.8.3 Encapsulation of Magnetic Nanoparticles

Numerous synthetic procedures have been developed for the synthesis of encapsulated magnetic nanoparticles. Due to the susceptibility of bare nanoparticles (*e.g.* Fe_3O_4) towards oxidation in air, various methods have been developed to avoid any stability

issues, and polymer shells which can help to protect the magnetic component are of interest. Magnetic-hybrid polymer composite nanoparticles attract a lot of interest among researchers because of their superparamagnetic properties. Indeed, polymer nanoparticles which encapsulate magnetic species display a vast range of applications, especially in environment and food analysis,[98] water treatment,[99] biotechnology and biomedical fields.[100] From the large volume of publications based on magnetite-based nanocomposites prepared *via* miniemulsion polymerization, only a few reports exist using magnetic nanoparticles not based on iron oxide,[96, 101] as most of the literature deals with superparamagnetic iron oxide.

Generally, magnetic-polymer composite nanoparticles can be prepared by a three step process utilizing a co-sonication process as reported by Ramirez and Landfester .[102] They demonstrated that magnetite nanoparticles in a size range of 10 nm in diameter can be produced by co-precipitation from a ferrous and ferric chloride solution. After hydrophobization of the magnetic nanoparticles with oleic acid, they were then dispersed in octane and miniemulsified in aqueous SDS solution. After evaporation of octane, the dispersion of SDS-stabilized magnetic nanoparticles was added to a monomer system. The last step was accomplished by sonication of the magnetic dispersion and styrene to form the miniemulsion, then polymerization to afford PS/magnetic composite nanoparticles. It was reported that up to 40 wt% of magnetite could be encapsulated and homogenously distributed within the PS matrix. However, partial oxidation was revealed either inside or on the surface of the magnetic nanoparticles, which may lead to the loss of magnetization. This phenomenon was also observed by several other authors.[103, 104]

Further investigation of PS/magnetite composite nanoparticles was performed by Mori and Kawaguchi.[105] They studied the effects of different types of initiators in miniemulsion polymerization upon the resulting particle characteristics of the products, focusing on size, morphology, magnetic properties and colloidal stability. By using water-soluble initiators polymer composite nanoparticles around 300 nm in diameter containing more than 30 wt% of magnetic nanoparticles could be obtained. It was found that magnetic nanoparticles were homogenously distributed within the polymeric matrix and no magnetic nanoparticles were observed on the outer surface of the polymer nanoparticles. In contrary, when AIBN, an oil-soluble initiator was used, the size of the polymer composite nanoparticles remained at most 100 nm in diameter. In addition, incomplete encapsulation of magnetic nanoparticles was obtained, with the majority of them observed upon the surface of the PS nanoparticles. It is thought that persulfate

initiates polymerization from the aqueous phase, confining the magnetic nanoparticles within the droplets. The oil-soluble initiator, AIBN, initiates the polymerization from within the monomer droplets, which are then subjected to a microphase separation between the polymer and the hexane-based ferrofluid nanoparticles.

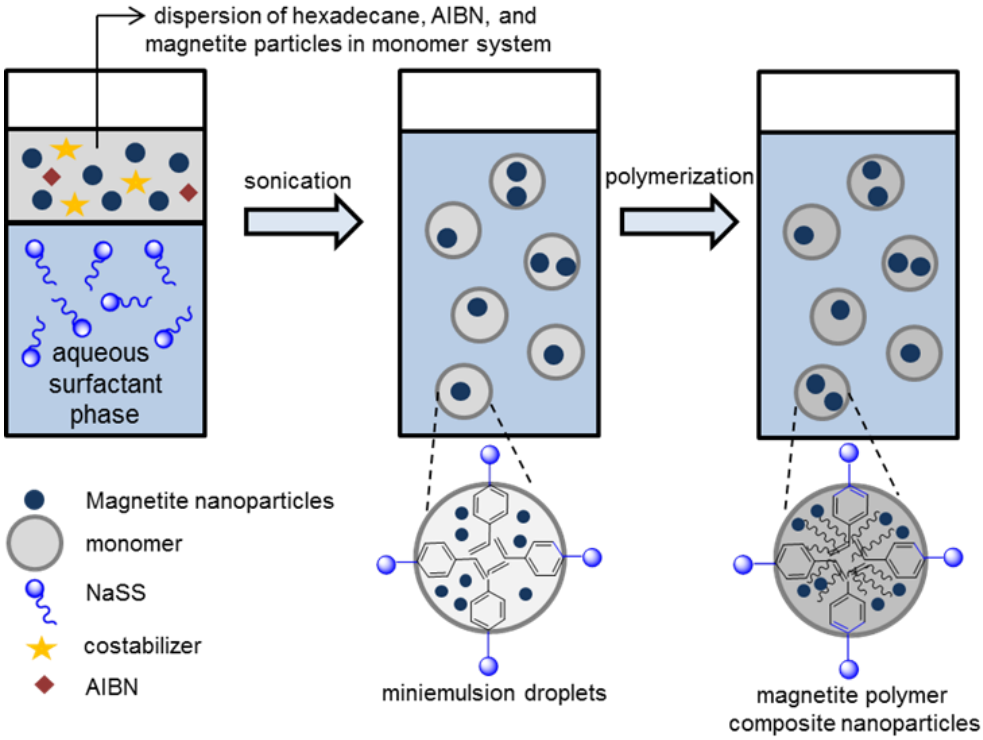

Figure 1.15 Schematic diagram of the synthesis magnetic polymeric composite nanoparticles obtained by emulsifier-free miniemulsion polymerization.[106]

In conventional miniemulsion polymerization, surfactant has been used to provide emulsion stability from droplet coalescence. Some researchers investigated emulsifier-free miniemulsion polymerization to encapsulate magnetite nanoparticles into a polymer matrix, which should avoid the migration of surfactant during polymerization.[106, 107] The preparation of magnetic polymeric composite particles *via* emulsifier-free miniemulsion polymerization using styrene as monomer and sodium-*p*-styrenesulfonate (NaSS) as an ionic comonomer was reported[106] by Lu *et al.* and successful incorporation of hydrophobic magnetic particles into polymer nanoparticles was accomplished (Figure 1.15). NaSS acts as a highly efficient stabilizer as a consequence of its sulfonate group, which can anchor upon the surface of polymer nanoparticles to help to improve stabilization by avoiding the migration/desorption of ionic groups which normally occurs with emulsifiers such as SDS. The unique features of this ionic comonomer helps to improve the distribution of magnetite particles inside

magnetic polymeric composite nanoparticles, produce small particles sizes with narrow particle size distributions, and reduces the number of pure polymer particles and bare (free) magnetite particles.

Work on magnetite/polymer composite nanoparticles by the group of El-Aasser involves[108] a novel approach towards designing polymer composite nanoparticles composed of three domains: poly(*n*-octadecyl methacrylate) (PODMA) or poly(*n*-octadecyl methacrylate-co-1-vinylimidazole) (P(ODMA-co-VIMZ)), magnetic nanoparticles, and AuNPs. Fe_3O_4 Nanoparticles were encapsulated within the monomer droplets (ODMA-VIMZ) and polymerized using the miniemulsion polymerization technique to afford magnetic-polymer composite nanoparticles. Morphology studies showed that Fe_3O_4 nanoparticles were dispersed homogenously inside the particles, and tend not to migrate towards the monomer/water interface during the polymerization process. The resulting Fe_3O_4/P(ODMA-co-VIMZ) composite nanoparticles were utilized as precursors for the adsorption of Au^{3+} ions upon the polymer nanoparticle surface, which led to the formation of Fe_3O_4/P(ODMA-co-VIMZ)/Au nanocomposite particles. This strategy affords polymer composite nanoparticles with three distinct potential applications arising from their magnetic properties, as well as plasmonic properties and chemical functionalization affinities of AuNPs. Moreover, they found that the deposition of Au nanoparticles did not affect the magnetization characteristics of encapsulated Fe_3O_4 nanoparticles.

The encapsulation of hydrophilic magnetic nanoparticles in hydrophilic polymer shells can be achieved *via* an inverse miniemulsion polymerization technique which includes water-based magnetic ferrofluid as the dispersed phase, and organic solvent and monomers as the continuous phase.[101] Usually, highly hydrophilic salts or low-molecular weight electrolytes, for example NaCl and $MgSO_4$, have been used as liphophobic costabilizers to minimise diffusional droplet degradation in inverse miniemulsion polymerization. The monomer droplets in a continuous organic medium (nonpolar) were stabilized with an oil-soluble non-ionic surfactant and the polymerization initiated from either the droplet or continuous phase.

1.8.4 Encapsulation of Oxide-Based Nanoparticles

The encapsulation of oxide-based nanostructured materials, such as silica, titanium dioxide, alumina or zinc oxide within polymeric particles has attracted great interest.

Oxide nanoparticles have been widely used in many applications ranging from paints, cosmetics, pharmaceuticals to catalysis and optics.

Silica has been the main focus on account of its low cost, easy processability, high chemical inertness, optically transparent properties and exceptional colloidal stability. Early approaches towards the encapsulation of silica within polymeric nanoparticles by miniemulsion polymerization techniques have utilized hydrophilic silica nanoparticles.[109] The most recent reported[110, 111] work on encapsulation of hydrophilic silica nanoparticles was performed by the group of Zhang, who prepared raspberry-like polymer composite microspheres consisting of polystyrene (PS) cores coated with 20 nm thick silica nanoparticle shells. The miniemulsion polymerization was performed using SDS as surfactant and 1-vinylimidazole[111] or 2-(methacryloyl)ethyltrimethylammonium chloride as cationic monomers. However, the work using hydrophilic silica nanoparticles showed its poor encapsulation within the polymer matrix. The grafting of silane coupling agents to modify the surface of silica was found as an effective way to improve the encapsulation efficiency of silica nanoparticles during miniemulsion polymerization.[112, 113]

Costoyas *et al.* prepared[113] hybrid core-shell silica/PS composite nanoparticles by miniemulsion polymerization possessing narrow particle size distributions (PSD) and high degrees of silica encapsulation. Instead of using common silane coupling agents, oleic acid (OA) was used as a surface modifier for the silica nanoparticles to improve their hydrophobicity. OA can be bonded to the silanol groups present on the surface of silica nanoparticles through a single hydrogen bond, and the double bond within OA is able to co-polymerize with vinyl monomers. A synergistic effect was observed when using OA and 3-(trimethoxysilyl)propyl methacrylate (TPM) in the compartmentalization step between the monomer phase and silica nanoparticles. The effect of different experimental variables, for example the size of silica nanoparticles, the ratio of styrene/ silica, the surfactant concentration, and the presence of ethanol in the reaction were analysed.

Work based on silica encapsulation was presented[114] by McKenna and co-workers, in which they performed a study of the mechanism of droplet formation and miniemulsion polymerization involving encapsulation of silica particles. Because most of the previous literature focused on controlling particle morphology, less attention has been paid to the mechanism of the miniemulsion polymerization itself during encapsulation of inorganic nanoparticles. Cryo-TEM studies showed that not all the droplets are equal; some droplets contain no silica whereas others contain many silica

nanoparticles. After the subsequent polymerization, it was shown that silica was buried inside the polymer nanoparticles. Further cryo-TEM studies also revealed that the inhomogeneity of the silica beads distribution in the particles is very similar in the final polymerized particles.

If the functionalization of the surfaces of silica nanoparticles is not performed, the negatively-charged silica particles can be used as Pickering "emulsifiers" to stabilize colloidal particles in heterophase systems, resulting in so-called Pickering systems.[89] This condition leads to the formation of a variety of structures of polymer/silica nanocomposite spheres. 'Pickering emulsion' refers to the situation when colloidal solid particles situate themselves at the oil-water interface and stabilize an emulsion of oil and water. The stabilization is achieved when the solid particles (*e.g.* colloidal silica) are added to the emulsion system; these particles will bind to the surface of the droplet and prevent the droplet from coalescing, making the emulsion more stable.[115] The most recent work based on Pickering miniemulsion polymerization was reported[116] by Cao *et al.* who synthesised raspberry-like nanocapsules possessing a hydrophobic liquid core *via* the copolymerization of styrene, divinylbenzene (DVB) and 4-vinyl pyridine (4-VP) as comonomers, silica nanoparticles as Pickering stabilizers and hexadecane as a liquid template. The colloidal stability of the systems was investigated in terms of the dispersion pH, the type and quantity of silica sols, and the content of 4-VP used. It was found that utilization of silica particles could promote the formation of capsules, which could not be obtained by using a conventional surfactant like Lutensol AT50 where solid particle will produce. Moreover, the morphology of particles is influenced by the dispersion pH, the weight content of HD and DVB, but not significantly affected by the 40VP contents.

Another oxide-based nanoparticle which has received much attention in recent literature is the aluminosilicates, more commonly known as clays. Clays offer many advantageous properties such as improvements in strength, toughness, elasticity and modulus whilst retaining optical transparency.[117] In comparison to pure polymer nanoparticles, the composite polymer/clay nanoparticles display excellent properties, for instance, enhanced resistance to tear, radiation, fire resistance, as well as lower thermal expansion and lower permeability to gases.[89]

Miniemulsion polymerization techniques possess an advantage over conventional emulsion polymerization for the encapsulation of clays. Huang *et al.* reported[118] the preparation of polymer/clay nanocomposite by suspension and emulsion polymerization of MMA with montmorillonite, a well-known type of clay. However,

the product obtained by suspension polymerization did not form thermodynamically-stable dispersion in water. Furthermore, the nanocomposite prepared through emulsion polymerization by a simple process of mixing clay with an as-prepared PMMA emulsion was unsuccessful and no substantial encapsulation was observed.

Khezri *et al.* described[119] a new strategy for the encapsulation of organo-modified montmorillonite within PMMA *via in situ* atom transfer radical polymerization with simultaneous reverse and normal initiation process (SR&NI ATRP). The use of SR&NI in ATRP can reduce the required catalyst concentration in comparison with reverse and normal ATRP. In addition, this initiation system allows for the control of molecular weight, and polymers with low polydispersity indices are obtained. In this study, 4,4'-dinonyl-2,2'-bipyridine (dNbPy) was used as a hydrophobic ligand to hold the metal complex in the polymerization loci, minimizing its entrance into the aqueous phase. Meanwhile, the cationic surfactant, CTAB was utilized due to its efficiency at the selected polymerization temperature (80 $^{\circ}$C). Homogenous distribution of droplets and polymer/clay composite nanoparticles possessing diameters of 170 nm were evaluated by dynamic light scattering (DLS) and scanning electron microscopy (SEM). Recent studies by Zengeni *et al.*[120, 121] have shown that highly filled polymer/clay hybrid composite nanoparticles (30 – 50 wt % clay) can be effectively prepared by a co-sonication polymerization method, which involves the separate preparation of two-dispersions; monomer miniemulsion and the inorganic dispersion. The two dispersions are then mixed together and co-sonicated to produce the final miniemulsion as a result of fission and fusion processes taking place during sonication.

Titanium dioxide (TiO_2) plays an important role, especially in the paint industry, owing to its high refractive index and its ability to reflect and refract light efficiently. Moreover, TiO_2 nanoparticles are also widely used as photo-catalysts for the degradation of organic pollutants, medical treatments and microorganism photolysis. In order to obtain a good encapsulation, the hydrophilic surface of TiO_2 should be modified. Erdem and co-workers showed[73, 122] that by modifying TiO_2 nanoparticles with polybutylene succinimide diethyl triamine, followed by their dispersion 5 wt% in styrene monomer prior to the miniemulsion reaction, resulted in 89% of TiO_2 being encapsulated within the resulting PS nanoparticles.

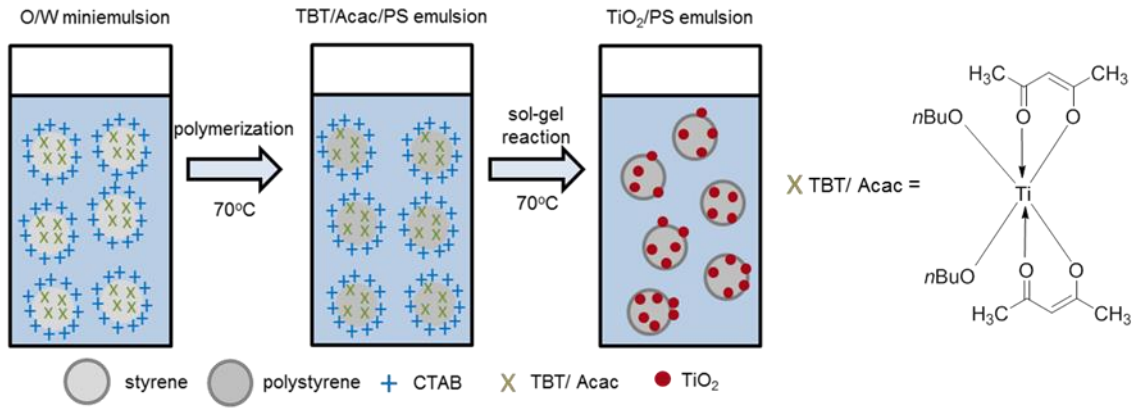

Figure 1.16 Formation of PS/TiO_2 nanocomposite particles.[123]

Wu *et al.* successfully used[123] a one-step miniemulsion polymerization method to prepare PS/TiO_2 composite nanoparticles with both organic monomers and inorganic precursors trapped in the miniemulsion droplets. Firstly, the organic monomer styrene and the inorganic precursor TBT/Acac (acetylacetone chelated tetra-*n*-butyl titanate) were compartmentalized in the miniemulsion droplets. The miniemulsion droplets were resulting in positively charged droplets which stabilized by cationic surfactants (CTAB) due to the adsorption of CTAB upon their surfaces. Hexadecane (HD) was used as a costabilizer in this polymerization system. When the reaction temperature reached 70 °C, the polymerization of styrene occurred simultaneously with the diffusion of TBT towards the oil/water interface due to its hydrophilic characteristics, and the sol-gel reaction was then initiated to form TiO_2 nanoparticles (Figure 1.16). Because the Ti-OH groups are weakly electronegative, the electrostatic interaction between the positively charged CTAB and the negatively charged TiO_2 nanoparticles encourages TiO_2 nanoparticles to coat the surface of polymer spheres, resulting in PS/TiO_2 composite nanoparticles (Figure 1.16).

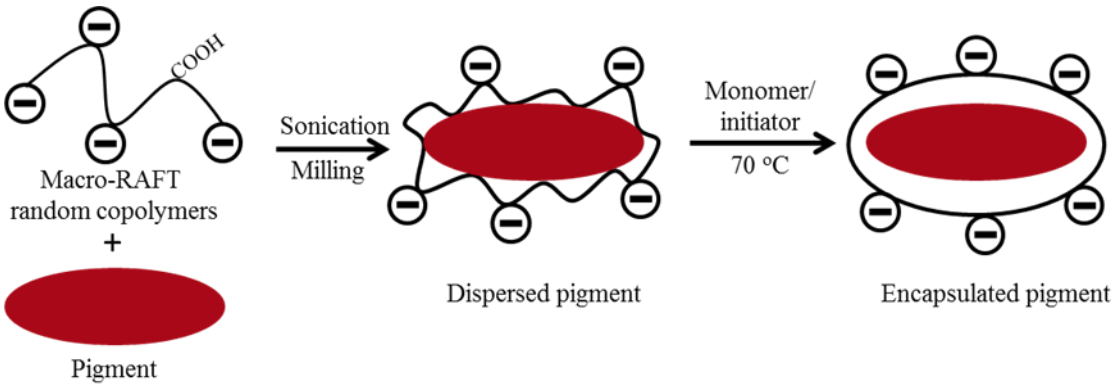

Figure 1.17 Schematic representation of the dispersion and encapsulation of pigment particles using macro-RAFT random copolymers.[124]

Hawkett *et al* employed[124] an emulsion polymerization using living amphipathic random macro-RAFT copolymers to encapsulate both hydrophilic inorganic (zirconia and alumina-coated titanium dioxide) and hydrophobic organic (phthalocyanine blue) pigments. Poly(methyl methacrylate)-co-(butyl acrylate) was the copolymer used which stabilized the initial pigment dispersion and facilitated the uniform growth of polymer on the pigment particle surface. The formation of encapsulated polymer composite nanoparticles showed a core-shell morphology structure with pigments particles located at the hydrophobic centre of thick polymer shells. The hydrophilic layer of negatively charged carboxyl groups on the surface (Figure 1.17) facilitated stabilization and dispersion of the encapsulated particles in the aqueous phase. It was demonstrated that 100% of the pigment particles were encapsulated and almost all of the polymer growth was within the encapsulating polymer shells. The reason for high encapsulation efficiency obtained is due to the use of a living amphipathic random macro-RAFT copolymer which do not self-assembles in the aqueous phase and hence avoids the formation of new particles by micelle nucleation.

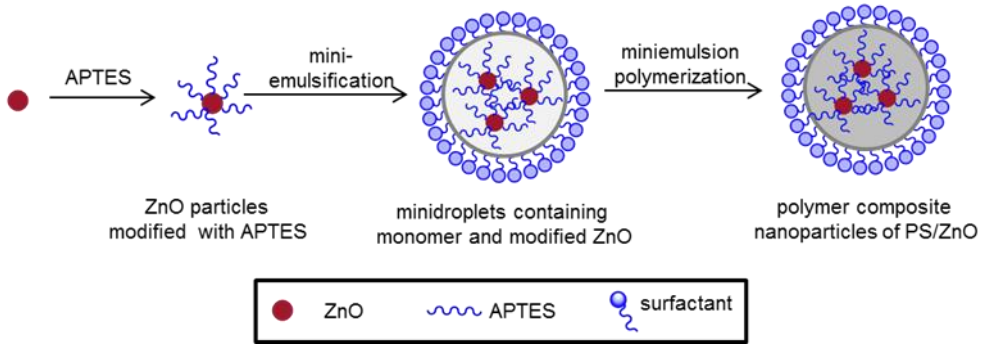

Figure 1.18 The preparation of ZnO/polystyrene nanocomposite by miniemulsion polymerization.[125]

Zinc oxide-based nanostructures are used as catalysts for chemical reactions, photocatalysts, photoelectric conversion, as antibacterial agents and bactericides, UV-shielding materials, and photoluminescent materials.[126, 127] Nanocomposite polymer nanoparticles of PS/ZnO prepared via miniemulsion polymerization were reported[125] by Tang and Dong. The surface of ZnO particles was modified by grafting with 3-aminopropyltriethoxysilane (APTES), which helps to improve the hydrophobicity of these inorganic materials and thus increases their encapsulation efficiency by 95% (Figure 1.18). The nanocomposite polymer particles obtained by miniemulsion polymerization possessed smaller particle diameters and narrow particle size distributions. Furthermore, the PS/ZnO composite nanoparticles exhibit good dispersion

ability with commercial polymers of poly(St-BA) coating films possessing good antibacterial activity.

The group of Ali Reza Mahdavian[128] successfully synthesised encapsulated nano-alumina as a core within poly[(styrene)-co-(methyl methacrylate)] shells under high shear ultrasonic irradiation miniemulsion polymerization. It is well known that alumina nanoparticles can be employed as fillers for polymers to improve mechanical, tribological, barrier, and conductive properties.[129]

1.9 Conclusions

The relatively recent advances in the development of inorganic/polymer composite nanoparticles have paved the way for the production of advanced and novel materials in colloidal nature based on both inorganic and polymer materials. The main motivation for the combination of inorganic materials with different properties within polymeric matrix is the multifunctionality of polymer composite nanoparticles. From the surveyed literature, it can be summarized that:

i) Miniemulsion polymerization proved a versatile technique in comparison to conventional emulsion polymerization for the synthesis of inorganic/polymer composite nanoparticles, in which the structure, morphologies, numbers and particle sizes of the nanocomposite can be effectively controlled.
ii) The nucleation and growth of the polymer *via* miniemulsion polymerization is primarily limited to the monomer droplets which offers better control in encapsulation efficiency of inorganic nanoparticle within polymer matrix.
iii) Miniemulsion polymerization techniques offer great opportunities for the encapsulation of a wide variety of materials in the form of small molecules, liquids and solids within polymer shells to generate multifunctional hybrid polymer composite nanoparticles.
iv) The ability to tailor the compatibility or dispersability between the inorganic species and organic monomer system is key to obtaining a good encapsulation of these otherwise incompatible compounds.
v) The relationships between miniemulsion composition, polymerization conditions, structures, properties and particles size of the inorganic species should be improved and optimized to ensure the desired products are prepared.

Taking into the account of the advantages and versatility of miniemulsion polymerization as a polymer encapsulation technique, and also the unique properties of

silicon quantum dots (SiQDs) as inorganic entities, sophisticated polymer composite nanoparticles possessing the luminescence characteristics of SiQDs and ease of functionalization and processability of polymer matrix will be discussed.

1.10 References

1. J. A. García-Calzón and M. E. Díaz-García, *TrAC Trends in Analytical Chemistry*, 2012, **35**, 27-38.
2. P. Alexandridis, *Chemical Engineering & Technology*, 2011, **34**, 15-28.
3. T. H. Chen, K. W. Kuo, W. T. Kuo, H. Y. Huang and Y. Y. Huang, *Journal of Bionanoscience*, 2008, **2**, 109-113.
4. M. C. Daniel and D. Astruc, *Chemical Reviews*, 2004, **104**, 293-346.
5. K. L. Kelly, E. Coronado, L. L. Zhao and G. C. Schatz, *The Journal of Physical Chemistry B*, 2002, **107**, 668-677.
6. X. Michalet, F. Pinaud, T. D. Lacoste, M. Dahan, M. P. Bruchez, A. P. Alivisatos and S. Weiss, *Single Molecules*, 2001, **2**, 261-276.
7. A. M. Smith and S. Nie, *Accounts of Chemical Research*, 2009, **43**, 190-200.
8. G. V. Ramesh, S. Porel and T. P. Radhakrishnan, *Chemical Society Reviews*, 2009, **38**, 2646-2656.
9. A. M. Smith, X. H. Gao and S. M. Nie, *Photochemistry and Photobiology*, 2004, **80**, 377-385.
10. F. Erogbogbo, C. W. Chang, J. May, P. N. Prasad and M. T. Swihart, *Nanoscale*, 2012, **4**, 5163-5168.
11. W. D. Lawson, F. A. Smith and A. S. Young, *Journal of The Electrical Society*, 1960, **107**, 206-210.
12. A. L. Éfros, *Advances in Physical Science*, 1974, **16**, 789.
13. A. I. Ekimov and A. A. Onushchenko, *JETP Letters*, 1981, **6**, 363-366.
14. J. P. Kuczynski, B. H. Milosavijevic and J. K. Thomas, *Journal of Physical Chemistry*, 1983, **87**, 3368-3370.
15. C. B. Murray, D. J. Norris and M. G. Bawendi, *Journal of the American Chemical Society*, 1993, **115**, 8706-8715.
16. M. Bruchez, M. Moronne, P. Gin, S. Weiss and A. P. Alivisatos, *Science*, 1998, **281**, 2013-2016.
17. W. C. W. Chan and S. M. Nie, *Science*, 1998, **281**, 2016-2018.
18. A. P. Alivisatos, *Science*, 1996, **271**, 933-937.
19. M. G. Bawendi, M. L. Steigerwald and L. E. Brus, *Annual Review of Physical Chemistry*, 1990, **41**, 477-496.
20. A. F. E. Hezinger, J. Tessmar and A. Goepferich, *European Journal of Pharmaceutics and Biopharmaceutics*, 2008, **68**, 138-152.
21. V. I. Klimov, *Semiconductor and Metal Nanocrystals: Synthesis and Electronic and Optical Properties*, Marcel Dekker Inc, 2003.
22. A. P. Alivisatos, *The Journal of Physical Chemistry*, 1996, **100**, 13226-13239.
23. X. H. Gao, W. C. W. Chan and S. M. Nie, *Journal of Biomedical Optics*, 2002, **7**, 532-537.
24. W. C. W. Chan, D. J. Maxwell, X. Gao, R. E. Bailey, M. Han and S. Nie, *Current Opinion in Biotechnology*, 2002, **13**, 40-46.
25. Y. T. Lim, S. Kim, A. Nakayama, N. E. Stott, M. G. Bawendi and J. V. Frangioni, *Molecular Imaging*, 2003, **2**, 50-64.

26. S. Kim, Y. T. Lim, E. G. Soltesz, A. M. De Grand, J. Lee, A. Nakayama, J. A. Parker, T. Mihaljevic, R. G. Laurence, D. M. Dor, L. H. Cohn, M. G. Bawendi and J. V. Frangioni, *Nature Biotechnology*, 2004, **22**, 93-97.
27. J. M. Klostranec and W. C. W. Chan, *Advanced Materials*, 2006, **18**, 1953-1964.
28. N. Tessler, V. Medvedev, M. Kazes, S. H. Kan and U. Banin, *Science*, 2002, **295**, 1506-1508.
29. M. Kazes, D. Y. Lewis, Y. Ebenstein, T. Mokari and U. Banin, *Advanced Materials*, 2002, **14**, 317-321.
30. W. U. Huynh, J. J. Dittmer and A. P. Alivisatos, *Science*, 2002, **295**, 2425-2427.
31. M. Peres, L. C. Costa, A. Neves, M. J. Soares, T. Monteiro, A. C. Esteves, A. Barros-Timmons, T. Trindade, A. Kholkin and E. Alves, *Nanotechnology*, 2005, **16**, 1969.
32. X. Michalet, F. F. Pinaud, L. A. Bentolila, J. M. Tsay, S. Doose, J. J. Li, G. Sundaresan, A. M. Wu, S. S. Gambhir and S. Weiss, *Science*, 2005, **307**, 538-544.
33. C. Kirchner, T. Liedl, S. Kudera, T. Pellegrino, A. M. Javier, H. E. Gaub, S. Stölzle, N. Fertig and W. J. Parak, *Nano Letters*, 2005, **5**, 331-338.
34. M. Green and E. Howman, *Chemical Communications*, 2005, 121-123.
35. E. Novo and M. Parola, *Fibrogenesis & Tissue Repair*, 2008, **1**, 5.
36. J. Lovric, S. J. Cho, F. M. Winnik and D. Maysinger, *Chemistry & Biology*, 2005, **12**, 1227-1234.
37. A. Shiohara, A. Hoshino, K. Hanaki, K. Suzuki and K. Yamamoto, *Microbiology and Immunology*, 2004, **48**, 669-675.
38. N. O'Farrell, A. Houlton and B. R. Horrocks, *International Journal of Nanomedicine*, 2006, **1**, 451-472.
39. N. H. Alsharif, C. E. M. Berger, S. S. Varanasi, Y. Chao, B. R. Horrocks and H. K. Datta, *Small*, 2009, **5**, 221-228.
40. A. Fucikova, J. Valenta, I. Pelant, K. Kusova and V. Brezina, *Physica Status Solidi C*, 2011, **8**, 1093-1096.
41. H. A. Santos, J. Riikonen, J. Salonen, E. Mäkilä, T. Heikkilä, T. Laaksonen, L. Peltonen, V.-P. Lehto and J. Hirvonen, *Acta Biomaterialia*, 2010, **6**, 2721-2731.
42. F. Erogbogbo, K. T. Yong, I. Roy, G. X. Xu, P. N. Prasad and M. T. Swihart, *ACS Nano*, 2008, **2**, 873-878.
43. F. Erogbogbo and M. T. Swihart, *AIP Conference Proceedings*, 2010, **1275**, 35-39
44. F. Erogbogbo, K. T. Yong, I. Roy, R. Hu, W. C. Law, W. Zhao, H. Ding, F. Wu, R. Kumar, M. T. Swihart and P. N. Prasad, *ACS Nano*, 2010, **5**, 413-423.
45. L. H. Lie, M. Duerdin, E. M. Tuite, A. Houlton and B. R. Horrocks, *Journal of Electroanalytical Chemistry*, 2002, **538-539**, 183-190.
46. J. K. Jaiswal and S. M. Simon, *Trends in Cell Biology*, 2004, **14**, 497-504.
47. L. Brus, *The Journal of Physical Chemistry*, 1994, **98**, 3575-3581.
48. A. Uhlir, *Bell System Technical Journal*, 1956, **35**, 333-347.
49. L. T. Canham, *Applied Physics Letters*, 1990, **57**, 1046-1048.
50. A. G. Cullis and L. T. Canham, *Nature*, 1991, **353**, 335-338.
51. G. Pucker, Serra, E. and Jestin, Y., in *Quantum Dots-A Variety of New Applications*, ed. A. Al-Ahmadi, InTech, edn., 2012.
52. D. P. Puzzo, E. J. Henderson, M. G. Helander, Z. Wang, G. A. Ozin and Z. Lu, *Nano Letters*, 2011, **11**, 1585-1590.
53. Y. Chao, L. Siller, S. Krishnamurthy, P. R. Coxon, U. Bangert, M. Gass, L. Kjeldgaard, S. N. Patoleo, L. H. Lie, N. O'Farrell, T. A. Alsop, A. Houlton and B. R. Horrocks, *Nature Nanotechnology*, 2007, **2**, 486-489.

54. M. Antonietti and K. Tauer, *Macromolecular Chemistry and Physics*, 2003, **204**, 207-219.
55. A. M. van Herk and K. Landfester, *Hybrid Latex Particles: Preparation with (Mini)emulsion Polymerization*, Springer, 2010.
56. K. Landfester, A. Musyanovych and V. Mailänder, *Journal of Polymer Science Part A: Polymer Chemistry*, 2010, **48**, 493-515.
57. E. Bourgeat-Lami, N. N. Herrera, J.-L. Putaux, A. Perro, S. Reculusa, S. Ravaine and E. Duguet, *Macromolecular Symposia*, 2007, **248**, 213-226.
58. R. O. Ebewele, *Polymer Science and Technology*, Taylor & Francis, 2010.
59. P. O'Brien, S. S. Cummins, D. Darcy, A. Dearden, O. Masala, N. L. Pickett, S. Ryley and A. J. Sutherland, *Chemical Communications*, 2003, 2532-2533.
60. A. Schmid, S. Fujii and S. P. Armes, *Langmuir*, 2006, **22**, 4923-4927.
61. A. Schmid, S. P. Armes, C. A. P. Leite and F. Galembeck, *Langmuir*, 2009, **25**, 2486-2494.
62. A. V. Fuchs and G. D. Will, *Polymer*, 2010, **51**, 2119-2124.
63. N. Joumaa, M. Lansalot, A. Theretz, A. Elaissari, A. Sukhanova, M. Artemyev, I. Nabiev and J. H. M. Cohen, *Langmuir*, 2006, **22**, 1810-1816.
64. J. M. Asua, *Polymeric Dispersions: Principles and Applications*, Kluwer Academic, 1997.
65. J. Forcada; and J. Ramos, in *Miniemulsion Polymerization Technology*, ed. V. Mittal, Wiley, Editon edn., 2011, 71-96.
66. K. Landfester, *Angewandte Chemie International Edition*, 2009, **48**, 4488-4507.
67. K. Landfester, *Macromolecular Rapid Communications*, 2001, **22**, 896-936.
68. F. J. Schork, Y. Luo, W. Smulders, J. Russum, A. Butté and K. Fontenot, in *Polymer Particles*, ed. M. Okubo, Springer Berlin Heidelberg, edn., 2005, **175**, 129-255.
69. V. Mittal, *Miniemulsion Polymerization Technology*, Wiley, 2011.
70. J. M. Asua, *Progress in Polymer Science*, 2002, **27**, 1283-1346.
71. A. Ethirajan and K. Landfester, *Chemistry - A European Journal*, 2010, **16**, 9398-9412.
72. A. Guyot, K. Landfester, F. Joseph Schork and C. Wang, *Progress in Polymer Science*, 2007, **32**, 1439-1461.
73. B. Erdem, E. D. Sudol, V. L. Dimonie and M. S. El-Aasser, *Journal of Polymer Science Part A: Polymer Chemistry*, 2000, **38**, 4431-4440.
74. A. López, A. Chemtob, J. L. Milton, M. Manea, M. a. Paulis, M. a. J. Barandiaran, S. Theisinger, K. Landfester, W. D. Hergeth, R. Udagama, T. McKenna, F. o. Simal and J. M. Asua, *Industrial & Engineering Chemistry Research*, 2008, **47**, 6289-6297.
75. K. Fontenot and F. J. Schork, *Industrial & Engineering Chemistry Research*, 1993, **32**, 373-385.
76. A. S. Kabalnov and E. D. Shchukin, *Advances in Colloid and Interface Science*, 1992, **38**, 69-97.
77. W. I. Higuchi and J. Misra, *Journal of Pharmaceutical Sciences*, 1962, **51**, 459-466.
78. C. S. Chern, T. J. Chen and Y. C. Liou, *Polymer*, 1998, **39**, 3767-3777.
79. J. Ugelstad, M. S. El-Aasser and J. W. Vanderhoff, *Journal of Polymer Science: Polymer Letters Edition*, 1973, **11**, 503-513.
80. F. K. Hansen and J. Ugelstad, *Journal of Polymer Science: Polymer Chemistry Edition*, 1979, **17**, 3069-3082.
81. J. L. Reimers and F. J. Schork, *Journal of Applied Polymer Science*, 1996, **60**, 251-262.

82. S. Wang and F. J. Schork, *Journal of Applied Polymer Science*, 1994, **54**, 2157-2164.
83. P. Walstra, *Chemical Engineering Science*, 1993, **48**, 333-349.
84. K. Landfester, N. Bechthold, F. Tiarks and M. Antonietti, *Macromolecules*, 1999, **32**, 5222-5228.
85. A. Gonenne and R. Ernst, *Analytical Biochemistry*, 1978, **87**, 28-38.
86. K. Landfester, N. Bechthold, F. Tiarks and M. Antonietti, *Macromolecules*, 1999, **32**, 2679-2683.
87. N. Bechthold, F. Tiarks, M. Willert, K. Landfester and M. Antonietti, *Macromolecular Symposia*, 2000, **151**, 549-555.
88. H. M. Ghazaly, E. S. Daniels, V. L. Dimonie, A. Klein and M. S. El-Aasser, *Journal of Applied Polymer Science*, 2001, **81**, 1721-1730.
89. J. Hu, M. Chen and L. Wu, *Polymer Chemistry*, 2011, **2**, 760-772.
90. F. Fleischhaker and R. Zentel, *Chemistry of Materials*, 2005, **17**, 1346-1351.
91. W. Yin, H. Liu, M. Z. Yates, H. Du, F. Jiang, L. Guo and T. D. Krauss, *Chemistry of Materials*, 2007, **19**, 2930-2936.
92. A. C. C. Esteves, L. Bombalski, T. Trindade, K. Matyjaszewski and A. Barros-Timmons, *Small*, 2007, **3**, 1230-1236.
93. A. C. C. Esteves, P. Hodge, T. Trindade and A. M. M. V. Barros-Timmons, *Journal of Polymer Science Part A: Polymer Chemistry*, 2009, **47**, 5367-5377.
94. A. Rubio-Ríos, B. Aguilar-Castillo, S. Flores-Gallardo, C. Hernández-Escobar, E. Zaragoza-Contreras, Z. Zhao and M. Carpenter, *Journal of Polymer Research*, 2012, **19**, art no. 9833.
95. K. Y. van Berkel and C. J. Hawker, *Journal of Polymer Science Part A: Polymer Chemistry*, 2010, **48**, 1594-1606.
96. K. Y. van Berkel, A. M. Piekarski, P. H. Kierstead, E. D. Pressly, P. C. Ray and C. J. Hawker, *Macromolecules*, 2009, **42**, 1425-1427.
97. R. Betancourt-Galindo, C. Cabrera Miranda, B. A. Puente Urbina, A. Castañeda-Facio, S. Sánchez-Valdés, J. Mata Padilla, L. A. García Cerda, Y. A. Perera and O. S. Rodríguez-Fernández, *ISRN Nanotechnology*, 2012, 1-5.
98. L. Cumbal, J. Greenleaf, D. Leun and A. K. SenGupta, *Reactive and Functional Polymers*, 2003, **54**, 167-180.
99. P. Polasek and S. Mutl, *Water SA*, 2002, **28**, 69-82.
100. S. Päuser, R. Reszka, S. Wagner, K. J. Wolf, H. J. Buhr and G. Berger, *Anti-Cancer Drug Design*, 1997, **12**, 125-135.
101. A. P. Romio, H. H. Rodrigues, A. Peres, A. Da Cas Viegas, E. Kobitskaya, U. Ziener, K. Landfester, C. Sayer and P. H. H. Araújo, *Journal of Applied Polymer Science*, 2012, **129**, 1426–1433.
102. L. P. Ramírez and K. Landfester, *Macromolecular Chemistry and Physics*, 2003, **204**, 22-31.
103. N. Joumaa, P. Toussay, M. Lansalot and A. Elaissari, *Journal of Polymer Science Part A: Polymer Chemistry*, 2008, **46**, 327-340.
104. A. R. Mahdavian, M. Ashjari and H. S. Mobarakeh, *Journal of Applied Polymer Science*, 2008, **110**, 1242-1249.
105. Y. Mori and H. Kawaguchi, *Colloids and Surfaces B-Biointerfaces*, 2007, **56**, 246-254.
106. S. Lu, J. Ramos and J. Forcada, *Langmuir*, 2007, **23**, 12893-12900.
107. J. Ramos and J. Forcada, *Langmuir*, 2011, **27**, 7222-7230.
108. Y. Yang, A. R. Mahdavian, E. S. Daniels, A. Klein and M. S. El-Aasser, *Journal of Applied Polymer Science*, 2013, **127**, 3768-3777.
109. F. Tiarks, K. Landfester and M. Antonietti, *Langmuir*, 2001, **17**, 5775-5780.

110. Y. Zhang, H. Chen and Q. Zou, *Colloid and Polymer Science*, 2009, **287**, 1221-1227.
111. Y. Zhang, H. Chen, X. Shu, Q. Zou and M. Chen, *Colloids and Surfaces A: Physicochemical and Engineering Aspects*, 2009, **350**, 26-32.
112. J. Zhou, S. W. Zhang, X. G. Qiao, X. Q. Li and L. M. Wu, *Journal of Polymer Science Part A: Polymer Chemistry*, 2006, **44**, 3202-3209.
113. Á. Costoyas, J. Ramos and J. Forcada, *Journal of Polymer Science Part A: Polymer Chemistry*, 2009, **47**, 935-948.
114. E. Bourgeat-Lami, G. A. Farzi, L. David, J. L. Putaux and T. F. L. McKenna, *Langmuir*, 2012, **28**, 6021-6031.
115. S. Melle, M. Lask and G. G. Fuller, *Langmuir*, 2005, **21**, 2158-2162.
116. Z. Cao, A. Schrade, K. Landfester and U. Ziener, *Journal of Polymer Science Part A: Polymer Chemistry*, 2011, **49**, 2382-2394.
117. E. Bourgeat-Lami and M. Lansalot, in *Hybrid Latex Particles*, eds. A. M. Herk and K. Landfester, Springer Berlin Heidelberg, edn., 2010, **233**, 53-123.
118. X. Huang and W. J. Brittain, *Macromolecules*, 2001, **34**, 3255-3260.
119. K. Khezri, V. Haddadi-Asl, H. Roghani-Mamaqani and M. Salami-Kalajahi, *Journal of Polymer Research*, 2012, **19**, art no. 9868.
120. E. Zengeni, P. C. Hartmann and H. Pasch, *ACS Applied Materials & Interfaces*, 2012, **4**, 6957-6968.
121. E. Zengeni, P. C. Hartmann and H. Pasch, *Macromolecular Chemistry and Physics*, 2013, **214**, 62-75.
122. B. Erdem, E. D. Sudol, V. L. Dimonie and M. S. El-Aasser, *Journal of Polymer Science Part A: Polymer Chemistry*, 2000, **38**, 4419-4430.
123. Y. Wu, Y. Zhang, J. Xu, M. Chen and L. Wu, *Journal of Colloid and Interface Science*, 2010, **343**, 18-24.
124. D. Nguyen, H. S. Zondanos, J. M. Farrugia, A. K. Serelis, C. H. Such and B. S. Hawkett, *Langmuir*, 2008, 24, 2140-2150.
125. E. Tang and S. Dong, *Colloid and Polymer Science*, 2009, **287**, 1025-1032.
126. N. S. Norberg and D. R. Gamelin, *Journal of Physical Chemistry B*, 2005, **109**, 20810-20816.
127. C. H. Hung and W. T. Whang, *Journal of Materials Chemistry*, 2005, **15**, 267-274.
128. A. Mahdavian, Y. Sarrafi and M. Shabankareh, *Polymer Bulletin*, 2009, **63**, 329-340.
129. H. Liu, H. Ye and Y. Zhang, *Colloids and Surfaces A: Physicochemical and Engineering Aspects*, 2008, **315**, 1-6.

Chapter 2

A Miniemulsion Polymerization Technique for Encapsulation of Silicon Quantum Dots in Polymer Nanoparticles

This chapter is based on the publication:

N.A. Harun, B.R. Horrocks and D.A. Fulton, "A Miniemulsion Polymerization Technique for Encapsulation of Silicon Quantum Dots in Polymer Nanoparticles", *Nanoscale*, 2011, **3**, 4733 – 4741.

2.1 Abstract

Miniemulsion polymerization techniques were used to encapsulate luminescent alkylated silicon quantum dots (SiQDs) within polymer nanoparticles composed of styrene and 4-vinylbenzaldehyde monomers. The polymer nanoparticles had mean diameters in the range 90 – 150 nm depending on the reaction conditions, however, all samples showed narrow particle size distributions, as determined by dynamic light scattering and atomic force microscopy. The SiQDs were found to have a small beneficial effect on the polymerization process by reducing the polydispersity of the final polymer particles, which is attributed to co-surfactant action of the undecene used to form the alkyl capping layer on the SiQDs. Confocal microspectroscopy was used to confirm that the luminescent alkylated SiQDs were encapsulated within the polymer nanoparticles and also provided luminescence and Raman spectra which show signals corresponding to both alkylated SiQDs and the polymer nanoparticles. Treatment of the polymer nanoparticles with dilute aqueous sodium hydroxide solution, which is known to corrode Si and extinguish the luminescence of alkylated SiQDs, results in only a partial reduction in luminescence suggesting that the majority of the alkylated SiQDs are encapsulated sufficiently deep within the polymer matrix to protect them from alkaline attack. Miniemulsion polymerization of the monomers styrene and 4-vinylbenzaldehyde affords polymer nanoparticles displaying reactive aldehyde groups upon their surfaces, which were decorated with a selection of molecules through imine, oxime, or hydrazine condensation reactions. It is speculated that SiQDs-polymer composite nanoparticles whose surfaces can be further decorated will increase the utility of luminescent SiQDs in applications such as anti-counterfeiting and as probes of biological processes.

2.2 Introduction

Over the past decades there has been a rapid development of semiconductor nanocrystals, also known as quantum dots (QDs), as these nanocrystals can be used extensively as valuable tools for diagnosis, imaging and optical tracking[1] in medical and biotechnology applications. Among the known semiconductor nanocrystals (QDs), silicon quantum dots (SiQDs) are of great interest because of their low cytotoxicity[2] profile which arises on account of the absence of heavy metal ion leaching,[2, 3] an issue which affects conventional cadmium chalcogenide-based QDs.

Various techniques have been reported for the synthesis of SiQDs, which generally can be divided into molecular/chemical routes starting from precursors such as silicon halides,[4-6] silsesquisiloxanes[7] or silicides,[8] and various physical techniques including electrochemical etching,[9-11] reactive sputtering,[12] sol-gel techniques,[13] SiO_2 implantation,[14] self-assembly,[15] laser ablation[16] and thermal vaporization.[17] The synthetic strategy to prepare SiQDs developed at Newcastle University involves[18] a two-step procedure involving electro-chemical etching of p-Si<100> wafers in fluoride media at high current densities, followed by reflux of the resulting porous Si chips in toluene solutions of an alkene, usually 1-undecene. A significant issue arising from this method of preparation is that the hydrophobic alkylated SiQDs lack water solubility, which limits the usefulness of alkylated SiQDs in biological applications, where water compatibility would be desirable. However, work has shown[19] that alkylated SiQDs can be dispersed as lyophobic aqueous sols by first dissolving them in small amounts of suitable organic solvents such as THF, and then dispersing this solution in water. It is also desirable to prepare SiQDs possessing functional groups which would facilitate their conjugation to other molecules. Even though, several examples of functional SiQDs, for instance amine-terminated SiQDs,[20, 21] have been reported, it is often difficult to perform organic reactions cleanly on the small quantities of available material. Furthermore, an attempt to synthesize SiQDs by electrochemical method which possesses suitable functional groups to facilitate their conjugation to other molecules has been largely unsuccessful.[22]

To increase the utility of alkylated SiQDs, a research program has been instigated aimed at encapsulating cargos of alkylated SiQDs within polymer nanoparticles. Achieving this goal will enable access to hybrid nanoparticles possessing the fluorescent properties of SiQDs and the processability offered by polymer nanoparticles, which benefit from increased chemical stability and further potential to functionalize the polymer nanoparticle shell as discussed in Chapter 1. Miniemulsion polymerization[23-25] is a robust and convenient method to encapsulate inorganic materials inside polymer nanoparticles. This technique delivers successful encapsulation because the hydrophobic inorganic species can be directly dispersed into the monomer phase, which is conventionally also hydrophobic, and encapsulated upon polymerization of miniemulsion droplets.[26]

To further utilize the usefulness of the polymer nanoparticles, the surface of polymer nanoparticles can be further decorated with other molecules including those of biological significance such as carbohydrate or peptides. The miniemulsion

polymerization technique allows the preparation of polymer nanoparticles featuring reactive functional groups upon their surfaces, such as terminal olefins,[27] carboxylic acids[28-31] and amines,[31-33] which can facilitate further chemical functionalization. The group of Costoyas[34] have demonstrated conjugation of hydrazine functions upon the surfaces of polymer nanoparticles by utilizing the monomers 4-vinylbenzyl hydrazine and styrene. Hydrazines react cleanly and efficiently with aldehydes and ketones to form stable hydrazones,[35] presenting a very useful route to adorn the surfaces of the polymer nanoparticles with biomolecules. The hydrazine functional group possesses higher reactivity and lower pK_a than the other amino groups, advantages which permit their conjugation to proceed under conditions when the amino group would normally be protonated. The relative stability of hydrazones compared to imines means that kinetic fixing of the products through reductive amination chemistry is not required.

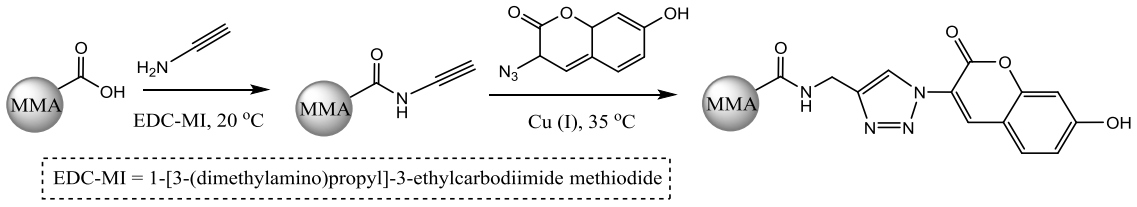

Scheme 2.1 Synthetic route for nanoparticle surface functionalization using 'click' chemistry.

Another interesting example involving surface functionalization was investigated by Lovell *et al.*[36]. They present the synthesis of polymer nanoparticles by starve-fed emulsion polymerization and their surface modification via post-polymerization 'click' chemistry. The main objective of this work was to demonstrate that 'click' chemistry could be successfully applied upon the surface of polymer nanoparticles dispersed in aqueous media. The alkyne-functionalized polymer nanoparticles were prepared (Scheme 2.1) by a starve-fed emulsion polymerization process involving copolymerization of methyl methacrylate (MMA) and methacrylic acid in the ratio of 80 : 20 mol % in order to form carboxylic core-shell particles, onto which were conjugated alkyne groups by reaction with *propargylamine*. The 'click' reaction on the surface of polymer nanoparticles was performed successfully using the fluorescent azide dye pro-fluorophore which only displays fluorescence after the 'click' reaction has successfully occurred. Demonstrating the feasibility of 'click' chemistry for surface modification in aqueous media provides a new approach to synthesize surface-functionalized polymer nanoparticles. This class of polymer nanoparticles could be very

useful in applications, for instance, drug delivery or diagnostics, as it should be possible to attach targeting molecules which would help direct the nanoparticles towards cells or tissues of interest.

This chapter describes the synthesis of polymer nanoparticles produced by miniemulsion polymerization in the absence and presence of SiQDs. Polymer nanoparticles displaying aromatic aldehyde groups on their surfaces are prepared, which allow access to surface-decorated polymer nanoparticles through their reactions with numerous nitrogen nucleophiles e.g. amines, hydrazines, acyl hydrazines and alkoxyamines will be discussed. The characterization of polymer composite nanoparticles both chemically and spectroscopically will also be discussed.

2.3 Results and Discussion

2.3.1 *Synthesis of Silicon Quantum Dots (SiQDs)*

The starting point for the synthesis of SiQDs is the preparation of a porous silicon layer, which is usually a few microns-thick film, and is produced by electrochemical etching of Si wafer in the presence of fluoride media.[2] The luminescence emitted from the porous Si surface originates from the quantum-confined structure nature of this nanocrystalline film.[2]

The SiQDs were prepared according to a modification[37] of the original procedure described by Lie *et al.*[18] using an electrochemical etching process. SiQDs were produced by refluxing hydrogen-terminated porous Si films in dry toluene solutions of 1-undecene. The porous Si films break up under the reflux conditions and 1-undecene undergoes a hydrosilylation reaction upon the surface of the particle, resulting in the formation of hydrocarbon monolayer which stabilizes the resultant particle against oxidation. It is also well known that the chemical modification of the surface of porous Si can be used to manipulate its photoluminescent, spectroscopic and electrochemiluminescent behaviour.[38-40] 1-Undecene has been chosen for the preparation of SiQDs because it has been reported[18] that a dispersion of SiQDs can be formed easily when the SiQDs are coated with 1-undecene. After the refluxing procedure, it was noted that the solution was observed to be a pale yellow colour and luminesced orange under a handheld UV-lamp (λ = 365 nm) (Figure 2.1a). Evaporation to dryness removes toluene and unreacted 1-undecene to afford an oily/ waxy residue which displays luminescence when irradiated under UV light (λ = 365 nm).

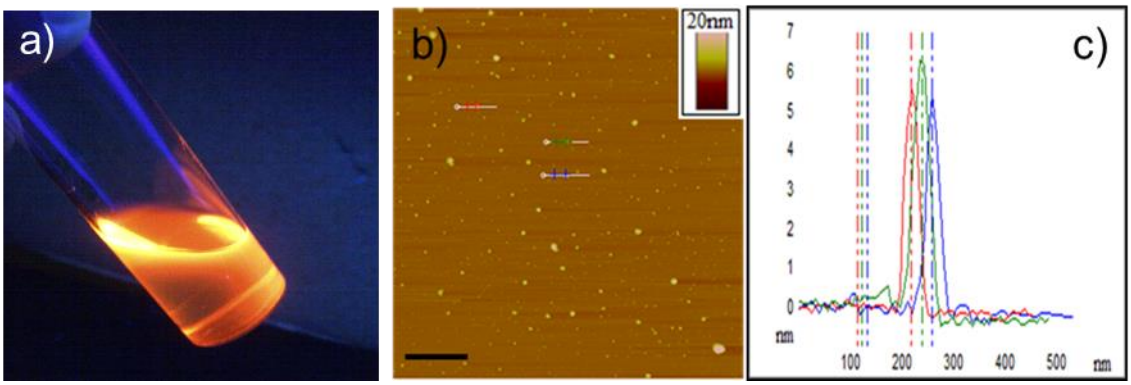

Figure 2.1 (a) The alkylated SiQDs dispersed in toluene luminesce orange under a UV lamp (λ = 365 nm) (b) The AFM image of SiQDs dispersed in CH_2Cl_2 drop cast onto mica (c) Cross section of SiQDs as measured by AFM.

This dried oily/ waxy residue contained the desired nanoscopic silicon particles whose surface is covered with a monolayer of Si-C bonded alkyl species formed by a hydrosilylation process. Such Si-C bonded surfaces possess a good resistance to oxidation under ambient conditions in comparison to hydrogen-terminated Si/monolayers anchored via Si-O bonds.[41, 42] As prepared, SiQDs are hydrophobic and are not soluble in aqueous media, forming a lyophobic colloid in organic solvents e.g. THF, CH_2Cl_2 and $PhCH_3$.

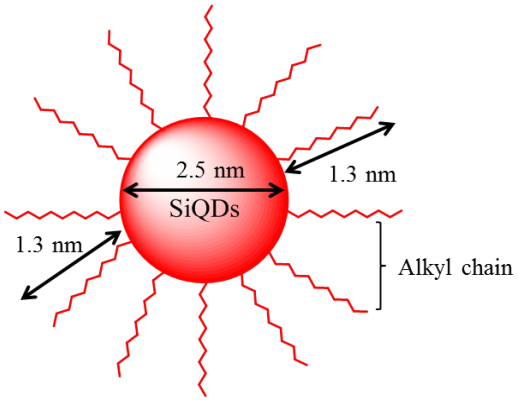

Scheme 2.2: Cartoon scheme of silicon quantum dots (SiQDs). The size is not in accurate scale.

The particle size of single alkylated SiQDs obtained from the electrochemical etching method is about ~ 6 nm as confirmed from the height of alkyl capped SiQDs measured by tapping mode™ AFM (Figure 2.1 b). This observation is consistent with the previously reported studies[19, 37] of SiQD structures which shows the Si core to be 2.5 nm in diameter and the shell of alkyl chains to be approximately 1.3 nm thick (Scheme 2.2), The large particle observed from the shown AFM image (Figure 2.1b) is most likely associated with a large clump of aggregated single SiQDs, and which may arise as a consequence of the drying of SiQDs solution on the mica substrate. The structure

and composition of alkyl capped SiQDs have been spectroscopically and microscopically characterized in considerable detail in previous studies.[18, 43, 44]

When the size of a SiQD becomes comparable to or smaller than the exciton Bohr radius, quantum confinement effects become important and its energy levels become discrete, as opposed to the continuous energy levels found in bulk Si crystal. In SiQDs, the energy required to excite an electron from the highest level of the valence band to the lowest level of the conduction band is higher, and shorter wavelength of light are absorbed which is shifted to the blue due to the effect of quantum confinement. The absorption spectra (Figure 2.2a) of alkyl-capped SiQDs in CH_2Cl_2 measured at different concentrations display features at ~ 360 nm which are attributed to the direct band gap transition (ca. 3.4 eV in bulk silicon). On account of the "indirect band gap" phenomenon in SiQDs, a weak light absorption is also observed in the wavelength region of 620 nm and 720 nm. The indirect band gap absorption of SiQDs is consistent with the experimentally measured emission spectra, as illustrated in Figure 2.2b.

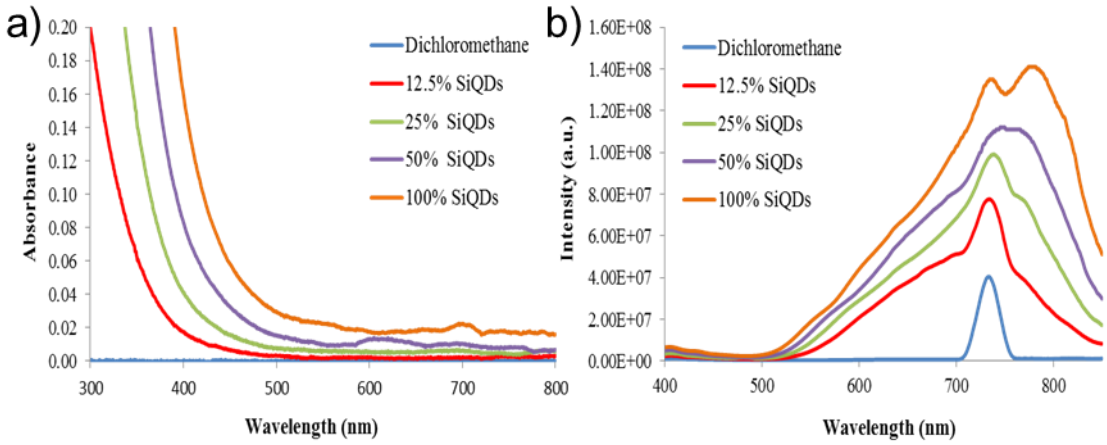

Figure 2.2 (a) Absorbance spectra of alkylated SiQDs dispersed in CH_2Cl_2 observed by UV-Vis spectroscopy (b) Emission spectra of SiQDs dispersed in CH_2Cl_2 (excitation λ = 365 nm).

The emission spectra of alkylated SiQDs dispersed in CH_2Cl_2 were measured by fluorescence spectroscopy (excitation wavelength = 365 nm) (Figure 2.2b). Four different concentrations of SiQDs solution were observed, with the emission spectra displaying broad photoluminescence (PL) in the range of 530 nm – 850 nm. These broad emission profiles of SiQDs probably arise on account of the absorption or emission of a lattice vibration (phonon), and also probably on account of the different particle sizes within the SiQDs sample. The maximum emission of SiQDs was found at approximately around 670 nm – 700 nm, similar to observations from previous work.[18] It is worth mentioning here that the intense and sharp peak at 730 nm corresponds to an

artifact of second order scattering, while the rest of other peaks belong to the emission spectra of SiQDs. Electronic structure[45] and photophysics[46, 47] of SiQDs prepared by electrochemical etching method was thoroughly studied and characterized several years ago in our research group. The absorbance and emission spectra that were measured here are consistent with the previously reported alkylated SiQDs, indicating their successful synthesis.

2.3.2 *Preparation of Polymer Composite Nanoparticles via Miniemulsion Polymerization*

The hydrophobic nature of alkylated SiQDs makes them ready-made candidates for encapsulation by miniemulsion polymerization methods as their hydrophobic alkyl monolayers ensure good stability in the organic phase of the monomer. The encapsulation of SiQDs using the monomers styrene (St), 4-vinyl benzaldehyde (4-VBA) and mixtures of both was investigated. 4-VBA is a styrenic monomer featuring an aromatic aldehyde function, which allows the preparation of polymer nanoparticles possessing aldehyde surface groups that may be further functionalized through the formation of imine, hydrazine or oxime bonds.

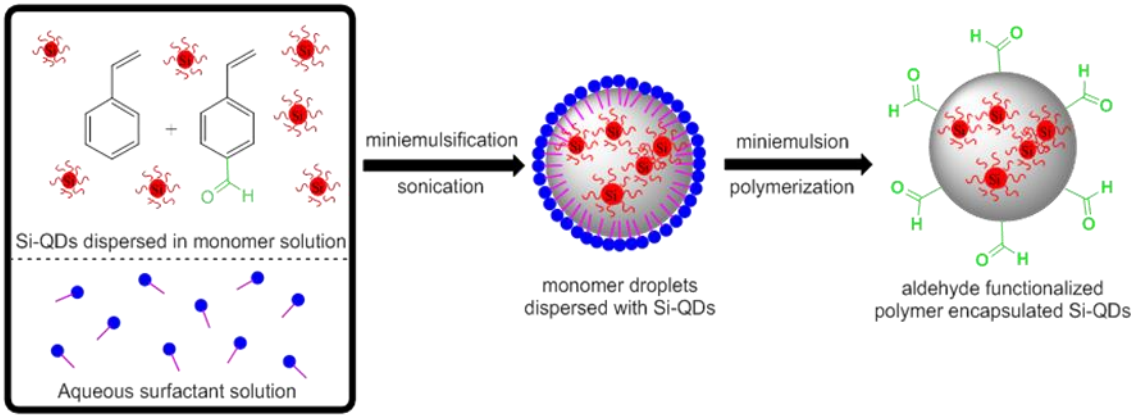

Scheme 2.3 Polymer composite nanoparticles encapsulating SiQDs prepared via miniemulsion polymerization techniques. An emulsion of monomer droplets dispersed with SiQDs is obtained by sonication of a mixture of SiQDs dispersed in monomer and aqueous surfactant. The monomer droplets are then polymerized into the desired polymer nanoparticles.

The miniemulsion polymerization (Scheme 2.3) utilized here is based upon the procedures described by the Landfester group,[48] using sodium dodecyl sulphate (SDS) as surfactant, hexadecane as co-surfactant and potassium persulfate (KPS) as the initiator. The hydrophobic nature of alkylated SiQDs ensures that they disperse in the

monomer organic phase. A concern is that the method of preparing alkylated SiQDs by electrochemical/ hydrosilylation results in the production of very small quantities of product (estimated yield of ~100 µg of alkylated SiQDs per individual 1 cm^2 Si chip), a fact which can have important consequences upon the ultimate distribution of SiQDs within the polymer nanoparticles. Hawker and co-workers have demonstrated[27] that working with low masses of inorganic components requires utilizing small total volumes of emulsion to encourage an even distribution of the inorganic particles throughout the polymer nanoparticles. Because the mass of alkylated SiQDs available for encapsulation is so small, the volume of the emulsion system therefore also needs to be scaled down. As a consequence, "small" scale miniemulsion polymerization was conducted at relatively low volumes (10 mL) and with total monomer content (0.25 g), such that the polymerizations were still experimentally practical. For comparison with more typical miniemulsion polymerization conditions, "large" scale reactions were also conducted at higher volumes (24 mL) and higher total monomer contents (6.00 g).

The desired polymer nanoparticles containing encapsulated alkylated SiQDs (**P3[QDs]**, **P6[QDs]**, and **P9[QDs]** were prepared by dissolving a sample of alkylated SiQDs in organic monomer phase and hexadecane to which water and SDS were added. The resulting mixture was then emulsified by sonication, and after measurement of the droplet size by dynamic light scattering (DLS), the emulsion was polymerized under nitrogen by addition of KPS initiator and heating at 72 $^{\circ}$C for 3 h. The resulting polymer nanoparticles were purified by dialysis and further characterized by DLS. To test the possible effects of SiQDs upon the miniemulsion polymerization process, polymerizations were also performed in the absence of SiQDs (**P1[Ls]** – **P2[Ss]**, **P4[Ls]** – **P5[Ss]**, and **P7[Ls]** – **P8[Ss]**); **Ls** is referred to a large scale miniemulsion while **Ss** corresponding to small scale miniemulsion polymerization. The complete protocols and summarized results of all miniemulsion polymerizations together with their characterization by DLS are presented in Table 2.1.

2.3.3 *Particle Sizes and Particle Size Distributions of Droplets and Polymer Nanoparticles as Determined by Dynamic Light Scattering (DLS)*

DLS provides characterization of particle sizes and particle size distributions of the monomer droplets and their resultant polymer nanoparticles. DLS, which is also known as Photon Correlation Spectroscopy/ Quasi-Elastic Light Scattering, is a well-established technique to determine the size and size distribution of molecules and which

exploits the Brownian motion phenomenon. The Brownian motion of particles or molecules in suspension causes laser light to be scattered at different intensities when the light hits the moving particles. By measuring the time scale of light intensity fluctuations, the average size, size distribution, and polydispersity of molecules and particles in solution can be quantified.[49] Mathematical analysis of these intensity fluctuations allows the determination of the diffusion coefficient and hence the particle size using the Stokes-Einstein relationship.[50]

Entry	Monomer	Total monomer content (g)	H_2O (mL)	D_h (nm)[a]		PDI[a]		10^{-14} (N_p/g^{-1})[b]		N_p/N_d
				Droplet	Nano particle	Droplet	Nano particle	Droplet	Nano particle	
P1[Ls]	St	6.00	24	136	129	0.132	0.032	1.84	2.15	1.17
P2[Ss]		0.25	10	156	137	0.150	0.178	0.124	0.184	1.48
P3[QDs]		0.25	10	150	154	0.105	0.102	0.140	0.129	0.92
P4[Ls]	4-VBA	3.00	12	119	112	0.085	0.083	2.66	3.19	1.19
P5[Ss]		0.30	10	168	146	0.123	0.290	0.109	0.166	1.52
P6[QDs]		0.30	10	130	124	0.143	0.186	0.235	0.271	1.15
P7[Ls]	4-VBA-St (1:4)	3.00	24	106	93	0.187	0.070	3.54	5.24	1.48
P8[Ss]		0.25	10	164	142	0.173	0.364	0.102	0.157	1.54
P9[QDs]		0.25	10	102	96	0.099	0.166	0.399	0.479	1.20

[a] Determined by dynamic light scattering (DLS).
[b] N_p or N_d are the number of particles or droplets per gram of water calculated from the diameter measured by DLS.

Table 2.1 Total monomer content, hydrodynamic mean droplet/particle diameter (D_h) and polydispersity index (PDI) for a series of miniemulsions. [**Ls**] indicates a large-scale polymerization, [**Ss**] indicates a smaller scale polymerization and [**QDs**] indicates a small-scale polymerization in the presence of silicon quantum dots. N_p/N_d is the ratio of number of particle over number of droplet. The concentration of surfactant, costabilizer and initiator used in the formulation are 0.01 M, 0.05 M and 0.02 M respectively.

It has to be mentioned that for the effective encapsulation of inorganic species by miniemulsion polymerization, it is important for the particles to be produced predominantly by polymerization of droplets. This requirement arises because the distribution of inorganic species in the particles will then reflect their distribution in the monomer solution, which is likely to be highly uniform. Therefore, DLS measurement of the ratio N_p/N_d is an important criterion on the quality of the encapsulation. Briefly, the number of particles per gram of water for either droplets or polymer nanoparticles (N_d or N_p) can be calculated from the average diameter of monomer droplets or polymer nanoparticles obtained from DLS according to equation (1) [51]:

$$N_p = \frac{W_m\left[\rho_m X_f + \rho_p\left(1 - X_f\right)\right]}{\frac{\pi}{6} D_p^3 W_w \rho_m \rho_p} \quad (1)$$

where W_m and W_w are the initial monomer weight and total weight of water respectively, ρ_m and ρ_p indicate the monomer density and polymer density, X_f is the final fractional conversion of monomer and D refers to the mean diameter of particles or droplets. X_f was obtained by weighing the dry mass of pure polymer. The mass of dissolved monomer is insignificant and all monomers are assumed to be presented as droplets. The masses of surfactant and costabilizer are also insignificant and are not included in the calculation. It should be noted that N_p is the particle number after polymerization (and therefore includes a small contribution from the unpolymerized monomer), whilst N_d is the particle number before polymerization and includes only the droplets. Typical values of X_f were ~0.8 and therefore the value of N_p is assumed to be dominated by the polymerized particles formed either by droplets nucleation or particles formation by homogenous nucleation of unreacted monomer. It worth pointing out that the number of particles (N_p) is based on the assumption that there is no contribution from SiQDs and no change of emulsion volume other than due to polymerization.

The N_p/N_d ratios calculated from equation (1) provide further information regarding the mechanism of droplet and micellar nucleation in this miniemulsion system. If the ratio of N_p/N_d is around unity, the mechanism of particle nucleation is primarily based upon on the radical entry into the droplets, and every droplet which is nucleated will lead to the formation of one particle. Values of N_p/N_d lower than unity suggest incomplete droplet nucleation has occurred. However, if higher values of N_p/N_d indicate that the micellar/ homogenous nucleation occurred because one droplet can feed monomer to more than one micellar nucleation particle, as likely often happens in conventional emulsion polymerization.[51]

From Table 2.1, it can be seen that “large” scale miniemulsion polymerizations (**P1[Ls]**, **P4[Ls]** and **P7[Ls]**) utilizing 3.00 g or 6.00 g of total monomer content produced polymer nanoparticles with mean diameters between 90 nm – 130 nm and with narrow PDIs in a range of 0.03 – 0.08. The N_p/N_d ratio for the polymer nanoparticles prepared were near to unity for entries **P1[Ls]** and **P4[Ls]**, which suggests that in these two instances the particles were formed predominantly by droplet nucleation.[52] However, under conditions where the total monomer content and volume of emulsion were scaled down by factors of 24 and 2.4 respectively (factor of 10 and 1.2

in the case of 4-VBA monomer), it becomes more difficult to control the polymer nanoparticle size and the breadth of their particle size distributions increased. The PDI of the polymer nanoparticles obtained from the "small scale" polymerizations (**P2[Ss]**, **P5[Ss]**, and **P8[Ss]**) showed broader size distributions, and the particle size also increased. According to the miniemulsion formulation employed here, the surfactant-to-monomer ratio, S (weight ratio of SDS to monomer) is 0.012, which is known to be below critical micelle concentration (CMC).[48] Therefore the higher values of N_p/N_d are not generated by micellar nucleation, but most likely due to particle coagulation which is presumably related to the low surface coverage of surfactant and hence broadening the particle size distribution.

Interestingly, the particle size distribution of the polymer nanoparticles which encapsulated SiQDs (**P3[QDs]**, **P6[QDs]**, and **P9[QDs]**), prepared at essentially similar total monomer content to the "small" scale polymerizations in the absence of SiQDs (**P2[Ss]**, **P5[Ss]** and **P8[Ss]**), showed narrower size distributions, as indicated by the PDI values between 0.10 – 0.19, and with particles sizes in a range of approximately 90 – 150 nm. In addition, the ratio of N_p/N_d is near unity for all polymers encapsulating SiQDs (**P3[QDs]**, **P6[QDs]**, and **P9[QDs]**), which also indicates particle nucleation is primarily by radical entry into the droplets. The presence of SiQDs in the miniemulsion system also appears to result in a decrease of the mean particle diameters of the resulting polymer nanoparticles. These observations suggest that traces of unreacted 1–undecene, leftover from the hydrosilylation process used to prepare SiQDs, acts as a co-stabilizer and helps to improve the stability of the miniemulsion system. To further support this hypothesis, a simple control experiment was performed. A "small" scale miniemulsion polymerization of St in the presence of 1-undecene (10 µL) was prepared. The sizes of monomer droplets and their resulting polymer nanoparticles are 88 nm and 85 nm, with narrower PDIs of 0.084 and 0.188 (as determined by DLS), respectively. Importantly, the ratio N_p/N_d was found to be near unity, which is comparable with the samples of all polymer nanoparticles encapsulating SiQDs (**P3[QDs]**, **P6[QDs]**, and **P9[QDs]**). It was clearly presented that by scaling down the volume of miniemulsion system, the PDI of the polymer nanoparticles is broadened, but can be improved by incorporation of SiQDs within polymer nanoparticles.

2.3.4 *Morphology Study and Particle Size Characterization by Atomic Force Microscopy*

A selection of polymer nanoparticles were analysed further by atomic force microscopy (AFM) in order to provide topographical information and to afford further insight into their sizes and size distributions. AFM is a Scanning Probe Microscopy (SPM) technique which was invented in 1986 by Binning et al.[53] In principle, AFM measures the surface morphology and properties through an interaction of the forces between a fine tip and a surface. This probing tip is supported on a flexible cantilever and is brought very close to the surface of the sample. Response to the attractive or repulsive forces between the tip and surface will produce a positive or negative bending of the cantilever. This bending phenomenon is detected using a laser beam which is reflected from the back side of the cantilever onto a photodiode. AFM images are scanned relative to the probing tip, digitizing the deflection of the cantilever or the Z movement of the piezo as a function of the lateral position x, y.[54] There are three primarily modes in AFM, namely, contact mode (< 0.5 nm probe-surface separation), tapping mode (0.5 – 2 nm probe-surface separation) and non-contact mode (0.1 – 10 nm probe-surface separation). Tapping mode AFM has been utilized in this research project to obtain the analysis of nanoparticle morphology and the sizes and sizes distribution of the polymer nanoparticles. In tapping mode AFM, the cantilever oscillates close to its resonance frequency. An electronic feedback loop ensures that the oscillation amplitude remains constant, and as a consequence, a constant tip-sample interaction is maintained during scanning.[55]

Figure 2.3 shows the tapping mode AFM images obtained from a series of polymer nanoparticles which encapsulate SiQDs (**P3[QDs]**, **P6[QDs]** and **P9[QDs]**). These images indicate that most of the polymer nanoparticles appear as prolate spheroids, probably as a consequence of particle-surface interactions and also on account of the tip, which does not track the topography perfectly. The poor AFM image obtained from **P9[QDs]** (Figure 2.3c) suggests an irregular mica surface, which may have occurred during the cleaning process to remove its top layer. The mean height of the polymer nanoparticles in the AFM images of **P6[QDs]** were calculated from an average of 50 polymer nanoparticles, showing the mean height was 114 ± 8 nm (mean ± standard deviation), which is slightly smaller than the hydrodynamic diameter obtained from DLS (124 ± 2 nm). This observation suggests that the particles are slightly deformed upon interaction with the mica substrate.

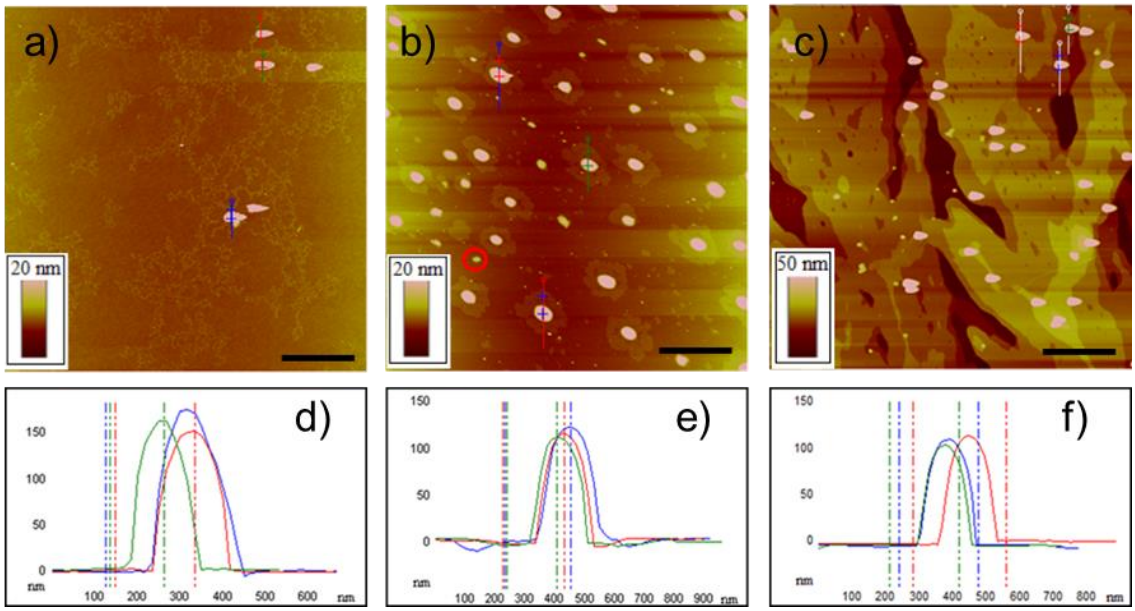

Figure 2.3 TappingMode AFM height images of (a) **P3[QDs]** (scan size = 8.5 μm), (b) **P6[QDs]** (scan size = 10 μm), (c) **P9[QDs]** (scan size = 6.5 μm); scale bar = 1 μm and cross sections of samples (d) **P3[QDs]**, (e) **P6[QDs]**, (f) **P9[QDs]**. Cross sections of interesting features were obtained by using the image analysis software of the microscope to acquire numerical topographical information.

Previously, it has been reported[56] that AFM provides systematically smaller mean diameters than DLS for polystyrene nanoparticles. It has to be noted that the appearance of small spheres (red circles) in Figure 2.3b is attributable to aggregates of SDS/ hexadecane, which are likely to be present in the samples. Furthermore, the polymer composite nanoparticles of **P3[QDs]** and **P9[QDs]** displayed average mean heights around 153 nm and 118 nm, respectively, which are consistent with the mean diameter obtained from DLS. In general, a reasonable agreement on mean particle diameter was obtained between AFM measurements and DLS, and these observations suggest polymer nanoparticles encapsulating SiQDs can be prepared with good control of particle sizes and size distributions.

2.3.5 *Luminescence (Epifluorescence) Microscopy*

Luminescence (epifluorescence) microscopy was used to monitor the luminescence and dark field scattering of the polymer nanoparticles prepared in the presence and absence of SiQDs. This technique involves the irradiation of the specimen with light of specific wavelength, and the much weaker emitted light (fluorescence) being separated from the excitation light, thus resulting in a fluorescent image, and the objects which are non-fluorescent, such as the background, remain dark.[57]

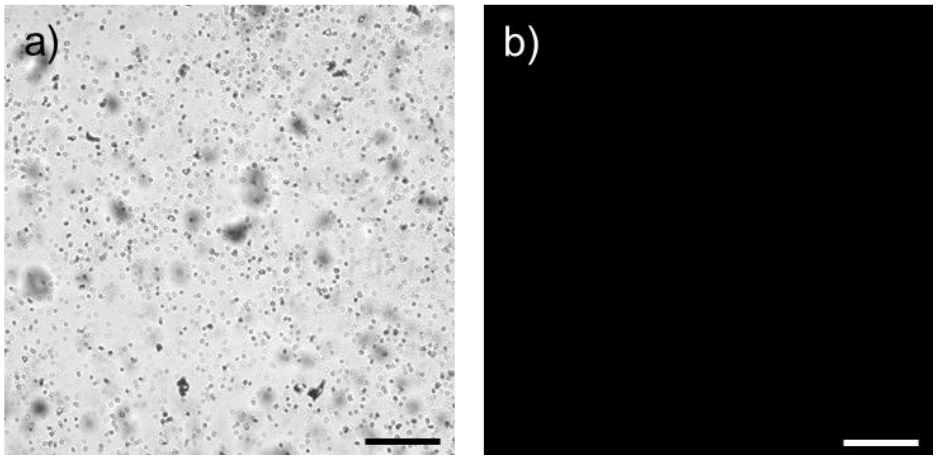

Figure 2.4 (a) Ordinary image and (b) fluorescence image of **P2[Ss]** at exposure times of 50 ms and 4598 ms respectively; scale bar = 100 μm.

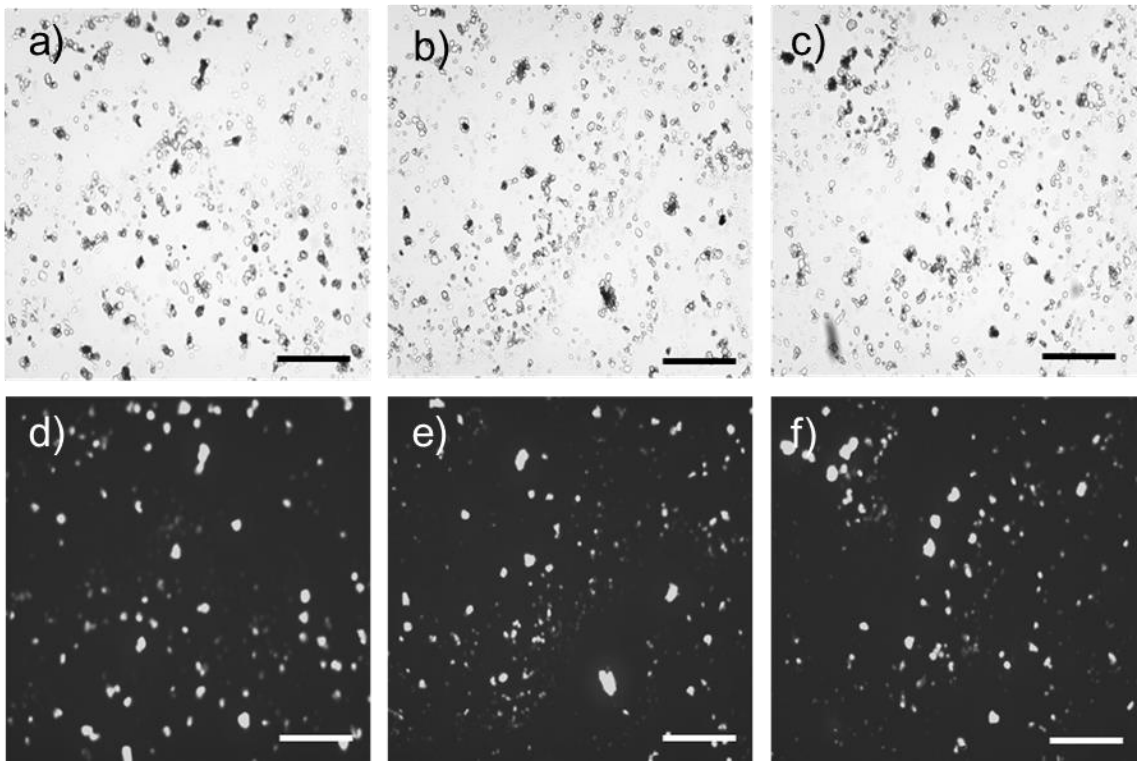

Figure 2.5 The ordinary images of (a) **P3[QDs]**, (b) **P6[QDs]** and (c) **P9[QDs]** at exposure times of 97 ms, 50 ms, and 2 ms, respectively, and the corresponding luminescence images of (d) **P3[QDs]**, (e) **P6[QDs]** and (f) **P9[QDs]** at exposure times of 4896 ms, 1498 ms and 1945 ms, respectively. Scale bar = 100 μm.

No luminescence effects were observed from the sample of polymer nanoparticles prepared in the absence of SiQDs (**P2[Ss]**, **P5[Ss]** and **P8[Ss]**) as shown from the fluorescence image of **P2[Ss]** (Figure 2.4b). In contrast, the luminescence images of all polymer nanoparticles containing encapsulated SiQDs (**P3[QDs]**, **P6[QDs]** and **P9[QDs]**) (Figure 2.5) show the existence of bright spots, confirming that the luminescence originates from the SiQDs and not from the polymer nanoparticles

themselves. In a previous study,[19] the quantum efficiency of the luminescence of SiQDs in organic solvents has been reported, and although there is not a marked variation, toluene was found to possess one of the highest efficiencies and therefore polystyrene, which possesses structured similarities with toluene can also be expected to present an environment where bright luminescence of SiQDs is observed.

Although there is variation in the brightness of the features in Figure 2.5 (d – f) as a consequence of some aggregation, it is clear that all the polymer nanoparticles observed in the optical image (Figure 2.5 a – c) emit luminescence. It may possible that there are some polymer nanoparticles that do not contain luminescent SiQDs. However, because alkylated SiQDs are essentially insoluble in water, their encapsulation efficiency can be estimated on the basis that it should be similar to the conversion efficiency of the polymerization, *i.e.*, approximately 80%.

2.3.6 *Confocal Microspectroscopy*

Confocal microspectroscopy studies were then performed to investigate the Raman and luminescence spectra of those polymer nanoparticles without SiQDs (**P2[Ss]**, **P4[Ss]** and **P6[Ss]**) and those which contained SiQDs (**P3[QDs]**, **P6[QDs]** and **P9[QDs]**). Confocal microspectroscopy is a type of optical microscopy pioneered by Marvin Minsky in 1955, who built a working microscope with the aim of scanning neural networks in unstained preparations of living brains.[58] This microscopy technique is based upon the ideas of point-by-point illumination of the specimen and rejection of out-of-focus information by the existence of a pinhole in front of the detector. As a result, less haze, better contrast and sharply focused images can be obtained as compared to conventional microscopes. The image formation in confocal microspectroscopy is fundamentally different from conventional wide-field microscope, where the source of light is mercury/ xenon lamp and the image can be viewed directly by eye. In contrast, the illumination in a confocal microscope is achieved by scanning one or more focused beams of light using a laser light source.

In this work, the sample was examined at an excitation wavelength of 488 nm supplied by an Ar ion laser and the scattered/ emitted light was dispersed on a grating of 150 lines mm^{-1} to obtain a broad spectral range covering both luminescence and Raman features of interest. Figure 2.6 (a – c) shows a reflected light (dark field) image and confocal luminescence images of the samples of polymer nanoparticles containing SiQDs (Figure 2.6d – f) drop cast onto a glass cover slip. The bright features obtained

from the confocal luminescence images of polymer nanoparticles encapsulating SiQDs (Figure 2.6d – f) are not obtained in the samples prepared in the absence of SiQDs (Figure 2.6f inset). This observation confirms the presence of SiQDs, which are encapsulated inside or associated with the polymer nanoparticles. It was clearly observed that the aggregates in Figure 2.6 arise on account of the drying process during sample preparation for microscopy, and they do not reflect the actual aggregation state of polymer nanoparticles in dispersion, where no aggregation was confirmed from DLS characterization.

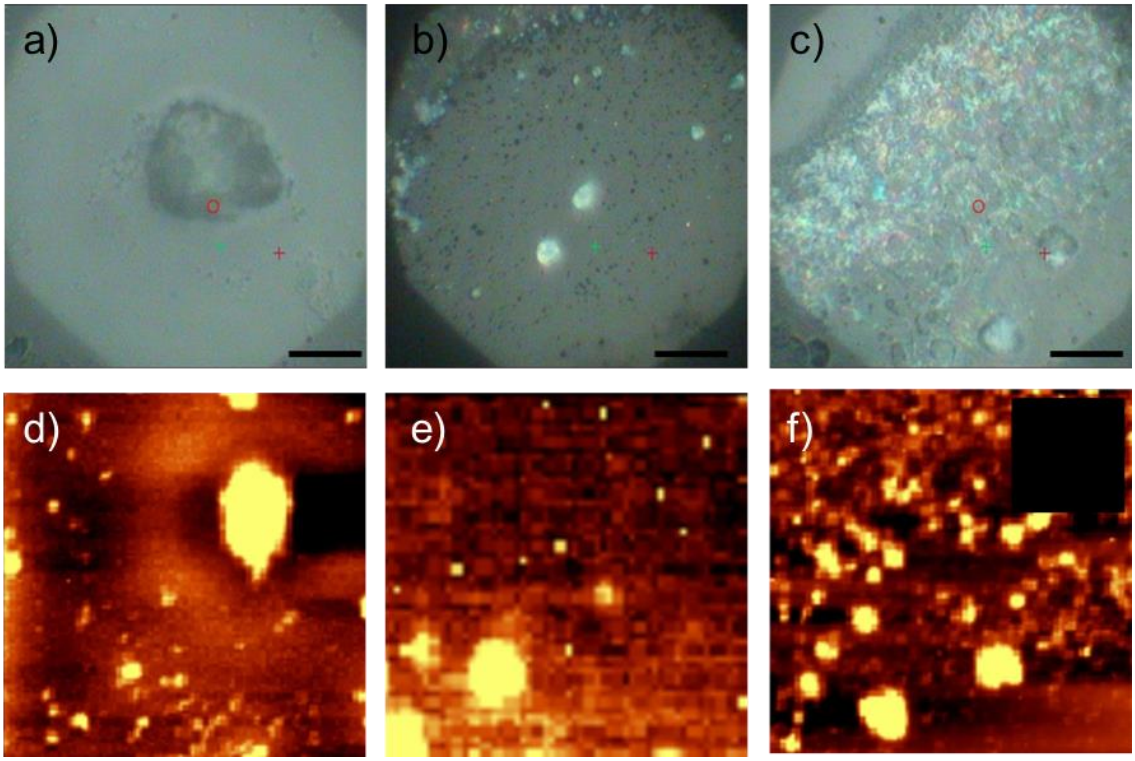

Figure 2.6 Reflected light images of (a) **P3[QDs]** (b) **P6[QDs]** (c) **P9[QDs]** acquired prior to the confocal luminescence spectrum images of (d) **P3[QDs]** (e) **P6[QDs]** (f) **P9[QDs]**. Inset is a control confocal luminescence spectrum image of **P2[Ss]**, black square, top right corner of the confocal luminescence spectrum image of **P9[QDs]**): in both cases the colour scale represents the integral of the spectral intensity from a Raman shift of 200 cm^{-1} to 7000 cm^{-1}, which corresponds to a mixture of luminescence and Raman signals which are analysed below. In order to facilitate direct comparison, the colour scale of the inset is set equal to that of the main image and appears entirely dark because of the weakness of the Raman scattering. The polymer nanoparticle samples were purified by dialysis and drop cast on a glass cover slip. Scale bar on the reflected light image = 10 μm and scan size of luminescence images = 50 x 50 μm.

The combination of these bright features (corresponding to individual and aggregates of polymer nanoparticles) affords average Raman spectra of polymer nanoparticles which show Raman bands corresponding to the aromatic and alkyl C–H groups present in **P3[QDs]**, **P6[QDs]** and **P9[QDs]** (Figure 2.7). An additional weak

signal corresponding to the carbonyl from the aromatic aldehyde functions was observed from the polymer nanoparticles samples of **P6[QDs]** and **P9[QDs]**. In the Raman region the spectrum was expressed as a sharp peak observed at 3500 cm^{-1} and below. In Raman spectroscopy, polar functional groups, such as carbonyl, amine and amides are weak, however, –S-S–, –SH, –CN, –C=C groups and aromatic rings display strong individual Raman signals.[59] The large and broad peak present in the spectra of **P3[QDs]**, **P6[QDs]** and **P9[QDs]** (Figure 2.7b – d) is attributable to the luminescence signals from SiQDs, which are incorporated inside or upon the surface of the polymer nanoparticles. The Raman peaks around 3070 – 3000 cm^{-1} correspond to aromatic C–H stretching associated with the polystyrene matrix of **P3[QDs]**, **P6[QDs]** and **P9[QDs]** polymer nanoparticles (Figure 2.7b – d). The signal at approximately 2833 – 2886 cm^{-1} was attributed to aliphatic C–H stretching modes, while the signal around 1616 cm^{-1} corresponds to the aromatic C–C region of the polymer nanoparticles. A weak signal around 1695 – 1714 cm^{-1} corresponding to the carbonyl group was presented for the samples **P6[QDs]** and **P9[QDs]** (Figure 2.7c – d).

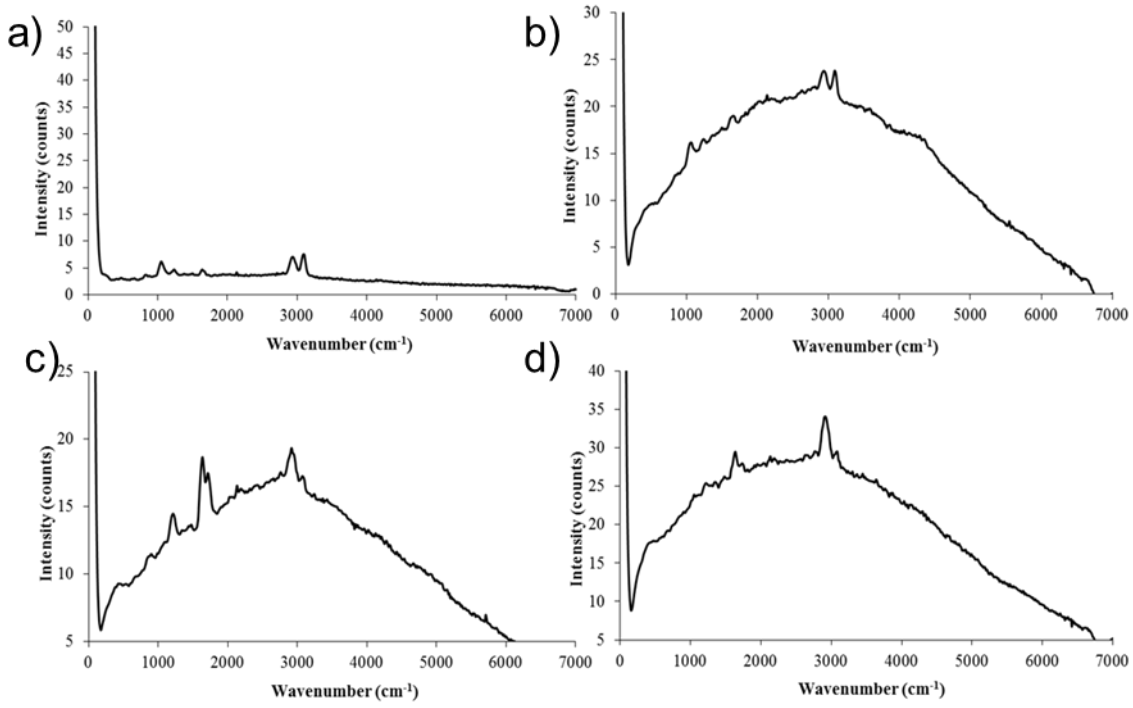

Figure 2.7 Average luminescence/Raman spectra of (a) **P2[Ss]** (b) **P3[QDs]** (c) **P6[QDs]** and (d) **P9[QDs]** polymer nanoparticles dispersed in 2.47mM[60] aqueous SDS solution of and drop cast onto glass cover slips for observation by confocal microspectroscopy (excitation wavelength, λ = 488 nm). The higher intensity peak at 0 cm^{-1} is the elastically scattered laser light. These spectra were obtained as averages over the particles identified in images such as presented in Figure 2.6 (d – f).

To further confirm the encapsulation of SiQDs inside polymer nanoparticles, the spectra were also obtained from polymer nanoparticle samples which do not encapsulate SiQDs. The mean luminescence/Raman spectrum of **P2[Ss]** (Figure 2.7a) shows significant Raman peaks for aromatic and alkyl vibration modes, but no luminescence was observed. This control experiment confirmed that the pure polymer nanoparticles do not show any luminescence and therefore the luminescence in the polymer nanoparticles encapsulating SiQDs samples are dominantly from SiQDs. The observation of both sharp Raman signals corresponding to the polymer together with the broad luminescence peak from SiQDs suggest strongly that the SiQDs are indeed encapsulated within or upon the surfaces of the polymer nanoparticles.

2.3.7 *Stability of Encapsulated SiQDs inside Polymer Nanoparticles*

Confocal microspectroscopy demonstrated that SiQDs are encapsulated inside or upon the polymer nanoparticles, but does not allow us to determine if the SiQDs are buried deep inside the polymer nanoparticles or if they are distributed at or near the surface. Transmission electron microscopy (TEM) studies were inconclusive because the scattering factor of Si is not sufficient to provide good contrast with the polymer. Therefore, an investigation of the luminescence SiQDs decay upon exposure to aqueous alkali was conducted.

It is well reported that SiQDs prepared in our laboratory are capped with 11-carbon monolayer and are thus very stable against corrosion by water and are resistant to oxidation under ambient conditions. SiQDs dispersions can retain bright orange luminescence under UV light (λ = 365 nm) and no flocculation was monitored over a time period of several months.[43] These suspensions can also retain their luminescence upon addition of strong acid (1 M HCl), but the bright orange luminescence of SiQDs can be destroyed completely in alkaline media (1 M NaOH). This treatment will lead to destruction of the luminescence SiQDs if they are on the surface of the polymer nanoparticles. In contrast, if the SiQDs are located inside the polymer nanoparticles, the luminescence should be lost at a much slower rate as the polymer shell will shield the SiQDs from the destructive influence of the alkaline media.

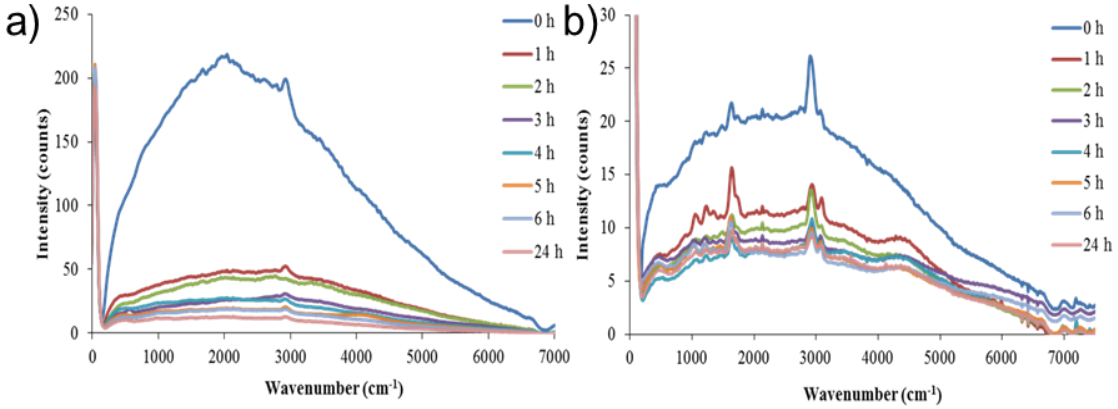

Figure 2.8 Average luminescence/Raman spectra of (a) alkylated SiQDs and (b) **P9[QDs]** nanoparticles before and after treatment with 0.02 M NaOH solution over a period of 24 h.

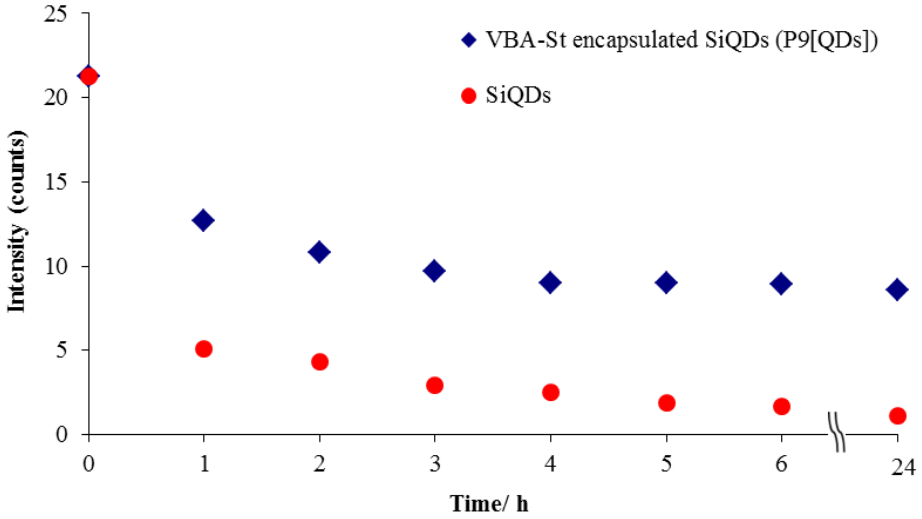

Figure 2.9 Luminescence intensity of (unencapsulated) alkylated SiQDs and **P9[QDs]** nanoparticles (at maximum wavelength) at different times of exposure to 0.2 mL of 0.02 M NaOH solution. The intensity of luminescence for the unencapsulated alkylated SiQDs has been normalized so that it matches the luminescence intensity of the **P9[QDs]** nanoparticles at t = 0.

Figure 2.8a shows the luminescence spectra of bare alkylated SiQDs before and after 24 h exposure to 0.02 M aqueous NaOH solution, which is known to dissolve SiQDs and cause their luminescence to diminish, as confirmed from visibly observing the sample under UV light (λ = 365 nm).[19] A massive decline in luminescence intensity (76 %) for bare alkylated SiQDs is observed after treatment with alkaline NaOH solution after only 1 hour of exposure. A comparison was then obtained with the polymer nanoparticles encapsulating SiQDs (**P9[QDs]**). Interestingly, a drop of 60 % of photoluminescence intensity is observed for sample (**P9[QDs]**) (Figure 2.8b) when exposed to the same concentration of NaOH solution. This observation, whereby ~40% of the luminescence is retained, suggests that at least some of the SiQDs are indeed

encapsulated within the polymer shells, which shield them from attack by alkaline media.

The graph of luminescence intensity selected at ma ximum wavelength of both bare alkylated SiQDs and **P9[QDs]** over different exposure times was plotted (Figure 2.9) to obtain a clearer relationship on the decay of photoluminescence intensity upon exposure to 0.02 M NaOH solution. Bare alkylated SiQDs display a rapid drop (76%) in luminescence intensity after 1 h treatment with 0.02 M NaOH. After 24 h, the luminescence intensity had dropped by 95% of its initial value. In comparison, sample **P9[QDs]** displays an approximate reduction of 38% in luminescence intensity after 1 h exposure to alkaline media, probably on account of accessible SiQDs on or near the surface of polymer nanoparticles being corroded by the alkaline solution. Surprisingly, even after 24 h a substantial fraction (40%) retain their luminescence suggesting that these SiQDs are buried sufficiently deeply within the polymer nanoparticles to be protected from the alkaline solution. This simple chemical test suggests that 40% of encapsulated SiQDs are located deep within the polymer nanoparticles and demonstrates that encapsulation greatly increases the stability of SiQDs to attack by alkaline reagents such as aqueous NaOH. Similar observations were demonstrate for the samples of **P3[QDs]** and **P6[QDs]**. Figure 2.10a – b indicates a drops in photoluminescence intensity of around 39% and 40% for **P3[QDs]** and **P6[QDs]** respectively after 24 h treatment with 0.02 M NaOH solution, an observation which again suggests at least some SiQDs are encapsulated deep inside polymer nanoparticles, shielding them from attack by NaOH solution.

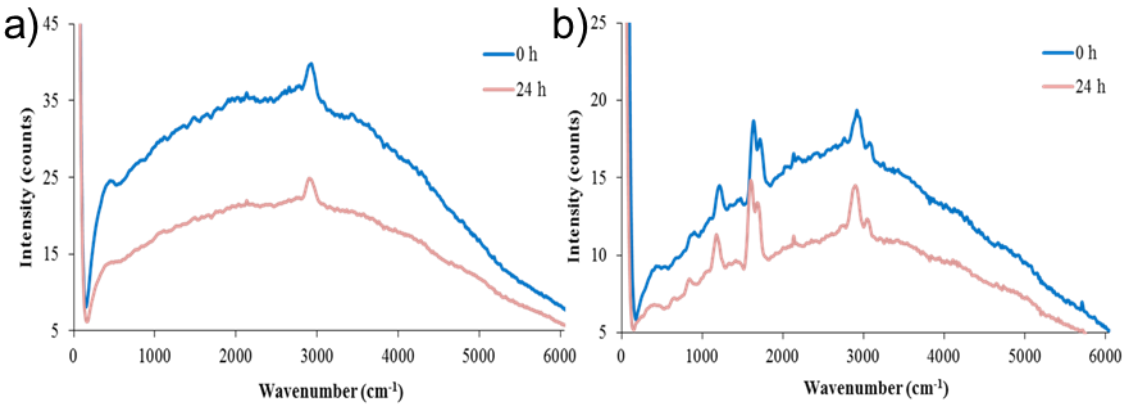

Figure 2.10 Average luminescence/Raman spectra of (a) **P3[QDs]** and (b) **P6[QDs]** nanoparticles before and after treatment with 0.02 M NaOH solution over a period of 24 h.

2.3.8 *Conjugation Studies on Aldehyde-Functionalized Polymer Nanoparticles*

The functionalization of the surfaces of polymer nanoparticles is of interest as it can increase the usefulness of the polymer nanoparticles in applications. It was therefore decided to investigate the decoration of the surfaces of polymer nanoparticles **(P8[Ss])** possessing reactive aldehyde groups through imine, oxime or hydrazone formation (Scheme 2.4).

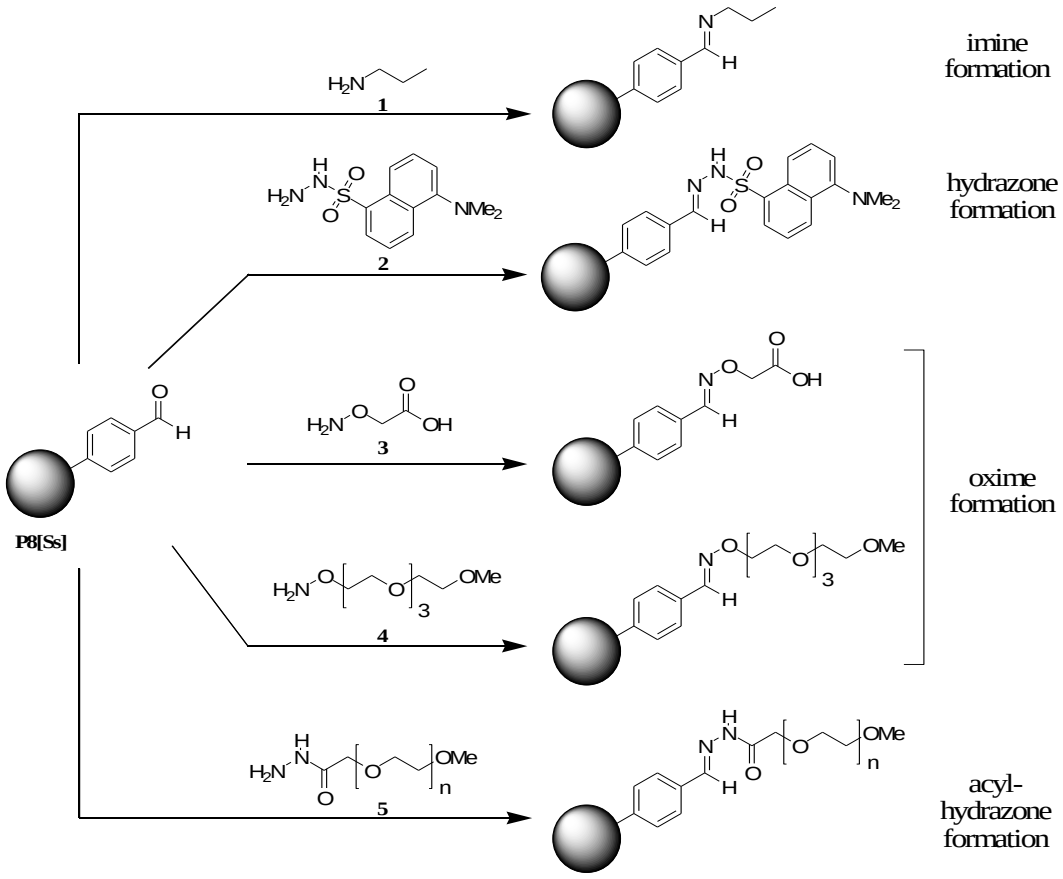

Scheme 2.4 Schematic of various conjugation studies of **P8[Ss]** with amine, dansyl hydrazine, alkoxyamine and PEG derivatives.

Initially, the copolymerization of 4-VBA and St prepared via miniemulsion polymerization was performed in the ratios 1:4, 1:20, 1:40 and 1:60 in order to obtain differing amounts of aldehyde groups onto the surface of polymer nanoparticle which could then be utilized in the conjugations studies. The formation of 4-VBA-St polymer nanoparticles was confirmed by ^{1}H NMR and FTIR spectroscopies. From Figure 2.11a – b, it is clearly shown that when the ratio of St increased, the intensity of the aldehyde signals obtained from ^{1}H NMR (δ = 9.89 ppm) and FTIR (CHO band = 1710 cm^{-1}) becomes diminished. Copolymerization of 4-VBA and St at a ratio of 1:4 gives the most

intense signal in both ^{1}H NMR and IR spectra. Consequently, the conjugation studies of aldehyde functionalized polymer nanoparticles were performed using 4-VBA:St polymer nanoparticles prepared with monomer ratio of 1:4 (**P8[Ss]**).

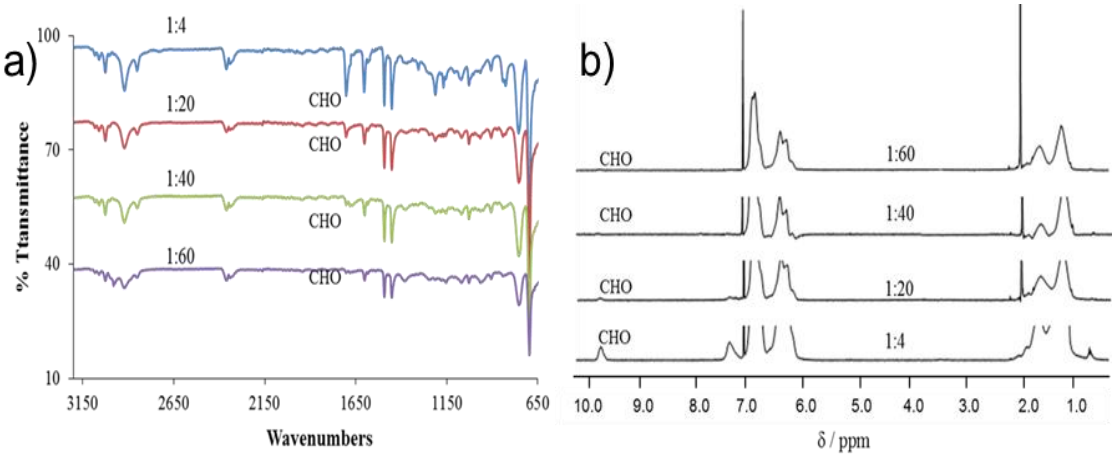

Figure 2.11 (a) FTIR spectra and (b) ^{1}H NMR (300 MHz, $CDCl_3$) of aldehyde functionalized polymer nanoparticles in the ratio of 1:4, 1:20, 1:40 and 1:60.

Propylamine (**1**) was chosen as a model compound for initial studies and the conjugation reaction (Scheme 2.4) was performed in chloroform with 1:1 equivalence by mass between **P8[Ss]** and 1-propylamine. After purification by dialysis, the ^{1}H NMR spectrum of the conjugate displayed a signal corresponding to the imine proton at δ = 8.20 ppm, which confirmed the success of the conjugation. The conjugation studies were further explored using hydrazine derivatives, which conjugate to the polymer nanoparticle through the formation of hydrazone bonds. Dansyl hydrazine (**2**) was chosen, as this molecule has been widely used as UV light-excitable fluorophore, especially in chromatographic analysis.[56] The conjugation of **P8[Ss]** with dansyl hydrazine (**2**) was performed in THF with a 1:1 ratio by mass of dansyl hydrazine and **P8[Ss]**, and the successful formation of the hydrazone bond (δ = 8.68) was confirmed by ^{1}H NMR spectroscopy (Figure 2.12a). The conjugation product was also confirmed using UV-Vis spectroscopy, which displayed a small red shift ~5 nm from 340 nm to 345 nm for the maximum absorption peak, evidence which suggests that the dansyl dyes are in close proximity to one another as they would expect to be conjugated onto a surface of aldehyde functionalized polymer nanoparticles (Figure 2.12b).

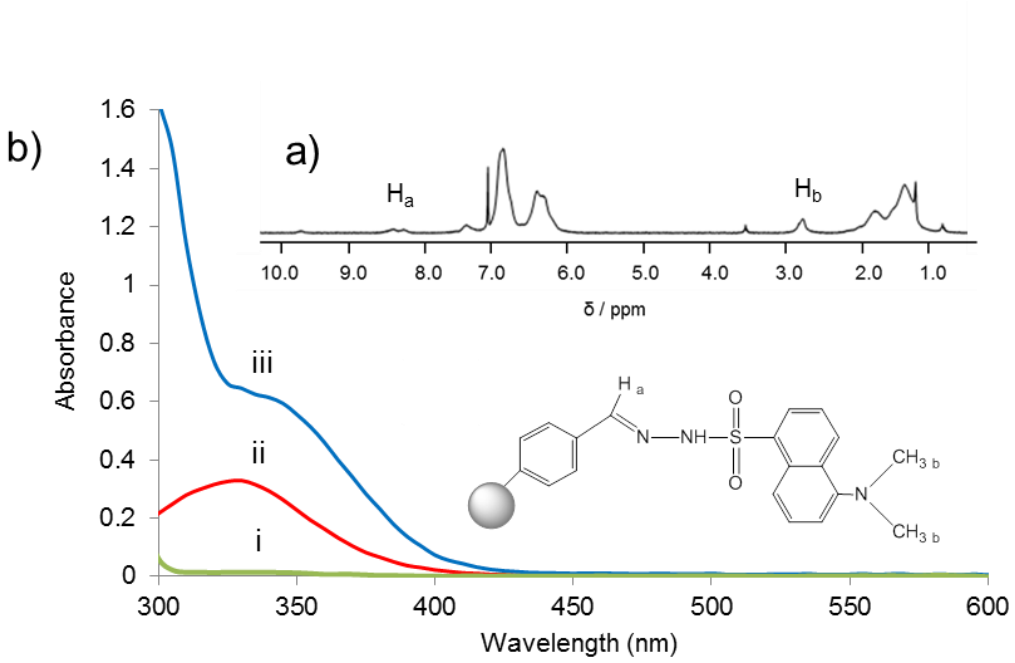

Figure 2.12 (a) ^{1}H NMR (300 MHz, $CDCl_3$) and (b) UV-Vis spectrum of the conjugation product of dansyl hydrazine with **P8[Ss]** where (i) VBA-St polymer nanoparticle; (ii) dansyl hydrazine and (iii) conjugated polymer nanoparticle respectively.

Conjugation through the formation of oxime bonds (Scheme 2.4) was further investigated using the alkoxyamine *O*-(carboxymethyl) hydroxylamine hemihydrochloride (**3**), where it was hoped its successful conjugation would impart water dispersity upon the polymer nanoparticles. The reaction was performed in a mixed solvent of $CHCl_3$ and MeOH (1:1 v/v) with 1:1 equivalence by mass of the alkoxyamine and **P8[Ss]**. ^{1}H NMR spectroscopy revealed a signal for the oxime proton at δ = 8.18 ppm, indicating the formation of the oxime bond. Unfortunately, the carboxylic acid groups adorned on the surface of the polymer nanoparticles did not impart the expected water dispersity upon the polymer nanoparticles. The possible explanation for this observation maybe attribute to the hydrophobic PS core, and also on account of the fact that the majority of aldehyde groups are probably contained inside the polymer core. To broaden the conjugation studies of **P8[Ss]**, the conjugation of a water soluble polyethylene glycol (PEG) derivative was investigated. PEG is a non-toxic, biocompatible, water-soluble polymer, and thus a potentially useful polymer to attach to the surfaces of the aldehyde-functionalized polymer nanoparticles should they be further developed as probes in biological processes. Furthermore, PEG is also the gold standard stealth polymer in drug delivery applications.[61] The conjugation was observed initially by using tetra-polyethylene glycol (**4**), a small molecule derivative of PEG containing a reactive alkoxyamine function at its terminus. The conjugation was

performed in $CHCl_3$ with a ratio of 1:1 by mass of **4** and **P8[Ss]**. After purification, ^1H NMR spectroscopy revealed a signal at δ = 8.08 ppm corresponding to the oxime proton, which indicates successful conjugation had occurred.

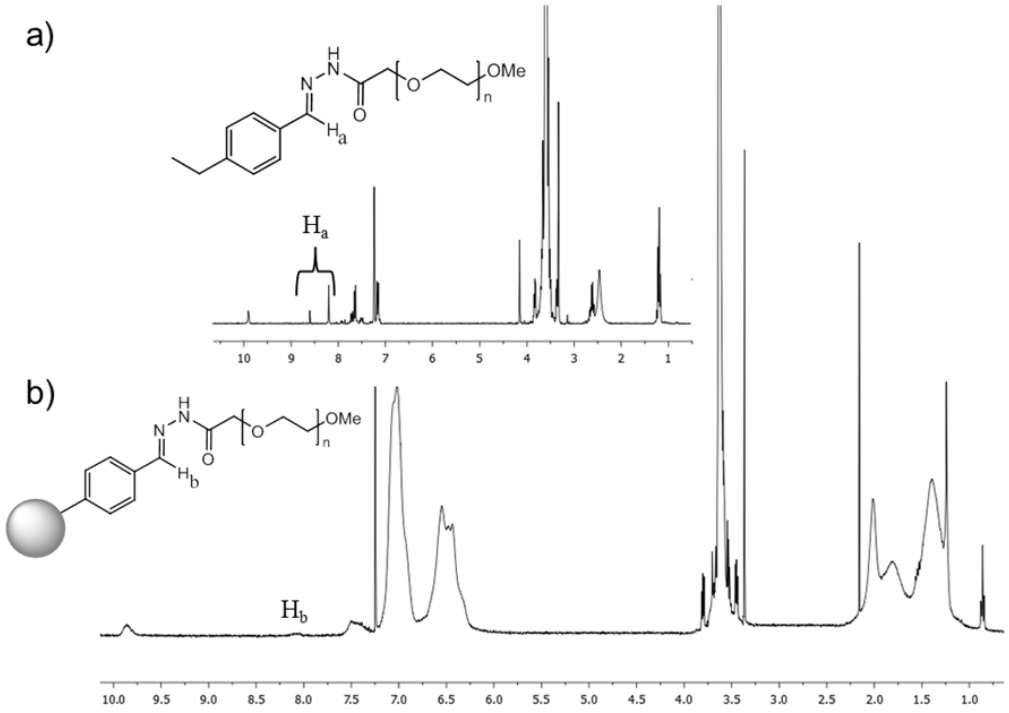

Figure 2.13 ^1H NMR (300 MHz, $CDCl_3$) spectra of (a) conjugated 4-ethyl benzaldehyde and (b) **P8[Ss]** with PEG hydrazide (**5**) (M_W = 5 kDa).

The conjugation of a commercial 5 kDa polyethylene glycol hydrazide (**5**) was then accomplished. To confirm the effectiveness of the conjugation with this PEG derivative, the reaction was initially investigated using a model reaction of **5** with a small aldehyde molecule, 4-ethyl benzaldehyde. It was noted that the reaction was complete overnight, as determined by the reduction in intensity of the aldehyde signal at δ = 9.98 ppm, and the formation of signals corresponding *cis* and *trans* hydrazine peaks observed at δ = 8.18 ppm and δ = 8.56 ppm, respectively (Figure 2.13a). The conjugation of **5** was then further investigated with **P8[Ss]** and the reaction was performed in $CHCl_3$ with a 1:1 equivalence by mass of **P8[Ss]** and **5**. In contrast to the other conjugation reactions, the conjugation of **5** onto the polymer nanoparticle surface was slow, taking several days to complete. The ^1H NMR spectrum (Figure 2.13b) of this conjugation shows an intense signal corresponding to the aldehyde proton and a very small signal corresponding to the hydrazone proton around δ = 8.18 ppm. Although this reaction was continued for a further several days, the intensity of the hydrazone signal did not change. In all of the conjugation studies described here, there was always a

significant ^{1}H NMR signal observed for the aldehyde functions, which is expected because the majority of aldehyde groups will be found inside of the polymer nanoparticles and are thus not available for conjugation.

The conjugation studies were then broadened to include aldehyde functionalized polymer nanoparticles encapsulating SiQDs (**P9[QDs]**). The conjugation was performed using PEG hydrazide (M_W = 5 kDa) (**5**), and observations similar to those obtained from conjugation PEG hydrazide with aldehyde-functionalized polymer nanoparticles prepared in absence of SiQDs (**P8[Ss]**) were made. A very small signal corresponding to hydrazones proton (δ = 8.08) was observed, suggesting little conjugation occurred. On the other hand, a significant signal corresponding to aldehyde protons revealed the incomplete conjugation reaction which arises most likely on account of unreacted aldehyde groups within the core of the polymer nanoparticles. The particle sizes and particle size distributions (PDI) of the polymer composite nanoparticles of **P9[QDs]** conjugated with PEG hydrazide (**5**) were determined by DLS. In comparison, the particle size of the conjugated polymer composite nanoparticles was four times larger and with broader PDI (D_h = 386 nm and PDI = 0.25 respectively) than the particle size of **P9[QDs]** (D_h = 96 nm, PDI = 0.17). This observation was further supported by the DLS histogram of the polymer composite nanoparticles (Figure 2.14), which displays an apparent increase in the hydrodynamic diameter of the system. Two significant peaks between 90 nm and 450 nm were obtained, an observation which suggests that aggregation occurred between the conjugated polymer composite nanoparticles. Additionally, the conjugated polymer composite nanoparticles encapsulating SiQDs display bright regions of luminescence with a broad peak attributable to the fluorescence of SiQDs as characterized by confocal microspectroscopy (Figure 2.15).

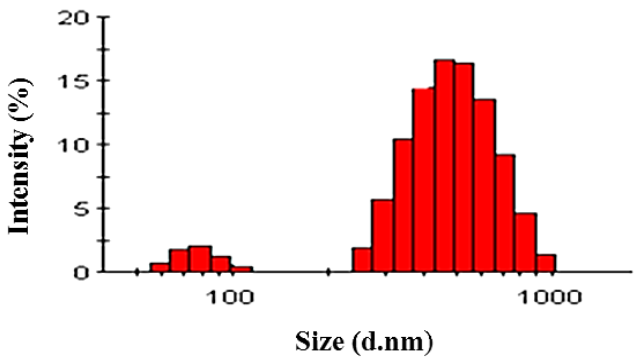

Figure 2.14 DLS histogram of particle sizes (diameters) of conjugated PEG hydrazide with **P9[QDs]**.

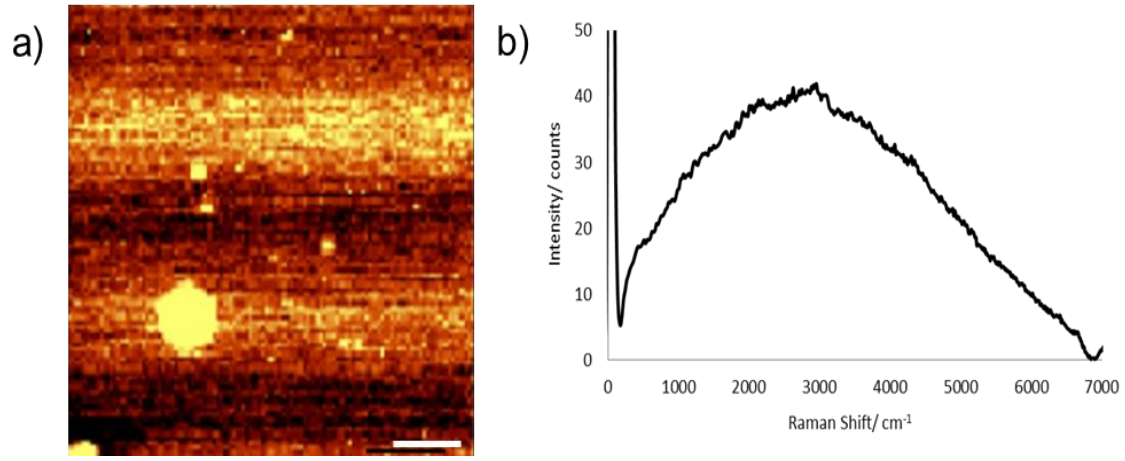

Figure 2.15 (a) The confocal luminescence spectrum images and (b) average luminescence/Raman spectra of conjugated PEG hydrazide with **P9[QDs]**.

We note that since the copolymer VBA-St polymer nanoparticles were dispersed in organic solvent for conjugation of aldehyde, there is a possibility that the conjugated polymer nanopaticles changed their morphology. However, since we observed SiQD luminescence from the conjugated polymer, we assume that the changes are minimal. These conjugation studies demonstrate that it was possible to successfully adorn the surface of aldehyde-containing polymer nanoparticles with a selection of organic molecules which may find further valuable applications in field such as in biological areas.

2.4 Conclusions

Miniemulsion polymerization of St or 4-VBA and mixtures of both monomers has been utilized to encapsulate luminescent SiQDs inside polymer nanoparticles. Dynamic light scattering and analysis of AFM images showed a narrow particle size distribution with mean particle diameters between 90 – 150 nm. Polymer nanoparticles prepared in the presence of SiQDs possessed narrower PDIs, which may attributed to a co-surfactant effect of the alkylated SiQDs or trace 1-undecene, which is likely to be present within the sample of SiQDs, improving the stability of the miniemulsion. An important feature of miniemulsion polymerization is that because the polymer nanoparticles are formed by polymerization of the monomer droplets rather than nucleation in solution, it is likely that the distribution of the SiQDs within the polymer nanoparticles will reflect the homogenous distribution of the SiQDs dissolved within the monomer phase. Microscopy experiments showed the polymer nanoparticles emit luminescence from encapsulated SiQDs. The luminescence and Raman spectra of polymer encapsulated

SiQDs were studied by confocal microspectroscopy, and the presence of SiQDs inside polymer nanoparticles was confirmed by the characteristic broad luminescence signal of SiQDs and the Raman signals corresponding to the polymer nanoparticles. To provide further evidence of encapsulation, chemical testing was performed to estimate the fraction of SiQDs buried deep inside the particles and therefore inaccessible to aqueous chemical reagents. About 40% of the luminescence of polymer encapsulated SiQDs (**P9[QDs]**) was retained after 24 h exposure to NaOH (aq) whereas 95% of non-encapsulated SiQDs luminescence was destroyed after 24 h. This observation suggests that 60% of the SiQDs are located on or near the surface of polymer nanoparticles and are destroyed by NaOH (aq), and 40% are deeply buried and protected. Furthermore, a similar observation was made with the sample of **P3[QDs]** and **P6[QDs]**, which showed a drop (~ 40%) of the luminescence after 24 hour treatment with alkaline media. To increase the scope and utility of the polymer nanoparticles, especially in possible biological applications, polymer nanoparticles displaying aldehyde functional groups upon their surfaces were also prepared via miniemulsion copolymerization of 4-VBA and St. It was shown that a number of organic molecules can be conjugated onto the surfaces of these polymer nanoparticles through the formation of imine, oxime and hydrazone bonds. However, one limitation of this conjugation system is that water disperse composite polymer nanoparticles could not be obtained by conjugating hydrophilic molecules such as PEG. This disappointing outcome may be attributable to the limited number of active aldehyde groups upon the surface of polymer nanoparticles, resulting in limited conjugation of the molecules onto polymer nanoparticles surface. We expect that with engineered polymer polymer-encapsulated SiQDs, together with methods to further functionalize the surface of these polymer nanoparticles, new chemical or spectroscopic probes can be synthesized using the convenience and control of miniemulsion polymerization.

2.5 Experimental

All chemicals were purchased from Sigma Aldrich or Alfa Aesar and were used as received without further purification. Styrene and vinylbenzaldehyde[62] were kept refrigerated until use and distilled under high vacuum before use. Water was deionized before use (nominal resistivity 18 MΩ cm, Nanopure purification system, Barnstead). Membranes for purification of polymer nanoparticles by dialysis were obtained from

Spectrum Laboratories (Spectra/Por® Dialysis Membrane Tubing, molecular weight cut-off: 3500, width: 18 mm and diameter: 11.5 mm).

Preparation of silicon quantum dots

Photoluminescent SiQDs were prepared according to the modification[37] of the procedure described by Lie *et al*.[18] The porous silicon layers were formed by electrochemical etching of a boron-doped p-Si<100> oriented wafer (1–10 Ω cm resistivity, Compart Technology, Peterborough, UK) in the presence of fluoride. The Si wafers were cut into squares approximately 1.2 cm^2 using a diamond scribe and etched in a 1 : 1 v/v solution of 48% aqueous HF and EtOH. A porous silicon layer was obtained at high current density (10 min at 250 mA cm^{-2}) that was supplied by a programmable power supply (Keithley 2601), and the porous layer luminesced orange when observed under a handheld UV lamp (λ = 365 nm). The dry porous silicon chips were then refluxed in 25 mL of dry toluene solution containing 0.4 mL of 1-undecene under N_2 for 3 h. The resulting solution emitted an orange-coloured luminescence under an UV light (λ = 365 nm). This fluorescent solution was filtered to remove undissolved silicon particles and then the solvent and unreacted 1-undecene was removed under reduced pressure. The product was an oily/waxy residue which luminesces under UV light (λ = 365 nm) and was soluble in nonpolar solvents e.g. THF, CH_2Cl_2 and $PhCH_3$. It was estimated that 100 µg of alkyl SiQDs were typically produced per Si chip.

General procedure for miniemulsion polymerizations

Oil-in-water miniemulsion polymerization was performed in a two phase system, consisting of an aqueous phase and a monomer phase. The aqueous phase employed deionised water and SDS (0.01M), whilst the monomer phase consisted of styrene (St), 4-vinylbenzaldehye (VBA) or mixtures of both, and hexadecane (0.05 M) as co-surfactant. The monomer solution was added into the aqueous phase and the mixture was stirred vigorously. After 1h, the miniemulsion was generated by ultrasonication of the emulsion for 15 min with a high intensity ultrasonic processor at 30% amplitude (VC750220, Fisher Scientific, tapered microtips, power: 750 W). During the sonication, the emulsion mixture was ice-cooled to avoid any unwanted polymerization due to heating of the sample. The resulting miniemulsion was then transferred into a three-necked 50 mL round-bottom flask equipped with a condenser and a nitrogen inlet. The polymerization was performed under N_2 at 72 $^{\circ}C$ and initiated by addition of aqueous

potassium persulfate (KPS) solution (0.02 M). The polymerization was completed after 3 h and the reaction was terminated by cooling to room temperature. Polymer nanoparticles were purified by dialysis (4 d with water exchanges twice a day and the polymer nanoparticles were obtained by removing water from the polymer dispersion via freeze-drying. Samples were taken prior to and after polymerization for particle size characterization. The experimental quantities and volumes used in all the polymerizations are displayed in Table 2.1.

Preparation of SiQDs encapsulated of polymer nanoparticles via miniemulsion polymerization

Miniemulsion polymerizations in the presence of SiQDs were prepared as above, with the addition of SiQDs inside the monomer phase system. On account of low quantities of SiQDs obtained from electrochemical etching process, the exact mass of SiQDs cannot be measured. However, in each polymerization, four batches of SiQDs which contained 24 Si chips were prepared, and it was estimated that the total amount of SiQDs obtained is 100 μg per chip.

General preparation for conjugation onto polymer nanoparticles functionalized with aldehyde groups

Dry solid of copolymer 4-VBA-St (1:4) nanoparticles (**P8[Ss]**) were mixed with propylamine in the ratio of 1 : 1 (w/w). To this mixture was added 10 mL of $CHCl_3$. The reaction mixture was stirred at room temperature under N_2 for 24 h. The solvent was removed under reduced pressure and the product was purified by dialysis in water for 4 d with water exchanges twice a day. A similar procedure was applied for the conjugation of functionalized aldehyde polymer nanoparticles with the molecules dansyl hydrazine, *O*-carboxymethyl hydroxylamine hemihydrochloride, tetra-polyethylene glycol alkoxyamine and polyethylene glycol-hydrazide by diluting in THF, a mixture of $CHCl_3$ and MeOH and $CHCl_3$, respectively.

Characterization of Polymer Composite Nanoparticles

Dynamic light scattering

Particle size and particle size distributions of the monomer droplets or polymer nanoparticles were performed by dynamic light scattering (DLS) measurements using a HPPS (Malvern) instrument at 25 ± 0.1 $^{\circ}C$ and a scattering angle of 173^{o} (backscatter detection). The emulsion of monomer droplets or polymer nanoparticles (0.5 μL) was

diluted with 10 mL of 2.47 mM SDS solution[60] to avoid the diffusion of surfactant and monomer molecules from the monomer droplet into water. The sample solutions were then placed in low volume disposable PMMA cuvettes and measurements were performed five times.

Atomic force microscopy

The particle morphologies and average particle sizes were further characterized by atomic force microscopy (AFM) measurements performed in Tapping Mode™ using a Multimode Nanoscope IIIA (Veeco Instruments Inc., Metrology Group, Santa Barbara) instrument. The tips used in this measurement were TESPW (0.01 – 0.025 Ω cm antimony n-doped Si cantilevers, Veeco Instruments Inc., Metrology Group) with a resonant frequency of 245 – 247 kHz and a spring constant of 20 – 80 N m^{-1}. The polymer nanoparticles samples were diluted in 10 mL of 2.47 mM sodium dodecyl sulfate (SDS) solution[60] and approximately 0.5 µL of sample solution was deposited onto mica wafer and left overnight to dry. AFM measurements were run on an air table (TMC) for noise and vibration isolation. Particle heights are reported as mean ± standard deviation based on a sample size of 50 polymer nanoparticles.

Luminescence microscopy (epifluorescence and bright field imaging)

The luminescence and bright field optical images of the polymer nanoparticles in the presence of SiQDs and absence of SiQDs, respectively, were observed using an Axioskop 2 plus Microscope (Carl Zeiss) equipped with a light source comprising a Hg arc lamp and Plan-Neofluar 40x/0.75 objective lenses. The excitation filter was a 300 – 400 nm bandpass filter and the emitted light was filtered by a longpass filter with cut-off at 420 nm. The sample was prepared by diluting 1 mg of polymer nanoparticles in 2 mL of 2.47 mM SDS solution[60] followed by sonication for 30 min at 25% amplitude to obtain well-dispersed polymer solutions. Approximately 0.5 µL of the sample dispersion was deposited on the glass slide and the measurements performed.

Confocal microspectroscopy (Luminescence & Raman)

Raman and luminescence spectra were collected using a confocal microscope (WiTec Confocal Raman Microscope model CRM 200, Ulm, Germany). A high intensity Argon Ion laser (Melles-Griot) with output power 35 mW at a wavelength of 488 nm was used as the excitation source. The collected light was analysed by a spectrograph equipped with a CCD detector; we chose a grating of 150 lines mm^{-1} was chosen in order to

capture the full spectrum including all Raman and luminescence bands of interest. All experiments were performed at scan size of 50 x 50 µm in 100 lines at 100 pixels per line with an integration time of 0.1 s/pixel. The preparation of the sample for analysis was similar to that of the luminescence microscopy measurements.

Nuclear magnetic resonance (NMR)

^{1}H NMR spectra were recorded on a Bruker Advance 300 spectrometer at 300MHz, with the $CDCl_3$ as a solvent. Compound numbers refer to those given in Scheme 2.4. ^{1}H NMR ($CDCl_3$) of the product of conjugation (**1**): δ 0.93 -1.01 (br, CH_3), 2.62 (br, CH_2), 3.53 (br, CH_2-NH), 6.59 (br, Ar, polymer backbone), 7.06 (br, Ar, polymer backbone), 8.20 (R-NH),; conjugation (**2**): δ 2.78 (br, CH_3), 6.59 (br, Ar, polymer backbone), 7.06 (br, Ar, polymer backbone), 8.68 (R-NH); conjugation (**3**) : δ 4.76 (br, O-CH_2-COOH), 6.59 (br, Ar, polymer backbone), 7.06 (br, Ar, polymer backbone), 8.18 (br, R-NH); conjugation (**4**) : δ 3.40 – 3.56 (br, OCH_3, of the chain terminus and PEG backbone), 4.35 (br, CH_2-O), 6.59 (br, Ar, polymer backbone), 7.06 (br, Ar, polymer backbone), 8.08 (br, R-NH); 4-ethyl benzaldehye : δ 1.17 (t, CH_3), 2.44 (br, CH_2-Ar), 3.53 (s, OCH_3), 3.56 (CH_2 PEG backbone), 4.13 (br, CH_2-CO), 7.13 – 7.16 (d, CH-Ar), 7.61 – 7.64 (d, CH-Ar), 8.18 (R-NH *cis*), 8.56 (R-NH *trans*); conjugation (**5**) : δ 3.53 (CH_2 PEG backbone), 8.08 (R-NH). All NMR spectra of conjugation system show the evidence of excess or unreacted aldehyde proton around δ 9.79.

Fourier transmission infra-red (FT-IR)

FT-IR spectroscopy was performed on a Varian 800 FT-IR instrument (Varian Inc.). FT-IR of aldehyde functionalized polymer nanoparticles (**P8[Ss]**) (wavenumber, cm^{-1}): 2910 (C-H, alkyl), 2840 (C-H, alkyl), 1702 (C=O), 1600 (C=C, aromatic), 1490 – 1450 (C=C, aromatic), 1202 (C-H, aromatic).

UV-Visible spectroscopy

UV-visible absorption spectra of conjugated dansyl hydrazine and **P8[Ss]** were obtained with a Cary 100 Bio UV-Visible spectrophotometer by using 1 cm path length glass cuvettes. THF has been used as a solvent for the baseline correction and also for sample dispersion.

2.6 References

1. A. P. Alivisatos, W. Gu and C. Larabell, in *Annual Review of Biomedical Engineering*, 2005, **7**, 55-76.
2. N. O'Farrell, A. Houlton and B. R. Horrocks, *International Journal of Nanomedicine*, 2006, **1**, 451-472.
3. F. Erogbogbo, K. T. Yong, I. Roy, G. X. Xu, P. N. Prasad and M. T. Swihart, *ACS Nano*, 2008, **2**, 873-878.
4. R. D. Tilley, J. H. Warner, K. Yamamoto, I. Matsui and H. Fujimori, *Chemical Communications*, 2005, 1833-1835.
5. M. Rosso-Vasic, E. Spruijt, B. van Lagen, L. De Cola and H. Zuilhof, *Small*, 2008, **4**, 1835-1841.
6. A. Shiohara, S. Hanada, S. Prabakar, K. Fujioka, T. H. Lim, K. Yamamoto, P. T. Northcote and R. D. Tilley, *Journal of the American Chemical Society*, 2009, **132**, 248-253.
7. J. A. Kelly and J. G. Veinot, *ACS Nano*, 2010, **4**, 4645-4656.
8. C. Tu, X. Ma, P. Pantazis, S. M. Kauzlarich and A. Y. Louie, *Journal of the American Chemical Society*, 2010, **132**, 2016-2023.
9. M. V. Wolkin, J. Jorne, P. M. Fauchet, G. Allan and C. Delerue, *Physical Review Letters*, 1999, **82**, 197-200.
10. G. Belomoin, J. Therrien, A. Smith, S. Rao, R. Twesten, S. Chaieb, M. H. Nayfeh, L. Wagner and L. Mitas, *Applied Physics Letters*, 2002, **80**, 841-843.
11. F. Hua, M. T. Swihart and E. Ruckenstein, *Langmuir*, 2005, **21**, 6054-6062.
12. S. Furukawa and T. Miyasato, *Physical Review B*, 1988, **38**, 5726-5729.
13. L. Zhang, J. L. Coffer and T. W. Zerda, *Journal of Sol-Gel Science and Technology*, 1998, **11**, 267-272.
14. D. Kovalev, H. Heckler, M. Ben-Chorin, G. Polisski, M. Schwartzkopff and F. Koch, *Physical Review Letters*, 1998, **81**, 2803-2806.
15. H. Kohno, T. Mabuchi, S. Takeda, M. Kohyama, M. Terauchi and M. Tanaka, *Physical Review B - Condensed Matter and Materials Physics*, 1998, **58**, 10338-10342.
16. K. Hata, S. Yoshida, M. Fujita, S. Yasuda, T. Makimura, K. Murakami and H. Shigekawa, *The Journal of Physical Chemistry B*, 2001, **105**, 10842-10846.
17. T. Van Buuren, L. N. Dinh, L. L. Chase, W. J. Siekhaus and L. J. Terminello, *Physical Review Letters*, 1998, **80**, 3803-3806.
18. L. H. Lie, M. Duerdin, E. M. Tuite, A. Houlton and B. R. Horrocks, *Journal of Electroanalytical Chemistry*, 2002, **538-539**, 183-190.
19. F. M. Dickinson, T. A. Alsop, N. Al-Sharif, C. E. M. Berger, H. K. Datta, L. Å iller, Y. Chao, E. M. Tuite, A. Houlton and B. R. Horrocks, *Analyst*, 2008, **133**, 1573-1580.
20. J. H. Warner, A. Hoshino, K. Yamamoto and R. D. Tilley, *Angewandte Chemie International Edition*, 2005, **44**, 4550-4554.
21. M. Rosso-Vasic, E. Spruijt, Z. Popovic, K. Overgaag, B. van Lagen, B. Grandidier, D. Vanmaekelbergh, D. Dominguez-Gutierrez, L. De Cola and H. Zuilhof, *Journal of Materials Chemistry*, 2009, **19**, 5926-5933.
22. B. R. Horrocks and D. A. Fulton, *Unpublished work*.
23. A. V. Fuchs and G. D. Will, *Polymer*, 2010, **51**, 2119-2124.
24. N. Joumaa, M. Lansalot, A. Theretz, A. Elaissari, A. Sukhanova, M. Artemyev, I. Nabiev and J. H. M. Cohen, *Langmuir*, 2006, **22**, 1810-1816.
25. A. C. C. Esteves, P. Hodge, T. Trindade and A. M. M. V. Barros-Timmons, *Journal of Polymer Science Part A: Polymer Chemistry*, 2009, **47**, 5367-5377.

26. B. Erdem, E. D. Sudol, V. L. Dimonie and M. S. El-Aasser, *Journal of Polymer Science Part A: Polymer Chemistry*, 2000, **38**, 4431-4440.
27. K. Y. van Berkel and C. J. Hawker, *Journal of Polymer Science Part A: Polymer Chemistry*, 2010, **48**, 1594-1606.
28. V. Holzapfel, A. Musyanovych, K. Landfester, M. R. Lorenz and V. Mailänder, *Macromolecular Chemistry and Physics*, 2005, **206**, 2440-2449.
29. V. Holzapfel, M. Lorenz, C. K. Weiss, H. Schrezenmeier, K. Landfester and V. Mailänder, *Journal of Physics Condensed Matter*, 2006, **18**, S2581-S2594.
30. A. Ethirajan, U. Ziener and K. Landfester, *Chemistry of Materials*, 2009, **21**, 2218-2225.
31. A. Musyanovych, R. Rossmanith, C. Tontsch and K. Landfester, *Langmuir*, 2007, **23**, 5367-5376.
32. C. Wu, C. Szymanski and J. McNeill, *Langmuir*, 2006, **22**, 2956-2960.
33. U. Paiphansiri, J. Dausend, A. Musyanovych, V. Mailänder and K. Landfester, *Macromolecular Bioscience*, 2009, **9**, 575-584.
34. A. Costoyas, J. Ramos and J. Forcada, *Journal of Polymer Science Part A: Polymer Chemistry*, 2009, **47**, 6201-6213.
35. S. Patai, *The Chemistry of The Carbon-Nitrogen Double Bond*, Interscience Publishers, London; New York, 1970.
36. C. E. Evans and P. A. Lovell, *Chemical Communications*, 2009, 2305-2307.
37. Y. Chao, L. Siller, S. Krishnamurthy, P. R. Coxon, U. Bangert, M. Gass, L. Kjeldgaard, S. N. Patoleo, L. H. Lie, N. O'Farrell, T. A. Alsop, A. Houlton and B. R. Horrocks, *Nature Nanotechnology*, 2007, **2**, 486-489.
38. M. J. Sailor and E. J. Lee, *Advanced Materials*, 1997, **9**, 783-793.
39. H. C. Choi and J. M. Buriak, *Chemistry of Materials*, 2000, **12**, 2151-2156.
40. M. P. Stewart and J. M. Buriak, *Angewandte Chemie International Edition*, 1998, **37**, 3257-3260.
41. J. M. Buriak, *Chemical Communications*, 1999, 1051-1060.
42. J. E. Bateman, R. D. Eagling, D. R. Worrall, B. R. Horrocks and A. Houlton, *Angewandte Chemie International Edition*, 1998, **37**, 2683-2685.
43. L. H. Lie, S. N. Patole, A. R. Pike, L. C. Ryder, B. A. Connolly, A. D. Ward, E. M. Tuite, A. Houlton and B. R. Horrocks, *Faraday Discussions*, 2004, **125**, 235-249.
44. Y. Chao, S. Krishnamurthy, M. Montalti, L. H. Lie, A. Houlton, B. R. Horrocks, L. Kjeldgaard, V. R. Dhanak, M. R. C. Hunt and L. Šiller, *Journal of Applied Physics*, 2005, **98**, 044316.
45. L. Siller, S. Krishnamurthy, L. Kjeldgaard, B. R. Horrocks, Y. Chao, A. Houlton, A. K. Chakraborty and M. R. C. Hunt, *Journal of Physics Condensed Matter*, 2009, **21**, 095005.
46. K. Zidek, F. Trojanek, P. Maly, L. Ondic, I. Pelant, K. Dohnalova, L. Siller, R. Little and B. R. Horrocks, *Optics Express*, 2010, **18**, 25241-25249.
47. R. J. Rostron, B. R. Horrocks and G. Roberts, *Journal of Applied Physics*, 2009, **105**, 094302.
48. K. Landfester, N. Bechthold, F. Tiarks and M. Antonietti, *Macromolecules*, 1999, **32**, 5222-5228.
49. B. J. Berne and R. Pecora, *Dynamic Light Scattering: With Applications to Chemistry, Biology, and Physics*, Dover Publications, 2000.
50. W. I. Goldburg, *American Journal of Physics*, 1999, **67**, 1152-1160.
51. G. Jia, Y. Xu, X. Tan and N. Cai, *Iranian Polymer Journal (English Edition)*, 2006, **15**, 979-987.
52. D. Mouran, J. Reimers and F. J. Schork, *Journal of Polymer Science Part A: Polymer Chemistry*, 1996, **34**, 1073-1081.

53. G. Binnig, C. F. Quate and C. Gerber, *Physical Review Letters*, 1986, **56**, 930-933.
54. E. Meyer, *Progress in Surface Science*, 1992, **41**, 3-49.
55. P. G. M. C.B. Prater, K.J. Kjoller, M.G. Heaton, *TappingMode Imaging Applications and Technology*, www.veeco.com, 2004.
56. C. Hoo, N. Starostin, P. West and M. Mecartney, *Journal of Nanoparticle Research*, 2008, **10**, 89-96.
57. S. Inoué and K. R. Spring, *Video Microscopy : The Fundamentals*, Plenum Press, New York [u.a.], 1997.
58. S. W. Paddock, *Applied Biochemistry and Biotechnology - Part B Molecular Biotechnology*, 2000, **16**, 127-149.
59. E. Smith, G. Dent and J. Wiley, *Modern Raman Spectroscopy: A Practical Approach*, Wiley Online Library, 2005.
60. C. S. Chern and Y. C. Liou, *Macromolecular Chemistry and Physics*, 1998, **199**, 2051-2061.
61. K. Knop, R. Hoogenboom, D. Fischer and U. S. Schubert, *Angewandte Chemie International Edition*, 2010, **49**, 6288-6308.
62. G. Sun, C. Cheng and K. L. Wooley, *Macromolecules*, 2007, **40**, 793-795.

Chapter 3

Gold Nanoparticle-Enhanced Luminescence of Silicon Quantum Dots Co-Encapsulated within Polymer Nanoparticles

This chapter is based on the publication:

N.A. Harun, M.J. Benning, B.R. Horrocks and D.A. Fulton, "Gold Nanoparticle-Enhanced Luminescence of Silicon Quantum Dots Co-Encapsulated within Polymer Nanoparticles", *Nanoscale,* 2013, **5**, 3817 – 3827.

3.1 Abstract

The preparation of two-component polymer composite nanoparticles encapsulating both Si quantum dots (SiQDs) and Au nanoparticles (AuNPs) by a single step miniemulsion polymerization of divinylbenzene is described. This simple and robust method affords well-defined polymer composite nanoparticles with mean diameters in a range of 100 – 200 nm and with narrow polydispersity indices as determined by dynamic light scattering and transmission electron microscopy (TEM). The successful encapsulation of AuNPs within poly(divinylbenzene) was confirmed by UV-Visible spectroscopy and from TEM images. Plasmon enhanced fluorescence of the luminescence of the SiQDs by AuNPs encapsulated within the polymer composite nanoparticles was evaluated by confocal microspectroscopy, and luminescence enhancements of up to 15 times were observed. These observations indicate that the luminescence of the SiQDs is enhanced by the proximity of the AuNPs. The polymer composite nanoparticles were successfully ink-jet printed onto a glass substrate, demonstrating that these composites are processable in printing applications.

3.2 Introduction

An exciting approach to expand the utilization of inorganic nanostructures in applications involves the combination of different nanoparticles possessing different functionalities within a single composite nanoparticle. Multicomponent composite nanoparticles can lead to improvements and enhancements in the properties of individual inorganic nanoparticles, whilst benefitting from the physical and chemical properties of the polymeric materials used in the fabrication of the nanocomposite. In particular, the surface derivatization of the polymer is typically much more facile than of the inorganic nanoparticles.

Quantum dots (QDs) are inorganic fluorophores that possess unique photophysical properties which are useful in a diverse range of applications.[1-8] In Chapter 2, it was shown that silicon quantum dots (SiQDs) can be encapsulated inside polymeric nanoparticles, resulting in a nanocomposite which possesses the luminescence of the SiQDs and the processability of the polymer matrix. However, it is often claimed that the overall brightness of SiQDs can be restricted by a low radiative emission rate as a consequence of the indirect band gap of bulk silicon,[9-11] which limits the possible utility of this class of nanoparticle.

Metallic nanoparticles of gold, silver and aluminium can in principle enhance the brightness of the luminescence fluorophore. This effect is known as metal-enhanced fluorescence, and occurs when metal nanoparticles are located near to a fluorophore and the plasmon mode is resonant with the incident light. In principle, the noble metallic nanoparticles possess interesting plasmonic properties which arise because of the collective oscillation of the conduction electrons when they are in resonance with electromagnetic radiation incident on the surface of the particles.[12-15] This phenomenon is confined near the boundary between the metal nanostructures and their surrounding dielectric matrix, resulting in a range of optical signal enhancements, such as surface enhanced Raman scattering (SERS), surface-enhanced fluorescence, and surface-enhanced infrared absorption.[16-19]

This chapter describes the enhancement of the fluorescent properties of SiQDs by co-encapsulating them with metallic nanoparticles within a polymer nanoparticle. Amongst the noble metal nanoparticles, gold nanoparticles (AuNPs) in particular are very attractive candidate nanoparticles to facilitate these fluorescence enhancements because of their high chemical stabilities on the nano-scale, high homogeneities, good biocompatibilities[20] and low toxicities.[1] Furthermore, the surface chemistry of AuNPs is well-understood and numerous chemistries are available to facilitate the surface modification of AuNPs.[21] To ensure effective fluorescent enhancements, another criterion is that the incident radiation must also be resonant with the absorption transition of the fluorophore. SiQDs are convenient in this case because they possess a featureless absorption spectrum with an absorbance that rises monotonically above the gap (~2 eV in the SiQDs used in this study) and therefore it is only necessary to match the excitation wavelength to the plasmon mode of the metal.

Work involving the preparation of polymer nanoparticles encapsulating more than one species of inorganic NPs has been reported previously. For example, the group of Hawker *et. al.* have described[22] a synthetic method for the preparation of composite nanoparticles composed of AuNPs and $MnFe_2O_4$ encapsulated within a spherical polymer (divinylbenzene) nanoparticle prepared by miniemulsion polymerization techniques. These composite nanoparticles display dual characteristics associated with the magnetism of the $MnFe_2O_4$ nanoparticles and surface plasmon resonance effects associated with the AuNPs. To facilitate their surface functionalization, these nanocomposite particles possessed reactive vinyl groups displayed upon their surfaces, allowing their functionalization with PEG utilizing thiol-ene click chemistry. Multifunctional nanocomposites comprised of magnetic (γ-Fe_2O_3 and Fe_3O_4),

semiconductor (CdSe/ZnS), and metal (Au) nanoparticles contained within block copolymer micelles of polystyrene-block-poly(acrylic acid) (PS-b-PAA) have also been constructed successfully.[23] This water-soluble multifunctional nanostructure was speculated to be useful in targeted drug delivery, providing long-circulating scaffolds for biomolecule presentation and tags for tracking cells.

AuNPs have also been successfully co-encapsulated with other fluorophores (dyes or quantum dots) to prepare nanocomposites with optically active properties. Recent work by Roy and co-workers[24] describes the design of high-brightness optical probes based upon a hybrid core-shell system of gold-silica, which was used to investigate plasmonic enhancement/quenching of a fluorescent dye which was incorporated within the silica shell. The combination of QDs and AuNPs within composite nanoparticles is also of great interest. One recent example reported by the group of Chandra describes[25] the development of a system for application in quantum dot solar concentrator (QDSC) devices. In this work, the group studied the influence of the plasmon-induced electromagnetic field of AuNPs upon the fluorescence properties of CdSe/ ZnS quantum dots (QDs) possessing core-shell type architectures, demonstrating that at certain concentration of AuNPs, a maximum of ~53% of fluorescent emission enhancement can be achieved. Lu and co-workers[26] investigated the effects of metal nanoparticle size, excitation wavelength and fluorescence wavelength on the photoluminescence (PL) enhancement and quenching of CdSe/PMMA composites by Au colloids. They observed that when the size of the AuNPs increased, strong PL enhancement of CdSe nanocrystals occurred. However, the PL of CdSe was quenched by small AuNPs (diameter approximately 25 nm). They speculate that this extinction occurs because of the dominance of the absorption component over the scattering component in smaller-sized AuNPs. This PL quenching cannot be adjusted by changing the excitation wavelength or the fluorescence wavelength of CdSe. In contrast, the excitation wavelength has a great influence on the PL enhancement for the larger AuNPs, where the enhancement factors for the longer excitation wavelength (530 nm or 550 nm) improved 4 times compared to the case using 370 nm excitation wavelengths. Moreover, the PL enhancement can be improved when the AuNPs are larger than 45 nm, and when the fluorescence wavelength of CdSe was longer than the wavelength of surface plasmon absorption of Au colloids.

When considering synthetic approaches to nanocomposite materials, miniemulsion polymerization has been reported as a convenient and powerful technique to encapsulate a range of different type of materials, including organic and inorganic

nanoparticles[27-34] inside polymeric nanoparticles.[35-42] Encapsulation of inorganic species inside polymer matrices affords composite materials which benefit from the outstanding properties associated with synthetic polymers *e.g.* their excellent mechanical, chemical, electrical, rheological, magnetic and optical properties.[28] The hydrophobic nature of inorganic species can facilitate their direct dispersion inside a suitable monomer system, which is conventionally also hydrophobic, and results in successful encapsulation of the inorganic species upon polymerization of miniemulsion droplets. We anticipated that the intense field near the AuNPs surface would produce substantial fluorescence enhancements of nearby SiQDs.[8, 11, 43-46] A search of chemical literature revealed there are no reports of composite nanoparticles prepared by miniemulsion polymerization encapsulating both AuNPs and SiQDs. Most of the methods reported where QDs are combined with plasmonic materials often involve the immobilization of the QDs upon films or substrates,[11, 47-51] which may limit some of advantages that come from co-encapsulation within a nanoparticle matrix. For example, Swihart *et al*.[47] investigated the energy transfer within a micelle platform where SiQDs were co-encapsulated with an anthracene-based dye in the hydrophobic core of micelles prepared from 1,2-distearoyl-*sn*-glycero-3-phosphoethanolaminate-*N*-[methoxy(polyethylene glycol)-2000] (DSPE-PEG). This work indicated that the luminescence of SiQDs from the core of 150 nm phospholipid micelles is enhanced by more than 80% upon addition of an anthracene dye. This composite colloidal solution can serve as a template for improving the QDs emission intensities, especially in biological and solar applications. In the work described in this Chapter, a synthetic route to prepare polymer composite nanoparticles which encapsulate plasmonic metal AuNPs and highly fluorescent SiQDs using miniemulsion polymerization techniques will be described, and the PL enhancement of the SiQDs as a consequence of their co-encapsulation with AuNPs will be demonstrated. This composite nanoparticle is expected to widen the scope of applications for both Si and noble metal-nano devices.

3.3 Results and Discussion

3.3.1 Modification of AuNPs Surfaces via the Polymer "Grafting To" Method

An important requirement in the preparation of polymer composite nanoparticles by miniemulsion polymerization methods is that the inorganic nanoparticles disperse well in the hydrophobic monomer system. Only by meeting this requirement can the

hydrophobic inorganic species be encapsulated within the polymer nanoparticle upon polymerization of the miniemulsion droplets.[52] Alkylated SiQDs prepared by the method developed in our laboratory can be readily dispersed in hydrophobic monomer systems on account of the solubilising 11-carbon alkyl monolayers surrounding their Si cores. Aqueous AuNPs were produced from the chemical reduction of $AuCl_4^-$ ions in a boiling sodium citrate solution.[53] In order to disperse aqueous AuNPs in hydrophobic organic monomers the surface of AuNPs must be modified to improve its hydrophobicity. There are numerous published procedures[54-62] describing the synthesis of hydrophobic AuNPs, most of which use long chain alkyl amines or thiols to alter the size, shapes and colloidal stability of the resulting AuNPs. These small-molecule ligands, however, have been demonstrated to be ineffective in promoting encapsulation into polymer matrices,[32, 63] and also oxidize easily at elevated temperatures.[30]

An alternative route towards increasing the hydrophobicity of AuNPs is by the covalent "grafting to" approach,[21, 64] where hydrophobic polymers featuring sulphur-containing functional groups such as dithioester, trithioester, thiol, thioether or disulphide groups either at their termini or displayed along the polymer chains, are grafted onto the surface of AuNPs to enable their dispersion in hydrophobic solvents and monomers. The "grafting to" technique offers a direct and facile method without the tedious synthesis and purification which is often required in the covalent "grafting from" technique,[21] which utilizes polymerization initiated from the substrate surface by covalent attachment of initiating groups. Monomer molecules penetrate through the grafted polymer easily and substantial grafting densities can be achieved.[65] Moreover, the grafting of polymer chains onto the surface of the AuNPs can discourage the aggregation of AuNPs,[66, 67] and it has also been suggested that the use of polymeric stabilizers for metal nanoparticles can enhance long term stabilities as well as promoting their compatibility and processability.[21] In this work, the "grafting to" approach was utilized successfully to conjugate polystyrene thiol chains onto the surface of AuNPs to afford hydrophobic AuNPs which can be easily re-dispersed in organic solvents, including the desired monomer system required for miniemulsion polymerization. Thiol-terminated polystyrene was synthesized (Scheme 3.1) via reversible addition fragmentation chain transfer (RAFT) polymerization,[68-71] a convenient method for the synthesis of a wide range of polymers of controlled architecture, molecular weight and narrow polydispersity indices. RAFT polymerization is mediated by a chain transfer agent (CTA) which is typically a dithioester or trithiocarbonate.

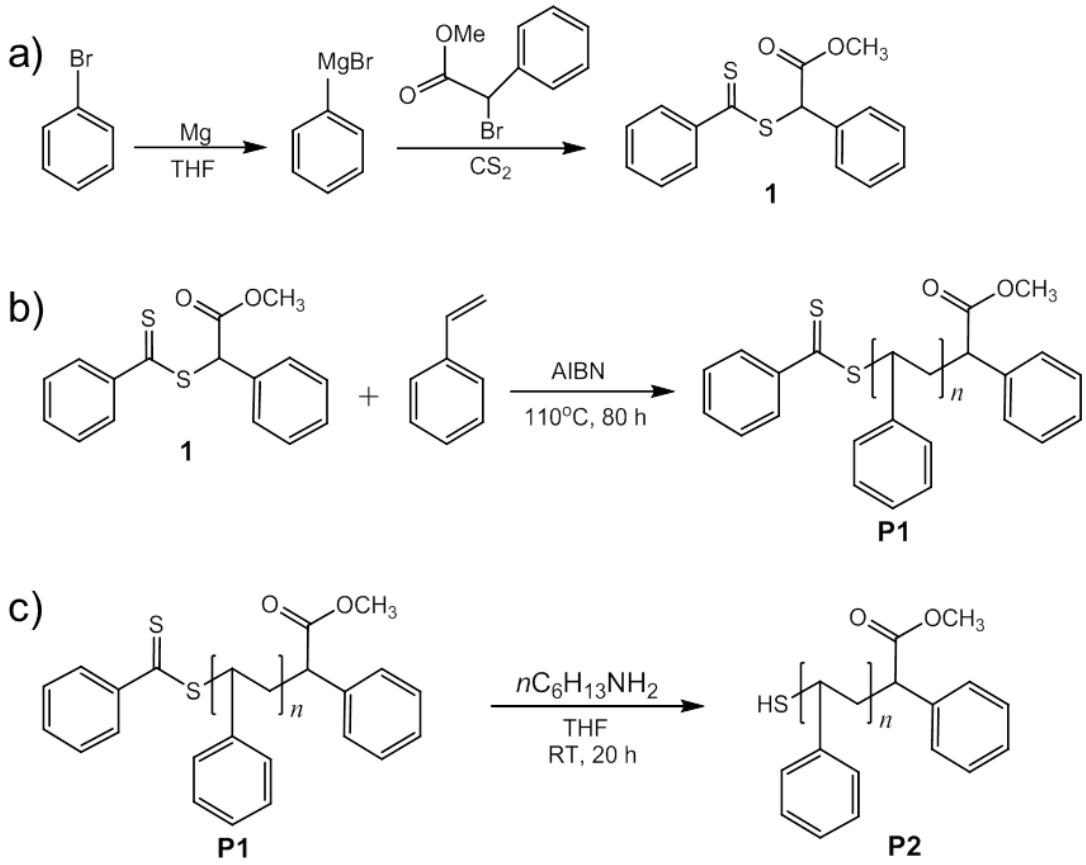

Scheme 3.1 Synthesis of (a) RAFT chains transfer agent (**1**) (b) PS polymer (**2**) and (c) thiol terminated PS (**3**).

Thus, RAFT CTA (**1**) was prepared[71] (Scheme 3.1a) in an overall yield of 40% by the addition of methyl-α-bromophenylacetate to a solution of phenylmagnesium bromide and carbon disulphide in THF. ^{1}H and ^{13}C NMR spectroscopies confirmed the identity of CTA (**1**) (Figure 3.1a). Polymerization of styrene mediated by RAFT CTA (**1**) afforded RAFT polymer (**P1**) (Scheme 3.1b). The RAFT polymerization was performed in the absence of solvent at 110 $^{\circ}$C for 80 h initiated with azobisisobutyronitrile (AIBN), yielding a total monomer conversion of 74% **P1**. The dithioester end group of the RAFT polymer was smoothly converted to the thiol through aminolysis with hexylamine at room temperature to afford thiol-terminated PS (**P2**) in a yield of 82% (Scheme 3.1c). The successful synthesis of PS polymer (**P1**) and thiol-terminated PS (**P2**) were confirmed by ^{1}H NMR spectroscopy (Figure 3.1b – c). The ^{1}H NMR proton spectrum of the aromatic end group of **P1** was present at δ 7.85 (Figure 3.1b), and after cleavage of the dithioester end group, the signal of the aromatic proton was no longer present (Figure 3.1c).

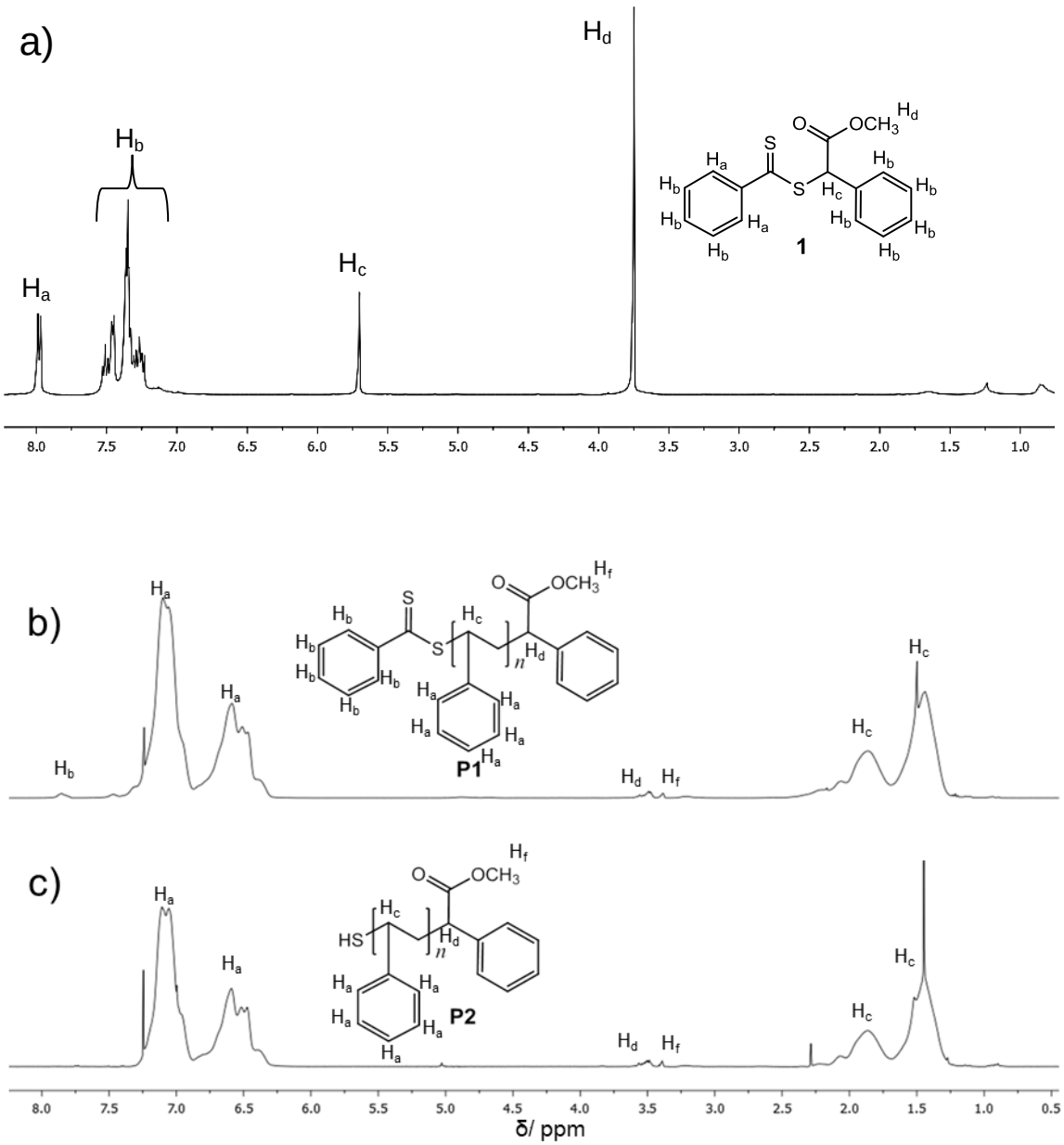

Figure 3.1 ^{1}H NMR spectra (400 MHz, $CDCl_3$) of (a) RAFT CTA (**1**), (b) PS (**P1**) and (c) thiol-terminated PS (**P2**).

PS (**P1**) and thiol-terminated PS (**P2**) were also characterized by GPC analysis (Table 3.1), indicating monomodal weight distributions and low polydispersities in both cases (Figure 3.2). The appearance of a small peak around 14.17 min, may suggest disulphide bond formation between thiol-terminated PS (**P2**) during GPC analysis, where two polymers have dimerized. The end-functionalized polymers were then grafted onto the surface of AuNPs to afford hydrophobic PS-thiol AuNPs (PS-AuNPs),[32] which were characterized by DLS, UV-Visible spectroscopy and TEM. Details explanations of the polymer characterizations are reported in the next sections.

Polymer	M_n (g mol^{-1})	M_w (g mol^{-1})	PDI (M_w/M_n)
P1	13 500	15 300	1.13
P2	14 200	15 900	1.12

Table 3.1 Characterization of polymers **P1** and **P2** as determined by gel permeation chromatography in THF (0.6 mL min^{-1}) calibrated against polystyrene standards.

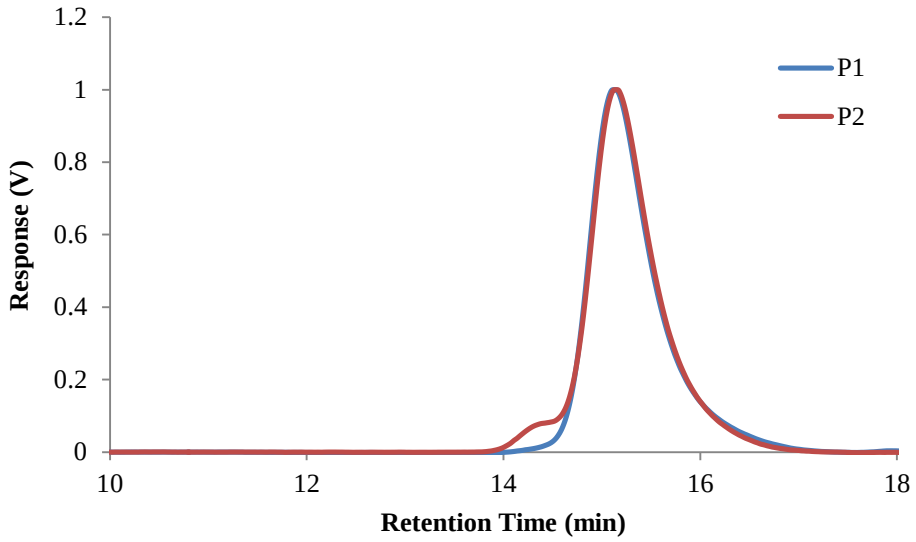

Figure 3.2 Gel permeation chromatography (GPC) traces for **P1** and **P2.**

3.3.2 Preparation of Au-Si Polymer Composite Nanoparticles via Miniemulsion Polymerization

To prepare polymer composite nanoparticles co-encapsulating both SiQDs and AuNPs, the miniemulsion polymerization procedures described[32] by Hawker *et al.* were employed (Scheme 3.2). AuNPs grafted with PS-thiol ligands (PS-AuNPs) and SiQDs were dispersed in divinylbenzene monomer, and subjected to miniemulsion polymerization. Divinylbenzene was chosen as a monomer as it has been demonstrated to successfully encapsulate PS-AuNPs to afford polymer–AuNPs composite particles.[22, 32] The monomer/inorganic species mixtures were mixed in an aqueous solution of cationic surfactant, cetyltrimethylammonium bromide (CTAB) and water soluble initiator, 2,2'-azobis-(2-amidinopropane) dihydrochloride (V-50). The mixture was miniemulsified by vigorous stirring before subjected to high intensity ultrasonication (750 Watt, 30% amplitude), then polymerized at 50 $^{\circ}$C. It is worth noting that although conventional miniemulsion polymerization utilizes a costabilizer (*e.g.*, hexadecane, cetyl alcohol or a polymeric costabilizer) in order to stabilize the emulsion droplets against coalescence and Ostwald ripening (diffusional degradation),[72] no co-stabilizer

was required here because hydrophobic PS-AuNPs appear themselves to sufficiently accomplish the function of a co-stabilizing agent.[32, 73] A major concern arising in miniemulsion polymerization is the issue of low levels of encapsulation and uneven distribution of inorganic particles throughout the polymer matrix. By scaling-down the total volume at which the miniemulsion is performed, ensuring a relatively higher ratio of inorganic nanoparticles to monomer, it was possible to achieve a good distribution of inorganic species within the polymer nanoparticles (as described in the transmission electron microscopy characterization on the following page).

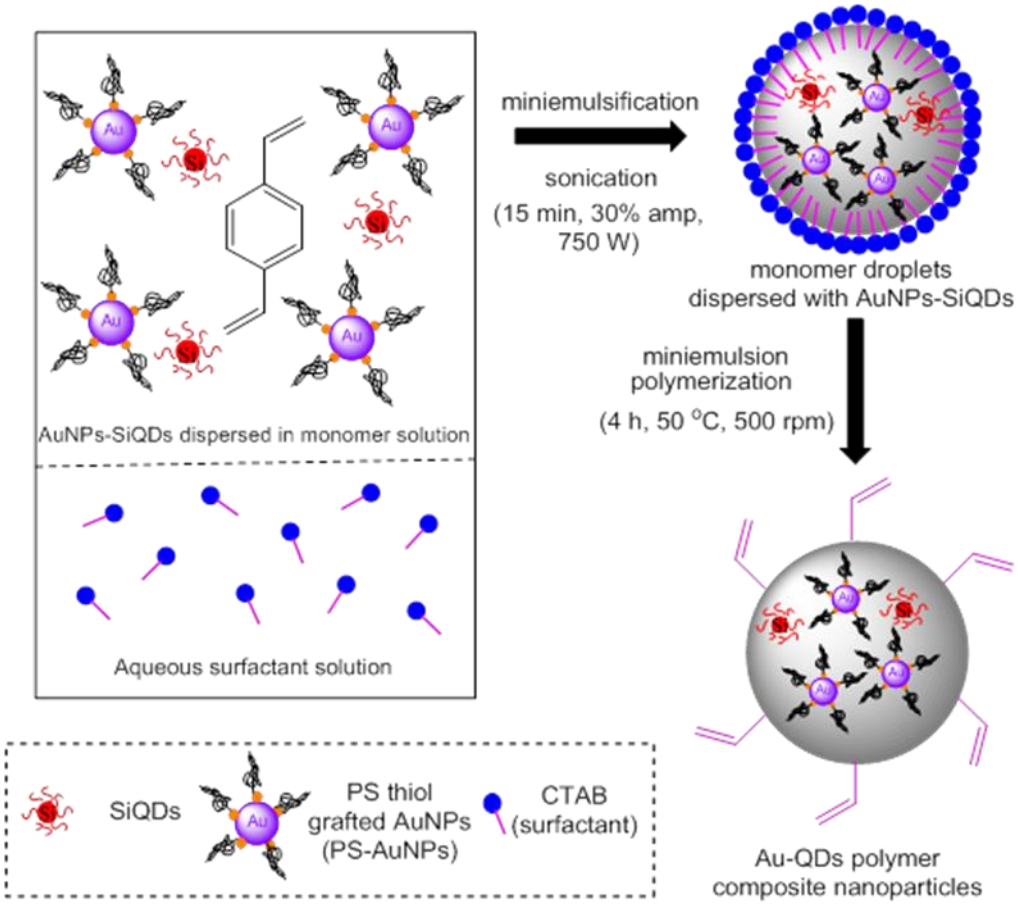

Scheme 3.2: Miniemulsion polymerization of Au-Si polymer composite nanoparticles

To explore the effects of different encapsulated ratios of AuNPs: SiQDs upon the fluorescence properties of the polymer composite nanoparticles, six batches of composite particles were prepared (Table 3.2) which contained different masses of PS-AuNPs but with constant masses of SiQDs. Because the electrochemical etching method affords low masses of SiQDs, it is not possible to determine the precise mass of SiQDs contained within each polymerization reaction, however, by dividing a SiQDs solution into six equal portions, it was possible to ensure a constant mass of SiQDs was

present within each polymerization and it can be assumed that all batches contain equal masses of encapsulated SiQDs. Because the molar mass of the AuNPs was not determined, the quantity of Au was simply reported as the total number of mg of PS-AuNPs used in each preparation, and it can be assumed this number is proportional to the actual level of encapsulated AuNPs.

3.3.3 Particle Size Characterization

Polymer Composite	PS-AuNPs[b] (mg)	Droplet and Particles Sizes Characterization[a]			
		Droplets		Purified Latex	
		Dh (nm)	PDI	Dh (nm)	PDI
P1[Au]	12	111.3 ± 2.9	0.24 ± 0.05	110.0 ± 0.8	0.29 ± 0.03
P2[Si]	0	110.4 ± 1.1	0.23 ± 0.07	118.2 ± 2.7	0.20 ± 0.02
P3[Au-Si]	3	144.0 ± 1.7	0.20 ± 0.08	147.4 ± 1.7	0.17 ± 0.03
P4[Au-Si]	6	139.1 ± 2.4	0.29 ± 0.02	146.4 ± 1.8	0.22 ± 0.01
P5[Au-Si]	12	151.3 ± 2.8	0.23 ± 0.03	160.7 ± 1.2	0.20 ± 0.03
P6[Au-Si]	18	162.6 ± 0.6	0.21 ± 0.04	158.7 ± 2.2	0.20 ± 0.02
P7[Au-Si]	24	166.2 ± 3.6	0.19 ± 0.01	161.5 ± 1.9	0.13 ± 0.02

Table 3.2 Particle size and particle size distribution (PDI) for a series of Au-Si polymer composites nanoparticles (**P3[Au-Si]**–**P7[Au-Si]**) and control polymer composite nanoparticles (**P1[Au]** and **P2[Si]**). [a] As determined by dynamic light scattering (DLS). [b] Total mass of PS-AuNPs used in the miniemulsion protocol.

The particle sizes and size distributions of the monomer droplets and their corresponding resultant polymer composite nanoparticles were measured by dynamic light scattering (DLS). The measurements involving monomer droplets were performed immediately after the reaction mixtures were emulsified by sonication, whilst for the polymer composite nanoparticles, the measurements were performed after the polymerizations were completed and purified by dialysis. The results obtained (Table 3.2 and Figure 3.3) show that the size of monomer droplets was essentially identical to the size of the resulting polymer nanoparticles and suggests that the distribution of Au–

Si in the polymer nanoparticles reflects their homogeneous distribution in the monomer solution.[74]

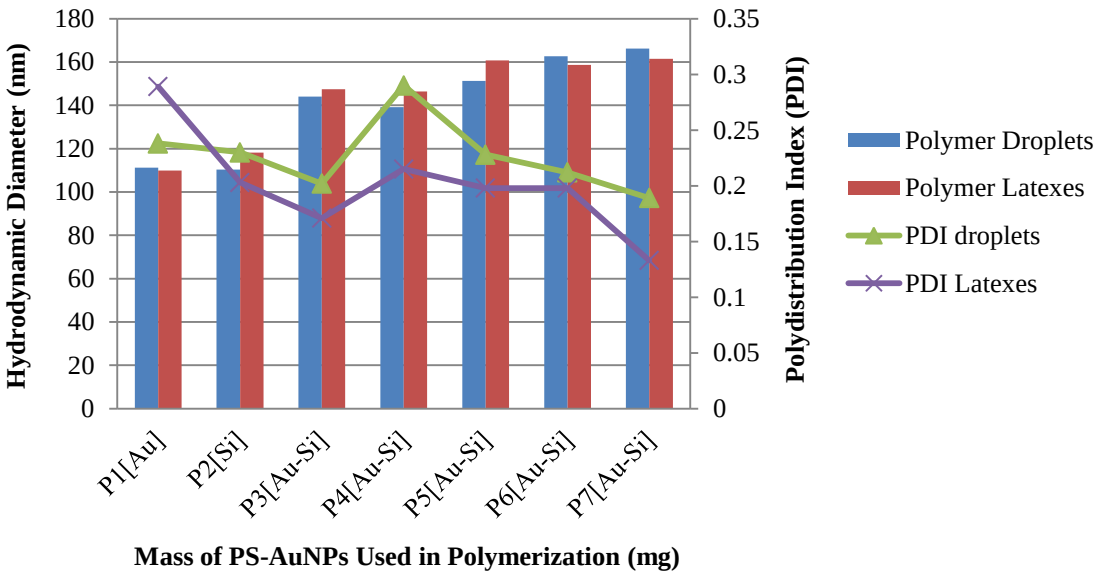

Figure 3.3 Hydrodynamic diameters (D_h) and PDI of Au-Si polymer composite nanoparticles containing different masses of PS-AuNPs.

To gauge any effect of the inorganic nanoparticles upon the outcome of the miniemulsion polymerizations, control samples were prepared which encapsulated only PS-AuNPs (**P1[Au]**) or SiQDs (**P2[Si]**). These controls indicated both the monomer droplets and polymer nanoparticles possessed mean diameters of 110 – 120 nm, and relatively narrow PDIs of 0.20 – 0.29, indicating no significant differences between these control samples in terms of particle size and particle size distributions. It should be noted that, the particles size of citrate stabilized AuNPs and PS-AuNP are 13.9 ± 0.7 nm and 13.4 ± 0.7 nm respectively as measured by DLS, while the size of alkyl capped SiQDs is approximately 5.0 nm.[75] The particle size of citrate stabilized AuNPs is slightly larger than PS-AuNPs because citrate stabilized AuNPs were measured in water, where hydration spheres around each particle increases their sizes. The average hydrodynamic diameters for the series of Au–Si polymer composite nanoparticles (**P3[Au–Si]**–**P7[Au–Si]**) (Figure 3.3) displayed an upward trend as the quantity of PS-AuNP increased, suggesting that increasing the mass of AuNPs in the miniemulsion polymerization did have a small effect upon the resultant particle sizes of the polymer composites.

The PDIs for both the monomer droplets and corresponding Au–Si polymer composite nanoparticles (**P3[Au–Si]**–**P7[Au–Si]**) showed fluctuating trends (Figure 3.3). The PDIs of the monomer droplets are generally higher (0.19 – 0.29) than the PDIs

of the corresponding polymer composite nanoparticles (0.13 – 0.29). The low PDIs values of Au–Si polymer composites nanoparticles (**P3[Au–Si]**–**P7[Au–Si]**) may be attributed to the traces of 1-undecene contaminants which are leftover from the synthesis of SiQDs, and which might help to improve the PDIs and the stability of the polymer composite nanoparticles.[74] In general, the PDIs observed for the Au–Si polymer composite nanoparticles are slightly broad (**P3[Au–Si]**–**P7[Au–Si]**), in the range of 0.13 – 0.29. However, it has been noted previously that the incorporation of inorganic materials can result in inhomogeneous dispersions on account of their strong interparticle interactions, which promotes agglomeration and hence broadening the size distribution.[30] Moreover, the requirement to scale down the total monomer content and volume of water may also contribute towards the increase of the PDIs.

3.3.4 UV-Visible Spectroscopy Characterization

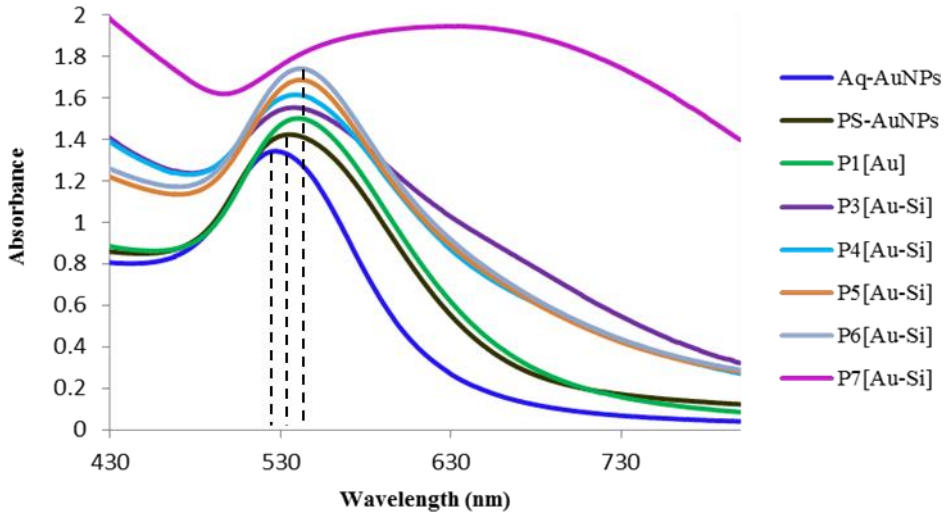

Figure 3.4 Comparison of UV-Vis spectra of aqueous-AuNPs, PS-AuNPs (in THF) and **P1[Au]** and **P3[Au-Si]** – **P7[Au-Si]**.

UV-visible spectroscopy (Figure 3.4) was used to compare the plasmon resonance bands of colloidal AuNPs (aq-AuNPs), PS-AuNPs and the Au–Si polymer composite nanoparticles (**P1[Au]** and **P3[Au–Si]**–**P7[Au–Si]**). It worth mentioning that the first observed evidence for the presence of AuNPs in the polymer composite nanoparticle was the purple colour observed in the aqueous emulsion solution. Further evidence for the presence of AuNPs was the shifting of the UV-Vis absorption peaks. The absorbance of the PS-AuNPs (530 nm) is red-shifted relative to the citrate-stabilized AuNPs (525 nm), whilst the Au–Si polymer composite nanoparticles (**P1[Au]** and

P3[Au–Si]–**P7[Au–Si]**) are further red-shifted to approximately 540 nm. The likely reason for this red-shifting is because the surface plasmon resonance band of AuNPs is sensitive to the changes in the dielectric environment of the surrounding medium and capping layer around the AuNPs.[21, 26] This red-shifting phenomenon is therefore expected; the surface plasmon resonance energy of the Au decreases as the refractive index of the medium surrounding the metal nanoparticles increases.[76] In contrast, for **P7[Au–Si]** a very broad surface plasmon resonance spectrum was observed, which is likely a consequence of the self-aggregation of PS-AuNPs during the polymerization process, suggesting incomplete encapsulation of AuNPs within the polymer matrix, as confirmed by TEM characterization in Section 3.3.5.

3.3.5 Transmission Electron Microscopy Characterization

Transmission electron microscopy (TEM) is an efficient and versatile tool for the characterization of materials over spatial ranges from the atomic scale through the 'nano' regime (from, 1 nm to ~ 100 nm) up to the micrometre level and beyond. The reason of development of TEM is due to the limited image resolution in typical light microscopes, which is imposed by the wavelength of the visible light. In contrast to conventional light microscopes, TEMs use electrons as the "light source", and their much lower wavelength results in higher resolution images of up to thousand times better than a light microscope.[77]

Transmission electron microscopy (TEM) micrographs (Figure 3.5) of Au–Si polymer composite nanoparticles (**P3[Au–Si]**, **P5[Au–Si]**, and **P7[Au–Si]**) were obtained and compared to those of citrate-stabilized AuNPs (aq-Au) and PS-AuNPs. Figure 3.5a shows typical TEM images of PS-AuNPs cast onto a carbon coated TEM grid, showing uniform distribution of nanoparticles upon the TEM grid. The polystyrene grafts upon the AuNPs cannot be observed under TEM on account of their low contrast between the carbon-coated grid and the polymer chains, and more importantly, the large contrast compared to the AuNPs.[68] In contrast, however, the citrate-stabilized AuNPs (Figure 3.5a (inset)) are clearly visible and tend to aggregate during sample preparation after evaporation of the aqueous solvent. The even distribution of AuNPs within the PS-AuNPs sample may be attributable to the polymer grafts upon the surface of AuNPs, which prevent aggregation between PS-AuNPs.[68] The particle sizes of citrate-stabilized AuNPs and PS-AuNPs are 13 – 30 nm as measured by TEM, and showed reasonable agreement with the hydrodynamic diameter of the nanoparticles obtained by DLS.

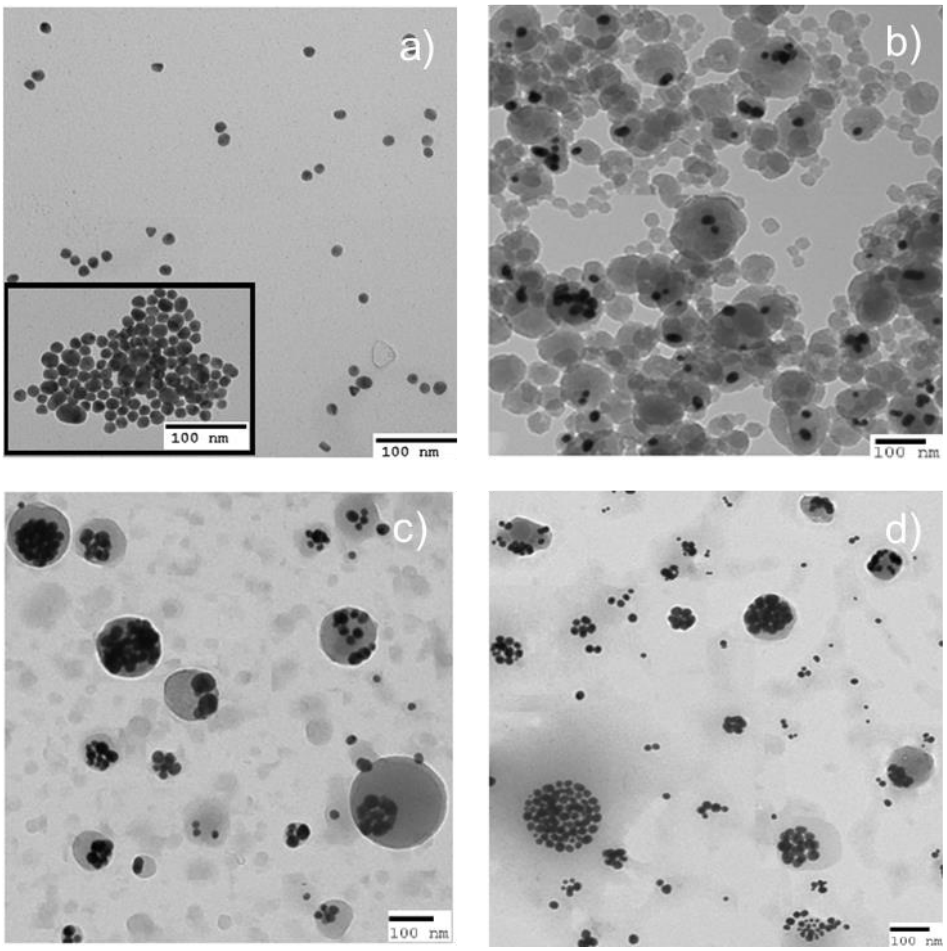

Figure 3.5 Transmission electron microscopy (TEM) images of (a) PS-thiol grafted AuNPs in THF (130 000x magnification). Inset shows TEM images of citrate-stabilized AuNPs in water (130 000x magnification) (b) **P3[Au–Si]** (64 000x magnification) (c) **P5[Au–Si]** (64 000x magnification) (d) **P7[Au–Si]** (64 000x magnification). Because of the low scattering factor of Si, TEM cannot confirm the presence or absence of SiQDs within the polymer matrix.

The TEM images of **P3[Au–Si]**, **P5[Au–Si]**, and **P7[Au–Si]** are depicted in Figure 3.5b – d. It can clearly be seen that the Au–Si polymer composite nanoparticles possess a spherical shape with diameters approximately 100 – 200 nm. TEM measurements (Figure 3.5) clearly show the encapsulation of AuNPs, however, because of the low scattering factor of Si, TEM cannot confirm the presence or absence of SiQDs within the polymer matrix. Sample **P3[Au–Si]** showed only a relatively small amount of encapsulated AuNPs with several empty polymeric nanoparticles observed (Figure 3.5b). In contrast, the sample **P5[Au–Si]** (Figure 3.5c), which is prepared with an increased mass ratio of PS-AuNPs to SiQDs, significant numbers of PS-AuNPs were incorporated into each polymer composite nanoparticle and no empty polymer particles were observed. **P7[Au–Si]** displays unusual morphology, as although it appears that some of the PS-AuNPs encapsulated successfully inside polymer matrix, most of the PS-AuNPs were observed outside the polymer shells in the form of PS-AuNPs clusters

(Figure 3.5d). This poor encapsulation of PS-AuNPs probably arises when the maximum possible mass of AuNPs was encapsulated within the polymer nanoparticles, resulting in excess PS-AuNPs aggregating with themselves to form unencapsulated clusters. This observation correlated with UV-Vis spectroscopy, which displayed a broad surface plasmon resonance (SPR) spectrum for this batch of polymer composite nanoparticles (Figure 3.4). These results suggest an 'upper-limit' of encapsulation of PS-AuNPs within the polymer nanoparticles, and that when the amount of PS-AuNPs further increases beyond this limit, poor encapsulation is obtained in the miniemulsion polymerization.

3.3.6 Evaluation of Fluorescence Enhancement Behaviour of Au-Si Polymer Composite Nanoparticles by Confocal Microspectroscopy

Confocal microspectroscopy studies were performed to evaluate the enhancements in the luminescence spectra of Au–Si polymer composite nanoparticles (**P3[Au–Si]**–**P7[Au–Si]**) relative to the control samples in which either SiQDs (**P1[Au]**) or AuNPs (**P2[Si]**) are absent. Luminescence enhancements were investigated with the polymer composite nanoparticles (**P3[Au–Si]**–**P7[Au–Si]**), which possess a constant amount of SiQDs but differing amounts of PS-AuNPs. Each sample was scanned by an Ar ion laser at excitation wavelength of 488 nm, and the emitted/ scattered light was dispersed on a grating of 150 lines per mm to exhibit both luminescence and Raman spectra. Figure 3.6 shows typical dark field images (reflected images) and confocal luminescence images of **P3[Au–Si]**, **P5[Au–Si]** and **P7[Au–Si]** drop-casted onto a glass cover slip. The bright regions observed in the confocal luminescence images belong to those polymer composite nanoparticles containing SiQDs, observations which suggest the successful encapsulation of SiQDs into the polymer matrix. In contrast, no luminescence was observed from the sample of polymer composite prepared in the absence of SiQDs (**P1[Au]**).

Figure 3.7 shows the average luminescence/Raman spectra obtained for **P3[Au–Si]**–**P7[Au–Si]** and the control specimen **P2[Si]**. These average spectra were obtained from the selection of bright regions collected from confocal images which were combined together to attain complete average luminescence/Raman spectra for the polymer composite nanoparticles. The large and broad signals present within the spectra correspond to the luminescence signals of SiQDs, which are incorporated inside or on the surface of the polymer nanocomposites. The Raman bands of poly(divinylbenzene)

(PDVB) appear around 3070–3000 cm^{-1} (aromatic C–H stretching) whilst the signal at approximately 2833–2886 cm^{-1} was attributed to aliphatic C–H stretching modes. Weak Raman signals were observed for **P2[Si]** and **P7[Au–Si]**, where both samples displayed small luminescence enhancements. However, the Raman bands of PDVB cannot be clearly identified from the average luminescence/Raman spectra in other samples because of the large broad luminescence peak which obscures the weak Raman signals.

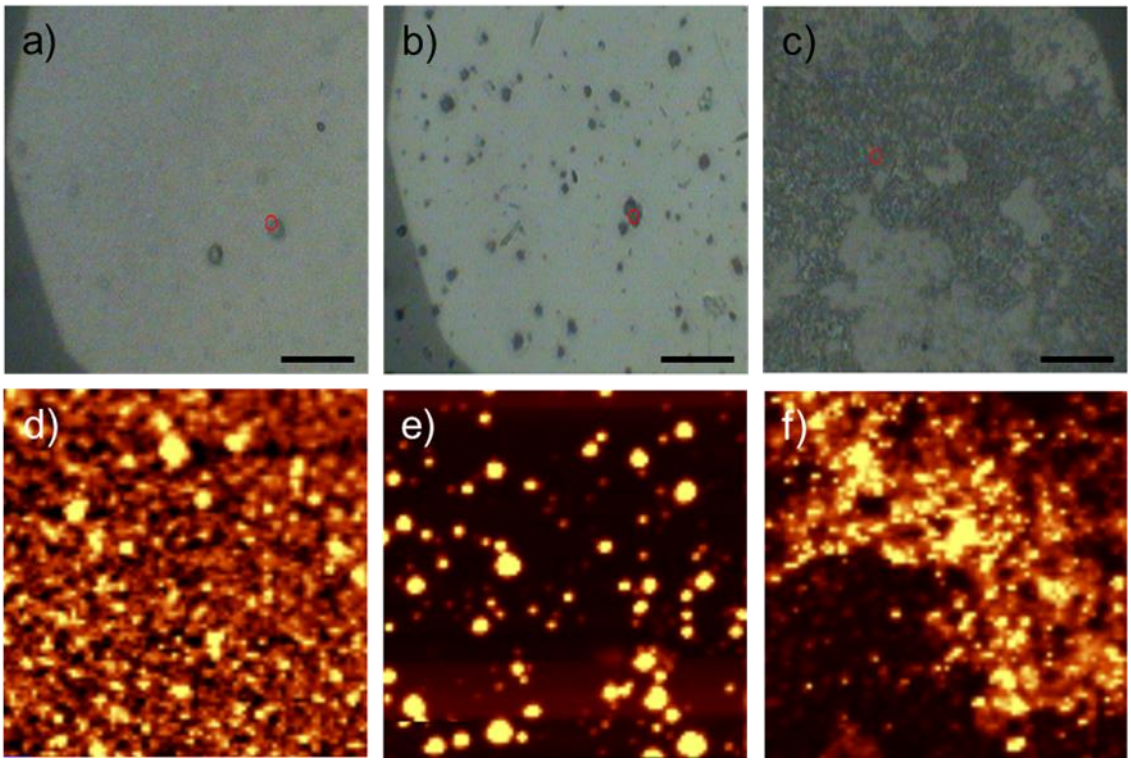

Figure 3.6 Reflected light image of (a) **P3[Au–Si]** (b) **P5[Au–Si]** and (c) **P7[Au–Si]** and confocal luminescence spectrum images of (d) **P3[Au–Si]** (e) **P5[Au–Si]** and (f) **P7 [Au–Si]** polymer composite nanoparticles, respectively. The polymer composite nanoparticles samples were purified by dialysis and drop cast on a glass cover slip. Scale bar on the reflected image = 10 μm and scan size of luminescence images = 50 x 50 μm.

The luminescence/Raman spectra of **P3[Au–Si]**–**P7[Au–Si]** displayed significant improvements in the luminescence of the encapsulated SiQDs as the relative mass of encapsulated AuNPs increased (Figure 3.7). The fluorescence intensity of Au–Si polymer composite nanoparticles were enhanced about 7 and 9 times when 3 mg and 6 mg of AuNPs were used in the miniemulsion polymerization (**P3[Au–Si]** and **P4[Au–Si]**), respectively, relative to polymer composite nanoparticles which encapsulated only SiQDs. For Au–Si polymer composite nanoparticles possessing 12 mg and 18 mg of PS-AuNPs (**P5[Au–Si]** and **P6[Au–Si]**), a 15- fold increase in the fluorescence intensity was observed as compared to **P2[Si]**. These observations indicate that the co-

incorporation of PS-AuNPs gives rise to a significant luminescence enhancement of the encapsulated SiQDs.

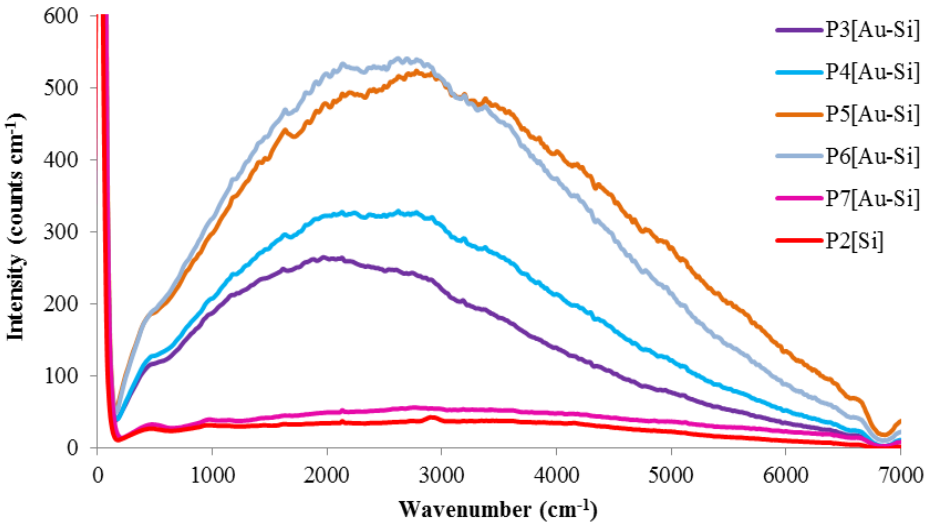

Figure 3.7 Average luminescence/Raman spectra of Au–Si polymer composite nanoparticles (**P3[Au–Si]**–**P7[Au–Si]**) and control polymer composite nanoparticles (**P2[Si]**). The higher intensity peak at 0 cm^{-1} is the elastically scattered laser light. The excitation wavelength, λ = 488 nm.

It is somewhat surprising that the **P7[Au–Si]**, which was prepared with the largest mass of PS-AuNPs, displays a significant drop in fluorescence enhancement. A likely explanation for this observation may be that when the concentration of PS-AuNPs used in the miniemulsion polymerization is increased beyond a certain limit, the metal nanoparticles tend to self-aggregate and are consequently poorly encapsulated within the polymer matrix. This interpretation is consistent with the results of the UV-Vis spectroscopy (Figure 3.4) and the TEM study (Figure 3.5), where a broad plasmon resonance band was observed in sample **P7[Au–Si]**, and further observations for the agglomeration of the AuNPs (Figure 3.5d). This observation is in agreement with the work reported by Chandra *et al.*[25] on the luminescence enhancement of CdSe/ZnS QDs by AuNPs, showing that the degree of fluorescence enhancement depends upon the relative amount of AuNPs encapsulated. Importantly, in their work the emission intensity is also initially enhanced when the concentrations of AuNPs increased, however, further increases in the quantity of encapsulated AuNPs causes a reduction in emission fluorescence intensity.

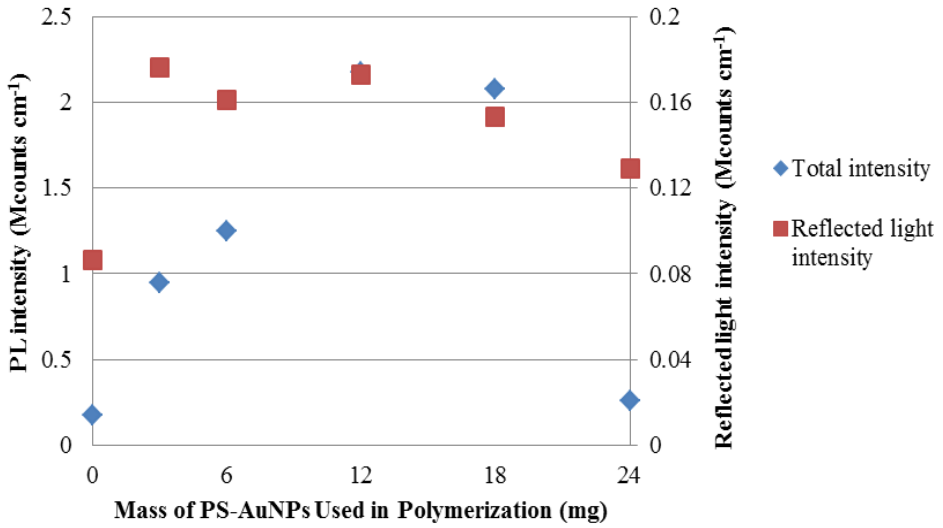

Figure 3.8 Total intensity and reflected light intensity of Au–Si polymer composite nanoparticles (**P3[Au–Si]**–**P7[Au–Si]**) and control polymer composite nanoparticles (**P2[Si]**). Total intensity was calculated as area underneath of the fluorescence peaks obtained from the averages over the particles identified in confocal images.

The total luminescence intensity and the intensity of elastically scattered light for co-encapsulated AuNPs and SiQDs are shown in Figure 3.8. These intensities are effectively normalised to the number of particles by averaging the spectra of all the particles in the field of view and therefore correspond to the intrinsic properties of an average particle and are not simply determined by the number of particles in the field of view. From Figure 3.8, it was noted that as the ratio of PS-AuNPs: SiQDs increased, the enhancement of total luminescence intensity increased until it reached a maximum (**P5[Au–Si]** and **P6[Au–Si]**). The optimum formulation in this study was obtained using 12 mg of PS-AuNPs (**P5[Au–Si]**), which gives the greatest total intensity (2 200 000 counts per cm). With further increases in the mass of PS-AuNPs used in the formulation, a massive drop of total intensity was then observed (**P7[Au–Si]**). In the sample prepared with 24 mg of PS-AuNPs (**P7[Au–Si]**), a 3 : 1 mole ratio PS-AuNP : SiQD was estimated from the particle sizes and masses used and therefore it is possible that the AuNPs actually reflect light at the polymer particle surface and that an inner filter effect occurs, reducing the emission from each polymer particle.

A large drop of total PL intensity for **P7[Au-Si]** sample may be explained by a number of different possibilities which are considered as the optical effects. The first possibility was attributed to the increase of the intensity of scattered light when a large amount of AuNPs have been encapsulated, *i.e.* all light is reflected by AuNPs before it reaches the SiQDs. As a result, the expected plot is depicted in Scheme 3.3a. Another possibility which can be expected to happen as seen in the massive drop of the total PL

intensity of **P7[Au-Si]**, is the drop of the inelastic scattered light (Scheme 3.3b) due to all the light being absorbed by large amounts of AuNPs encapsulated inside polymer matrix before it can reach the SiQDs.

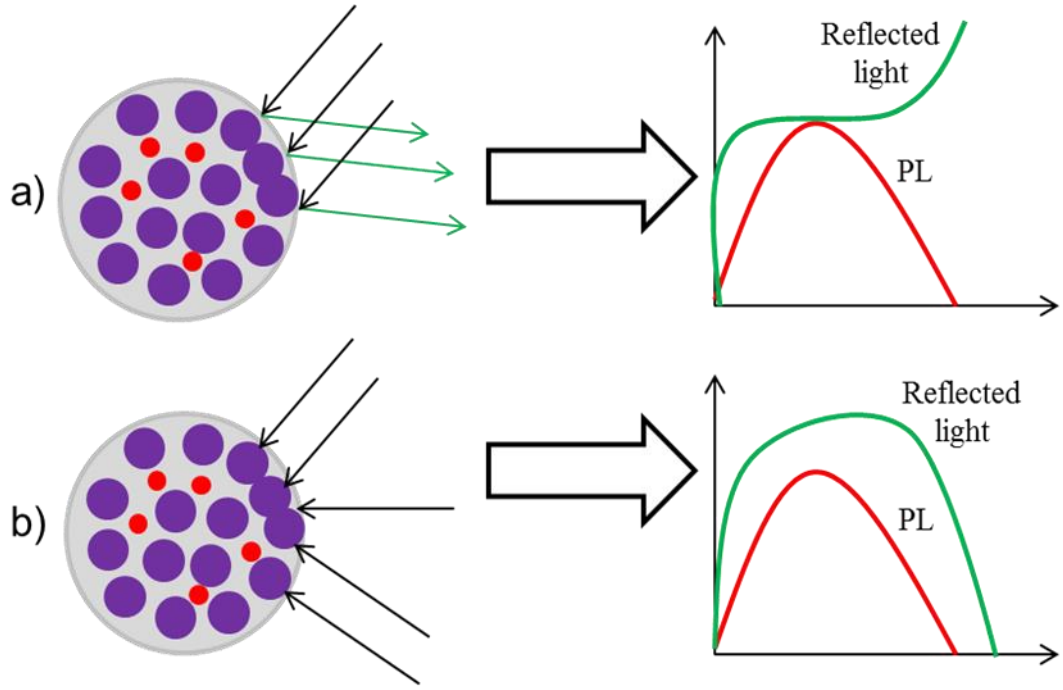

Scheme 3.3 Possible optical effects which may occur in the relationship between total PL intensity and total elastically scattered light intensity of **P7[Au-Si]**. AuNPs are shown as purple spheres while SiQDs are illustrated as red spheres.

These hypotheses were tested by plotting the intensity of elastically scattered light against the mass of PS-AuNPs used in the polymerization (Figure 3.8), but it was found that no increase in reflectivity occurs. Equally, the observation that the reflected light intensity does not decrease markedly also suggests that the low emission from **P7[Au–Si]** is not due to absorption of light by the AuNPs. In view of the observations of aggregation of the PS-AuNPs by TEM and absorption spectroscopy, it appears that the loss of intensity is not related to the optical effects but due to this aggregation and failure of encapsulation of AuNPs within polymer nanoparticles. If the size data to estimate the mole ratio of PS-AuNPs: SiQDs was used, the number of each nanoparticle inside every polymer particle can be calculated to be about 40 SiQDs per polymer particle and about 120 AuNPs per polymer for **P7[Au–Si]**. The high number of encapsulated PS-AuNPs appears to be too large for complete encapsulation, most likely leading to the breakdown of encapsulation by overloading the polymer particles. The aggregation of the AuNPs also leads to poor coupling of the excitation light at 488 nm to the red-shifted plasmon of the aggregate. Interestingly, there is also a significant

blue-shift in the PL maximum of the samples which show enhancement, but this is absent in the **P7[Au–Si]** and the **P2[Si]** sample which is absence of Au. This observation is consistent with the explanation based on loss of the enhancement mechanism.

3.3.7 Inkjet Printing Application

Inkjet printing has emerged as an important technology in recent years for many applications beyond simply printing text on paper, including the fabrication of organic transistors, full colour emissive polymer displays, ceramics and biopolymer arrays.[78] The rapid growth of inkjet technology is based upon its ability to precisely deposit picolitre volumes of solutions or suspensions in well-defined patterns. This facility, also known as "direct-write", is achieved by using computer-controlled translation stages and ink-dispensers, which readily facilitates the production of complex patterns. Inkjet printing eliminates the need for masks, which offers several advantages, for instance cost savings, efficient use of materials and waste elimination. Furthermore, since inkjet printing is a non-contact deposition method, contamination also can be minimized.[79]

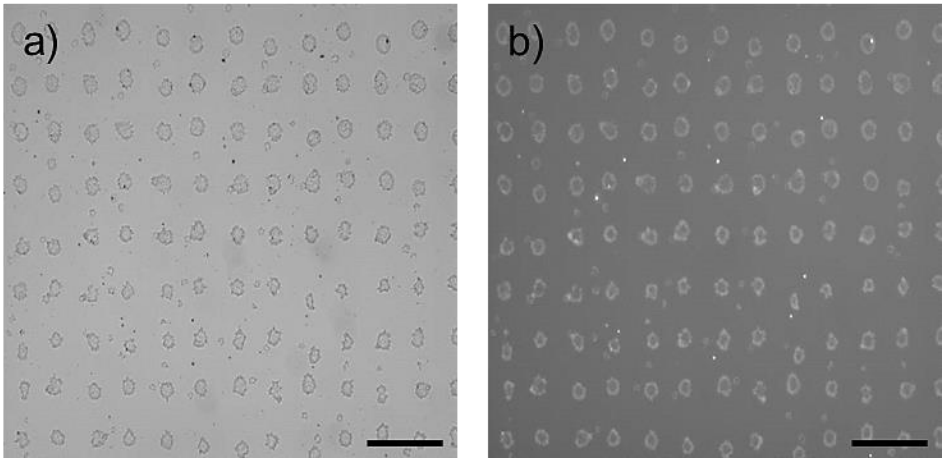

Figure 3.9 Inkjet printed images of **P6[Au–Si]** of (a) bright field optical image and (b) the corresponding luminescence image at exposure time of 5000 ms measured in an epifluorescence microscopy (excitation provided by an Hg Lamp/bandpass filter 300 – 400 nm and the emission was filtered by a 420 nm longpass filter); scale bar = 100 μm.

To demonstrate the potential processability of the Au-Si polymer composite nanoparticles in inkjet printing, a sample was inkjet printed onto a glass substrate. The inkjet printing experiment was performed in the Mechanical Engineering Laboratory at Newcastle University by Dr. Matthew J. Benning. An ink sample for printing was obtained from **P6[Au–Si]** suspended in cyclohexanone. Cyclohexanone was chosen as a

solvent because of good compatibility with the substrate and favourable viscosity properties. A regular pattern of small spots (diameter between 20 and 25 mm) was printed on the glass slide and the dark field scattering and luminescence images were monitored by using luminescence microscopy (epifluorescence). Figure 3.9a shows the bright field optical image of a square lattice of small spots of **P6[Au–Si]** which has been uniformly printed upon a glass slide. The luminescence image (Figure 3.9b) shows the existence of small bright spots possessing a very similar regular pattern. The spots are annular rather than disc shaped. It should be noted that neither the ink nor the printing method have been optimized and so it is likely that there is considerable scope for improvement. The results of these preliminary ink-jet printing studies suggest that these composite polymer nanoparticles can be printed onto surfaces with a reasonable degree of fidelity, and hence are suitable of use as components within more complex materials fabricated by ink-jet printing techniques.

3.4 Conclusions

Multicomponent polymer composite nanoparticles encapsulating two different inorganic nanoparticles, namely SiQDs and AuNPs, have been prepared using miniemulsion polymerization techniques. Six different batches of Au-Si polymer composite nanoparticles possessing different quantities of PS-AuNPs and with constant quantities of SiQDs have been prepared and studied. The modification of AuNP surfaces with thiol-terminated polymer by the "grafting to" method improved the hydrophobicity of aqueous AuNPs and showed excellent dispersion in the organic monomer system. The mean particle diameters of Au-Si polymer composite nanoparticles increased steadily when the mass quantity of PS-AuNPs in every polymerization increased. The encapsulation of PS-AuNPs inside polymer nanoparticles was observed by UV-Visible spectroscopy, which showed red shifting of surface plasmon resonance band of Au-Si polymer composite nanoparticles compared to citrate stabilized AuNPs and PS-AuNPs. From TEM images, it was further confirmed that Au-QDs have been successfully encapsulated inside spherical poly(divinylbenzene) nanoparticles. Because of the low contrast of SiQDs it was not possible to see the distribution of SiQDs inside polymer nanoparticles by TEM characterization. However, the luminescence spectra of Au-Si polymer composite nanoparticles obtained by confocal microspectroscopy displayed the characteristic broad luminescence signal of SiQDs, confirming the presence of SiQDs inside the polymer nanoparticles. Co-encapsulation of AuNPs and SiQDs was found to

enhance the luminescence of the SiQDs presumably because the excitation light is coupled to the plasmon band of the AuNPs, and in turn the intense field at the AuNPs surface couples strongly to the SiQDs. Enhancement factors up to 15 times were observed. This study also suggests that there exists an optimum loading of AuNPs within the polymer nanoparticles, beyond which the encapsulation fails and aggregation of Au-NPs occurred. This observation correlated with the evidence from the broad plasmon resonance band obtained from UV-Visible spectroscopy, and evidence for aggregation of un-encapsulated PS-AuNPs observed from TEM images. To further demonstrate the utility of the polymer composite nanoparticles, the inkjet printing onto a glass substrate was demonstrated. A regular pattern of bright small spots was observed under luminescence microscopy which indicates that the fluorescence effect originates from SiQDs. This work provides a synthetic route to prepare highly fluorescent SiQD probes through the generation of multimodal polymer composite nanoparticles benefitting from using a diversity of inorganic species with different functionalities and combinations.

3.5 Experimental

Materials and general experimental

Water was deionized before use (nominal resistivity 18 MΩ cm, Nanopure™ purification system, Barnstead). All chemicals were purchased from Sigma Aldrich or Alfa Aesar and were used as received without further purification. Divinylbenzene was refrigerated and used without purification. Membranes for purification by dialysis of polymer composite nanoparticles were obtained from Spectrum Laboratories (Spectra/Por® Dialysis Membrane Tubing, molecular weight cut-off: 3500 Da, width: 18 mm and diameter: 11.5 mm). Toluene was dried over sodium and distilled as required.

Preparation of silicon quantum dots (SiQDs)

Refer to Chapter 2, page 71.

Preparation of citrate stabilized AuNPs

Aqueous-AuNPs were synthesized using a citrate reduction method described in the literature.[53] To boiling distilled water (400 mL) was added $HAuCl_4 \bullet 3H_2O$ (0.16 g, 0.41

mM) to afford a yellow solution. A solution of 3.28 mM sodium citrate (34 mL) was added to the gold (III) chloride solution and the colour changed from light yellow to dark purple. The reaction mixture was boiled for 30 min, and the resulting aqueous dispersion of AuNPs possessed a ruby-red colour. The average diameter of the resulting aqueous-AuNPs was measured to be 13 – 30 nm by TEM and DLS analysis.

Synthesis of RAFT chain transfer agent (S-Methoxycarbonylphenylmethyl dithiobenzoate*)*

The RAFT CTA was prepared according to a literature procedure.[71] Mg Turnings (0.25 g) were dissolved in dry THF (20 mL) to which was added bromobenzene (1.57 g). The mixture was heated to 40 °C, and upon the complete dissolution of Mg, CS_2 (0.8 g) was added dropwise over approximately 15 min to afford a dark brown solution. Methyl-α-bromophenyl acetate was then added in one portion and the reaction temperature raised to 80 °C and stirred for 24 h. Ice cold water (10 mL) was then added to the solution before extracting the organic products with Et_2O (100 mL) three times. The combined organic extracts were washed with water (100 mL) and dried over anhydrous magnesium sulphate, filtered and evaporated to dryness. The organic products were purified by column chromatography (Hexane/ EtOAc 95: 5) to afford 0.62 g pure products (39.5 % yields). ^{1}H NMR (400 MHz, $CDCl_3$): δ 3.70 (3H, s, O-CH_3), δ 5.65 (1H, s, -S(Ph)CH–CO_2Me), δ 7.20 – 7.60 (8H, m, Ar-H), δ 7.98 (2H, dd, Ar-H). ^{13}C NMR (400 MHz, $CDCl_3$): δ 53.33 (CH), δ 58.62 (O-CH_3), δ 127.07, 128.53, 128.95, 129.05, 129.20, 132.94, 133.40, 144.0 (CH, Ar), δ 169.52 (C=O), δ 225.97 (CS_2).

Synthesis of thiol-terminated PS by RAFT polymerization

Thiol-terminated polystyrene was prepared by RAFT polymerization of styrene followed by aminolysis to convert the dithioester end group into a thiol.[32] The RAFT CTA (*S*-Methoxycarbonylphenylmethyl dithiobenzoate) (1 eq relative to St), AIBN (0.022 g, 0.09 eq) and a magnetic stirrer bar were added to a Schlenk flask which was then sealed. The reaction mixture was degassed by three freeze–pump–thaw cycles, and then heated with stirring at 110 °C for 80 h under an atmosphere of N_2. The product was precipitated into cold MeOH, filtered and dried under vacuum to afford polystyrene as a pink powder (5.18 g, 74%). A solution of this polymer (1.06 g) in THF (20 mL) was subjected to five freeze–pump–thaw cycles. Hexylamine (3.5 eq.) was then added using a N_2-purged syringe, and the reaction mixture was heated at 60 °C for 30 min, and then stirred under an atmosphere of N_2 at room temperature for 20 h. The resulting thiol-

terminated polystyrene was purified by precipitation in cold MeOH to afford a white powder (0.88 g, 82%). ^{1}H NMR (400 MHz, $CDCl_3$): δ 1.45 (br, $CHCH_2$, polymer backbone), δ 1.88 (br, $CHCH_2$, polymer backbone), δ 3.49 (br, OCH_3, of the chain terminus), δ 6.59 (br, Ar, polymer backbone), δ 7.06 (br, Ar, polymer backbone).

Preparation of polymer-grafted AuNPs

Thiol-terminated polystyrene (10 mg) was dissolved in inhibitor free THF (100 mL) and mixed with an aqueous dispersion of AuNPs (100 mL) in a separating funnel, resulting in formation of a dark-purple coloured solution. $CHCl_3$ (50 mL) was added and the organic and aqueous layers separated. The organic layer was collected and evaporated to dryness to afford a dark purple film. This film was then re-dissolved in a small volume of inhibitor free THF and then isolated by using centrifugation (7000 rpm for 30 min) to afford the product (PS-AuNPs) as dark purple solid.[32]

General procedure for miniemulsion polymerizations

Composite polymer nanoparticles were prepared following the oil-in-water miniemulsion polymerization method described by Hawker and van Berkel.[32] In brief, 2,2'-azobis-(2-amidinopropane) dihydrochloride (V-50) (7.5 mg) and cetyltrimethylammonium bromide (CTAB) (1.3 mg) were dissolved in 2mL of deionized water. PS-AuNPs (3 mg, 6 mg, 12 mg, 18 mg or 24 mg) were each dispersed in the monomer phase (55 mg of divinylbenzene containing dispersed SiQDs), and the resulting mixture was added into the aqueous solution and emulsified by stirring vigorously (600 rpm) for 30 min. The emulsion mixture was then subjected to sonication over an ice bath for 15 min using a high intensity ultrasonic processor at 30% amplitude (VC750220, Fisher Scientific, tapered microtips, power: 750 W). The reaction vessel was fitted with a condenser and a N_2 inlet and the polymerization was performed at 50 $^{\circ}$C under an atmosphere of N_2, with continuous stirring for 4 h. The resulting polymer nanocomposites were purified by dialysis against deionized water (3 – 4 days with water exchanges twice a day) and the purified polymer composites were stored as dispersions in aqueous solution. Because of the very low quantities of SiQDs obtained by the synthetic approach used here, it is not possible to control the exact amount of the SiQDs in each formulation. Therefore, to ensure a constant concentration of SiQDs in each formulation, multiple batches of SiQDs were combined and dispersed in CH_2Cl_2 (60 mL) and the resulting solution divided to six equal proportions which

were subsequently used for each polymer synthesis. For composite polymer nanoparticles encapsulating only SiQDs (**P2[Si]**), a similar procedure was applied as above, without the addition of PS-AuNPs inside the monomer phase system. The complete protocols are given in Table 3.2.

Preparation of printing ink containing Au–Si polymer composite nanoparticles

A colloidal suspension of **P6[Au–Si]** was subjected to vacuum centrifugation to afford 2 mg of solid powder. Printing inks were prepared by adding 1 mL of cyclohexanone to a powder of **P6[Au–Si]** (2 mg) and the resulting suspension then sonicated in an ultrasonic bath for 30 min.

Ink-jet printing of Au–Si polymer composite nanoparticles microdots

The prepared ink was loaded into a cartridge (Dimatrix Material Catridges) fitted with a 10 picoliter piezo print head (Fujifilm Dimatix Inc., DMC-11610 series, USA). Arrays were obtained by printing the ink using a materials printer (Fujifillm Dimatix Inc., DMP-2831 series, USA). 100 x 100 droplet arrays were printed onto untreated glass slides with the diameter of each droplet in a range of 25 μm and at spacing of 15 μm. The cartridges were viewed ejecting droplets under a stroboscope at 1 kHz and 5 kHz ejection frequencies using the DMP-2831 on-board drop watcher facility. Manual droplet optimisation was performed using a single orifice resulting in the following print settings: print orifice = 8, firing frequency = 1 kHz, cartridge temperature = 30 $^{\circ}$C, meniscus set point = 4 inch of water, piezo voltage = 18.5 V, wave form = multi step trapezoidal with a pulse width of 12.101 μs, drop velocity = 6 ms^{-1}, print head substrate clearance = 1000 μm. Prior to printing, the print heads were cleaned using the standard "spit purge- blot" procedure and several dot arrays were then printed in order to increase the likelihood of generating a regular deposition of droplets for post-process viewing.

Characterization of Polymer Composite Nanoparticles

Gel permeation chromatography (polystyrene and thiol-terminated polystyrene)

Gel permeation chromatography (GPC) was performed using THF as solvent at a flow rate of 0.6 mL min^{-1} on a Varian ProStar instrument (Varian Inc.) equipped with a Varian 325 UV-Vis dual wavelength detector (254 nm), a Dawn Heleos II multiangle laser light scattering detector (Wyatt Technology Corp.), a Viscotek 3580 differential RI detector and a pair of PL gel 5 μm Mixed D 300 x 7.5 mm columns with guard column

(Polymer Laboratories Inc.) in series. Near monodisperse polystyrene standards (Polymer Laboratories) were used for calibration. Data analysis was achieved with Galaxie software (Varian Inc.) and chromatograms characterized with the Cirrus software (Varian Inc.) and Astra Software (Wyatt Technology Corp.).

Dynamic light scattering

Refer to Chapter 2, page 72.

UV-Visible spectroscopy

UV-Visible absorption spectra of the aq-AuNPs, PS-AuNPs and Au–Si polymer composite nanoparticles (**P1[Au]**, **P3[Au–Si]**, **P4[Au–Si]**, **P5[Au–Si]**, **P6[Au–Si]** and **P7[Au–Si]**) were obtained with a Cary 100 Bio UV-Visible spectrophotometer by using 1 cm path length quartz cuvettes.

Transmission electron microscopy (TEM)

Samples for TEM were prepared by drop casting 20 μL of the polymer nanoparticle emulsion onto the surface of plastic film (parafilm); the face of a glow discharge-treated carbon support film on 400 mesh copper EM grid was then placed in contact with the sample solution. The polymer emulsion solution transferred onto the grid was diluted by placing in contact with water droplets on the plastic film. The edge of a filter paper was used to wipe-off the excess sample solution on the TEM grid and the samples left to dry in air for approximately 5 min. Transmission electron microscopy measurements were performed at ambient temperature using a Zeiss EM900 operated at 80 kV. Electron micrographs were recorded on Kodak type 4489 electron image film.

Confocal microspectroscopy (luminescence and Raman)

Luminescence and Raman spectra were obtained using a confocal Raman microscope (WiTec model CRM200, Ulm, Germany). A high intensity argon ion laser (Melles-Griot) with output power 35 mW at a wavelength of 488 nm was used as excitation source. The collected light was analysed by a spectrograph equipped with a CCD detector; a grating with 150 lines per mm was chosen in order to capture the full spectrum including all Raman and luminescence bands of interest. All experiments were performed at scan size of 50 x 50 μm with 100 lines at 100 pixels per line and an

integration time of 0.2 s per pixel. Emulsions of polymer composite nanoparticles dispersed in aqueous solution were drop cast onto glass cover slips for observation by confocal microspectroscopy.

Luminescence microscopy (epifluorescence and bright field imaging)

The luminescence and bright field optical images of the inkjet printed sample (**P6[Au–Si]**) was observed using an Axioskop 2 plus Microscope (Carl Zeiss) equipped with a light source comprising a Hg arc lamp and Plan-Neofluar 10x/0.30 objective lenses. The excitation filter was a 300 – 400 nm bandpass filter and the emitted light was filtered by a longpass filter with cut-off at 420 nm.

3.6 References

1. T. H. Chen, K. W. Kuo, W. T. Kuo, H. Y. Huang and Y. Y. Huang, *Journal of Bionanoscience*, 2008, **2**, 109-113.
2. A. Fu, W. Gu, C. Larabell and A. P. Alivisatos, *Current Opinion in Neurobiology*, 2005, **15**, 568-575.
3. J. K. Jaiswal, H. Mattoussi, J. M. Mauro and S. M. Simon, *Nature Biotechnology*, 2003, **21**, 47-51.
4. R. Bakalova, Z. Zhelev, H. Ohba and Y. Baba, *Journal of the American Chemical Society*, 2005, **127**, 11328-11335.
5. X. Gao, Y. Cui, R. M. Levenson, L. W. K. Chung and S. Nie, *Nature Biotechnology*, 2004, **22**, 969-976.
6. S. Kim, Y. T. Lim, E. G. Soltesz, A. M. De Grand, J. Lee, A. Nakayama, J. A. Parker, T. Mihaljevic, R. G. Laurence, D. M. Dor, L. H. Cohn, M. G. Bawendi and J. V. Frangioni, *Nature Biotechnology*, 2004, **22**, 93-97.
7. R. Sarkar, S. S. Narayanan, L. O. Palsson, F. Dias, A. Monkman and S. K. Pal, *Journal of Physical Chemistry B*, 2007, **111**, 12294-12298.
8. Y. Fu, J. Zhang and J. R. Lakowicz, *Chemical Communications*, 2009, 313-315.
9. J. S. Biteen, N. S. Lewis, H. A. Atwater, H. Mertens and A. Polman, *Applied Physics Letters*, 2006, **88**, 131109.
10. J. S. Biteen, D. Pacifici, N. S. Lewis and H. A. Atwater, *Nano Letters*, 2005, **5**, 1768-1773.
11. J. S. Biteen, L. A. Sweatlock, H. Mertens, N. S. Lewis, A. Polman and H. A. Atwater, *Journal of Physical Chemistry C*, 2007, **111**, 13372-13377.
12. L. M. Liz-Marzán, *Materials Today*, 2004, **7**, 26-31.
13. P. Mulvaney, *Langmuir*, 1996, **12**, 788-800.
14. L. M. Liz-Marzán, *Langmuir*, 2005, **22**, 32-41.
15. M. A. Martins, S. Fateixa, A. V. Girão, S. S. Pereira and T. Trindade, *Langmuir*, 2010, **26**, 11407-11412.
16. A. M. Schwartzberg and J. Z. Zhang, *Journal of Physical Chemistry C*, 2008, **112**, 10323-10337.
17. W. L. Barnes, A. Dereux and T. W. Ebbesen, *Nature*, 2003, **424**, 824-830.
18. F. Le, D. W. Brandl, Y. A. Urzhumov, H. Wang, J. Kundu, N. J. Halas, J. Aizpurua and P. Nordlander, *ACS Nano*, 2008, **2**, 707-718.

19. W. A. Murray and W. L. Barnes, *Advanced Materials*, 2007, **19**, 3771-3782.
20. S. Lee, S. Kim, J. Choo, S. Y. Shin, Y. H. Lee, H. Y. Choi, S. Ha, K. Kang and C. H. Oh, *Analytical Chemistry*, 2007, **79**, 916-922.
21. J. Shan and H. Tenhu, *Chemical Communications*, 2007, 4580-4598.
22. K. Y. van Berkel, A. M. Piekarski, P. H. Kierstead, E. D. Pressly, P. C. Ray and C. J. Hawker, *Macromolecules*, 2009, **42**, 1425-1427.
23. B.-S. Kim and T. A. Taton, *Langmuir*, 2006, **23**, 2198-2202.
24. S. Roy, C. K. Dixit, R. Woolley, R. O'Kennedy and C. McDonagh, *Nanotechnology*, 2012, **23**, 325603.
25. S. Chandra, J. Doran, S. J. McCormack, M. Kennedy and A. J. Chatten, *Solar Energy Materials and Solar Cells*, 2012, **98**, 385-390.
26. L. Lu, D. Chen, F. Sun, X. Ren, Z. Han and G. Guo, *Chemical Physics Letters*, 2010, **492**, 71-76.
27. K. Landfester and C. Weiss, *Modern Techniques for Nano and Microreactors/ Reactions*, ed. F. Caruso, Springer Berlin Heidelberg, 2010, 1-49.
28. J. Ramos and J. Forcada, *Langmuir*, 2011, **27**, 7222-7230.
29. N. Bernardy, A. P. Romio, E. I. Barcelos, C. D. Pizzol, C. L. Dora, E. Lemos-Senna, P. H. H. Araujo and C. Sayer, *Journal of Biomedical Nanotechnology*, 2010, **6**, 181-186.
30. A. V. Fuchs and G. D. Will, *Polymer*, 2010, **51**, 2119-2124.
31. K. Landfester, A. Musyanovych and V. Mailänder, *Journal of Polymer Science Part A: Polymer Chemistry*, 2010, **48**, 493-515.
32. K. Y. van Berkel and C. J. Hawker, *Journal of Polymer Science Part A: Polymer Chemistry*, 2010, **48**, 1594-1606.
33. Y. Xu, H. Xu and H. Gu, *Journal of Polymer Science Part A: Polymer Chemistry*, 2010, **48**, 2284-2293.
34. R. Chen, F. Chu, C. Gauthier, L. Chazeau, I. Chaduc, E. Bourgeat-Lami and M. Lansalot, *Journal of Polymer Science Part A: Polymer Chemistry*, 2010, **48**, 2329-2339.
35. B. Erdem, E. D. Sudol, V. L. Dimonie and M. S. El-Aasser, *Journal of Polymer Science Part A: Polymer Chemistry*, 2000, **38**, 4419-4430.
36. N. Joumaa, M. Lansalot, A. Theretz, A. Elaissari, A. Sukhanova, M. Artemyev, I. Nabiev and J. H. M. Cohen, *Langmuir*, 2006, **22**, 1810-1816.
37. Y. Mori and H. Kawaguchi, *Colloids and Surfaces B: Biointerfaces*, 2007, **56**, 246-254.
38. J. K. Oh, D. J. Siegwart and K. Matyjaszewski, *Biomacromolecules*, 2007, **8**, 3326-3331.
39. U. Paiphansiri, P. Tangboriboonrat and K. Landfester, *Macromolecular Symposia*, 2007, **251**, 54-62.
40. M. Takasu, T. Shiroya, K. Takeshita, M. Sakamoto and H. Kawaguchi, *Colloid Polymer Science*, 2004, **282**, 740-746.
41. F. Tronc, M. A. Winnik, B. L. Kaul and J.-C. Graciet, *Journal of Polymer Science Part A: Polymer Chemistry*, 2004, **42**, 1999-2009.
42. T. Chifeng, Y. Yunhua and G. Mingyuan, *Nanotechnology*, 2008, **19**, 105601.
43. S. Dutta Choudhury, R. Badugu, K. Ray and J. R. Lakowicz, *Journal of Physical Chemistry C*, 2012, **116**, 5042-5048.
44. N. Sui, V. Monnier, Y. Zakharko, Y. Chevolot, S. Alekseev, J. M. Bluet, V. Lysenko and E. Souteyrand, *Journal of Nanoparticle Research*, 2012, **14**, 1004.
45. J. R. Lakowicz, *Analytical Biochemistry*, 2001, **298**, 1-24.
46. K. Ray, R. Badugu and J. R. Lakowicz, *Journal of the American Chemical Society*, 2006, **128**, 8998-8999.

47. F. Erogbogbo, C. W. Chang, J. May, P. N. Prasad and M. T. Swihart, *Nanoscale*, 2012, **4**, 5163-5168.
48. J. H. Song, T. Atay, S. Shi, H. Urabe and A. V. Nurmikko, *Nano Letters*, 2005, **5**, 1557-1561.
49. O. Kulakovich, N. Strekal, A. Yaroshevich, S. Maskevich, S. Gaponenko, I. Nabiev, U. Woggon and M. Artemyev, *Nano Letters*, 2002, **2**, 1449-1452.
50. E. Hwang, I. I. Smolyaninov and C. C. Davis, *Nano Letters*, 2010, **10**, 813-820.
51. K. Munechika, Y. Chen, A. F. Tillack, A. P. Kulkarni, I. J. L. Plante, A. M. Munro and D. S. Ginger, *Nano Letters*, 2010, **10**, 2598-2603.
52. B. Erdem, E. D. Sudol, V. L. Dimonie and M. S. El-Aasser, *Journal of Polymer Science Part A: Polymer Chemistry*, 2000, **38**, 4431-4440.
53. J. Turkevich, P. C. Stevenson and J. Hillier, *Discussions of the Faraday Society*, 1951, **11**, 55-75.
54. N. Zheng, J. Fan and G. D. Stucky, *Journal of the American Chemical Society*, 2006, **128**, 6550-6551.
55. M. M. Maye, W. Zheng, F. L. Leibowitz, N. K. Ly and C.-J. Zhong, *Langmuir*, 1999, **16**, 490-497.
56. X. M. Lin, C. M. Sorensen and K. J. Klabunde, *Journal of Nanoparticle Research*, 2000, **2**, 157-164.
57. X. M. Lin, H. M. Jaeger, C. M. Sorensen and K. J. Klabunde, *Journal of Physical Chemistry B*, 2001, **105**, 3353-3357.
58. B. L. V. Prasad, S. I. Stoeva, C. M. Sorensen and K. J. Klabunde, *Chemistry of Materials*, 2003, **15**, 935-942.
59. M. Kanehara, J. I. Sakurai, H. Sugimura and T. Teranishi, *Journal of the American Chemical Society*, 2009, **131**, 1630-1631.
60. C. Li, K. L. Shuford, Q. H. Park, W. Cai, Y. Li, E. J. Lee and S. O. Cho, *Angewandte Chemie International Edition*, 2007, **46**, 3264-3268.
61. P. N. Njoki, I. I. S. Lim, D. Mott, H.-Y. Park, B. Khan, S. Mishra, R. Sujakumar, J. Luo and C.-J. Zhong, *Journal of Physical Chemistry C*, 2007, **111**, 14664-14669.
62. M. José Yacamán, J. A. Ascencio, H. B. Liu and J. Gardea-Torresdey, *Journal of Vacuum Science and Technology B: Microelectronics and Nanometer Structures*, 2001, **19**, 1091-1103.
63. M. K. Corbierre, N. S. Cameron, M. Sutton, S. G. J. Mochrie, L. B. Lurio, A. Rühm and R. B. Lennox, *Journal of the American Chemical Society*, 2001, **123**, 10411-10412.
64. M. K. Corbierre, N. S. Cameron and R. B. Lennox, *Langmuir*, 2004, **20**, 2867-2873.
65. S. Minko, *Polymer Surfaces and Interfaces*, ed. M. Stamm, Springer Berlin Heidelberg, 2008, 215-234.
66. P. Alexandridis, *Chemical Engineering and Technology*, 2011, **34**, 15-28.
67. X. Wang, G. Li, T. Chen, M. Yang, Z. Zhang, T. Wu and H. Chen, *Nano Letters*, 2008, **8**, 2643-2647.
68. Z. Merican, T. L. Schiller, C. J. Hawker, P. M. Fredericks and I. Blakey, *Langmuir*, 2007, **23**, 10539-10545.
69. C. Barner-Kowollik, T. P. Davis, J. P. A. Heuts, M. H. Stenzel, P. Vana and M. Whittaker, *Journal of Polymer Science Part A: Polymer Chemistry*, 2003, **41**, 365-375.
70. G. Moad, Y. K. Chong, A. Postma, E. Rizzardo and S. H. Thang, *Polymer*, 2005, **46**, 8458-8468.
71. S. Perrier, P. Takolpuckdee, J. Westwood and D. M. Lewis, *Macromolecules*, 2004, **37**, 2709-2717.

72. D. Crespy and K. Landfester, *Soft Matter*, 2011, **7**, 11054-11064.
73. M. S. El-Aasser and E. D. Sudol, *Journal of Coatings Technology Research*, 2004, **1**, 20-31.
74. N. A. Harun, B. R. Horrocks and D. A. Fulton, *Nanoscale*, 2011, **3**, 4733-4741.
75. Y. Chao, L. Siller, S. Krishnamurthy, P. R. Coxon, U. Bangert, M. Gass, L. Kjeldgaard, S. N. PatoleO, L. H. Lie, N. O'Farrell, T. A. Alsop, A. Houlton and B. R. Horrocks, *Nature Nanotechnology*, 2007, **2**, 486-489.
76. H. Y. Chen, S. Abraham, J. Mendenhall, S. C. Delamarre, K. Smith, I. Kim and C. A. Batt, *Chemical Physics and Physical Chemistry*, 2008, **9**, 388-392.
77. D. B. Williams and C. B. Carter, *Transmission Electron Microscopy: A Textbook for Materials Science*, Springer London, Limited, 2009.
78. E. Tekin, B.J. de Gans and U. S. Schubert, *Journal of Materials Chemistry*, 2004, **14**, 2627-2632.
79. E. Tekin, P. J. Smith and U. S. Schubert, *Soft Matter*, 2008, **4**, 703-713.
80. L. H. Lie, M. Duerdin, E. M. Tuite, A. Houlton and B. R. Horrocks, *Journal of Electroanalytical Chemistry*, 2002, **538-539**, 183-190.

Chapter 4

Simultaneous SERS and Metal-Enhanced Fluorescence of Co-Encapsulated Au-Ag Alloy Nanoparticles and Silicon Quantum Dots within Polymer Nanoparticles

4.1 Abstract

The co-encapsulation of Raman-active Au-Ag alloy nanoparticles and silicon quantum dots within poly(divinyl)benzene by a single step miniemulsion polymerization is presented. The resulting multicomponent polymer composite nanoparticles were successfully characterized by dynamic light scattering, UV-Visible spectroscopy and transmission electron microscopy. Plasmon enhanced surface-enhanced Raman scattering and fluorescence of Raman-active Au-Ag alloy nanoparticles and silicon quantum dots encapsulated inside polymer composite nanoparticles was investigated by confocal microspectroscopy, where simultaneous and significant surface-enhanced Raman scattering and fluorescence enhancement up to five-fold were observed. These observations indicate that when the Raman-active Au-Ag alloy nanoparticles and silicon quantum dots were co-encapsulated within the polymer layer, the surface-enhanced Raman scattering and luminescence are enhanced, presumably on account of their close proximity of the Raman-active Au-Ag alloy nanoparticles to the silicon quantum dots. It was anticipated that this multicomponent polymer composite displaying SERS-metal enhanced fluorescence could have potential in labelling applications.

4.2 Introduction

Metal nanoparticles are well-known to possess interesting and useful electronic, magnetic, optical and catalytic properties which are different from those of their bulk counterparts. Nanoparticles of the noble metals (silver, and gold) offer broad absorption bands in the visible region of the electromagnetic spectrum, and their solutions possess very intense colours which are absent in the bulk material.[1] This behaviour is attributed to the collective oscillation of the free conduction electrons when they are resonant with an applied electromagnetic field and these metals possess localized surface plasmon resonance (LSPR) properties. The unique characteristics of LSPR form the basis of a plethora of applications in diverse fields ranging from electronics and photonics,[2] sensing and catalysis,[3, 4] to biology and medicine.[5, 6] Furthermore, LSPR is also responsible for the electromagnetic field enhancements that lead to surface-enhanced Raman scattering (SERS) and other surface-enhanced spectroscopic processes.[7]

It is well established that molecules adsorbed at (rough) metal surfaces and nanoparticles show strong SERS, a phenomenon which was discovered[8] by

Fleischmann *et al.* in 1974. This effect was observed whilst using Raman scattering to probe the electrochemical reaction of pyridine at roughened silver (Ag) electrodes, and is responsible for an enhancement of up to 10^{16} fold in Raman scattering from the adsorbed molecules. There are two sources of the SERS effect: electromagnetic and chemical. The latter is considered to arise from the effect of the metal on the bonding in molecules adsorbed at the metal surface. The electromagnetic SERS phenomenon is observed when incident light excites localized plasmons of the metal, increasing the electromagnetic field near the metallic surface and resulting in an enhancement of the Raman signal of nearby molecules by many orders of magnitude.[9, 10] Because each molecule has a distinct vibrational spectrum, exploitation of the SERS effect allows molecules upon noble metal nanoparticles to be uniquely identified by Raman spectroscopy.[11, 12]

Gold (AuNPs) and silver nanoparticles (AgNPs) have most notably been used in SERS applications because their plasmon resonance frequencies fall within the visible and near-infra red regions of the electromagnetic spectrum, and are thus ideal to excite Raman modes. It is well known that AgNPs possess an intense SERS enhancement, however, these species are prone to oxidation. Consequently, AuNPs are used in SERS applications on account of their stability, biocompatibility and scope for surface chemistry, although their SERS enhancements are not as significant as with Ag.[10] Bimetallic nanoparticles consisting of Au and Ag can combine the signal enhancement of AgNPs with the advantages of the AuNPs.[13] The absorption spectra of Au-Ag alloy nanoparticles provide a single surface plasmon band which is related to the composition of the alloy,[14] and their synthesis is easy to achieve using reducing agents such as citrate,[1] sodium borohydride[15] or hydrazine.[16] Furthermore, the composition of Au and Ag can be tuned as desired.[17]

Most SERS studies have been conducted using direct attachment of Raman reporter molecules onto metal nanoparticles. However, the efficiency and reliability of these reporter molecules are often influenced by ligand dissociation or exchange processes, which limit their utility. Furthermore, Raman reporter molecules exposed upon surfaces can be easily affected by their chemical or biological environments.[18] To deal with these issues, numerous encapsulation techniques have been developed to enhance the stability of the SERS probes including coating with biomolecules,[19, 20] polymer[21] or SiO_2.[22]

Considerable work has been performed in the area of metal-containing polymer composite nanoparticles, which have been investigated as SERS substrates.[23] These

polymer hybrid nanoparticles offer an interesting alternative to conventional metal colloids or roughed metal surfaces on account of their facile processability into new materials and potential for chemical functionalization. Trindade *et al.* have reported[11] poly(*tert*-butyl acrylate)-based nanocomposites (P*t*BA) for SERS analysis prepared *via in situ* miniemulsion polymerization in the presence of organically-capped AgNPs and thiosalicylic acid, which acts as the SERS reporter. The synthetic strategy enables the production of versatile SERS substrates that can be used either as aqueous emulsions or solid films. Furthermore, the effect of temperature on the performance of the nanocomposite was also investigated, and it was shown that temperature variations appear not to affect the SERS signal of the analyte. This observation suggests that the molecules of thiosalicylic acid are still adsorbed upon the AgNPs, protected by the polymer matrix. More recent work from the same group reported[23] a new SERS substrate produced from blends of colloidal Au nanospheres and nanorods with P*t*BA. They found that Au-containing PtBA nanocomposites display a more intense SERS spectrum than the starting Au colloids, probably on account of particle clustering of Au assemblies at the polymer surface which leads to absorption increases in the spectral region close to the laser wavelength.

Chen *et al.* have demonstrated[18] a facile preparation of SERS nanoprobes where Raman reporter-tagged metal nanoparticles were encapsulated within polymer micelles consisting of amphiphilic diblock copolymers of polystyrene-*block*-poly(acrylic acid). This new class of SERS nanoprobe possesses a core-shell structure with uniform thickness. Nearly all metal nanoparticles were encapsulated and evenly spaced within the core, and it was found that the SERS reporter molecules fully covered the surface of the metal nanoparticles. Importantly, the self-assembled polymer micelle shell acts as a protecting layer; the hydrophobic PS layer protects the encapsulated SERS nanoprobes from ionic oxidants and the hydrophilic PAA layer prevents aggregation and functions as an anchoring point for biological-targeting vectors. Other examples of polymer composite nanoparticles designed for SERS include durable, stable and optically translucent SERS-active substrates prepared by depositing PVP/AgNPs colloidal solutions onto poly(methyl methacrylate) (PMMA) slides.[24] Poly(vinyl pyrrolidone) (PVP) was used as stabilizing polymer to prevent AgNPs from precipitation, and the SERS activity was evaluated by detecting the signal from a Rhodamine-based Raman reporter molecule.

Polymer composite nanoparticles encapsulating two or more different inorganic nanoparticles which display different properties have attracted interest for advanced

applications because they can exhibit novel physical and chemical properties. The combination of high nanoparticle loading and their localization within polymeric nanoparticles presents opportunities in applications where the close proximity of the inorganic species is critical. In Chapter 3, the co-encapsulation of SiQDs and AuNPs was shown to result in composite particles possessing metal-enhanced fluorescence properties. In this Chapter, the development of multicomponent polymer composite nanoparticles composed of SiQDs and Au-Ag alloy nanoparticles encoded with Raman reporter molecules co-encapsulated inside polymeric nanoparticles is described. SiQDs have been chosen because they possess large Stokes shifts (as discussed in Chapter 1) and therefore their luminescence is obtained at longer wavelength and interferes much less with the Raman spectrum of SERS label than luminescence from direct gap QDs such as CdSe. These composites offer dual optical characteristics associated with SERS of the Raman-active Au-Ag alloy NPs and metal-enhanced fluorescence effects associated with SiQDs. Preliminary studies investigating their SERS and luminescence enhancement effects are described.

4.3 Results and Discussion

4.3.1 Aqueous Gold-Silver (Au-Ag) Alloy Nanoparticles

AuNPs were utilized initially in this work on account of their successful encapsulation within polymer nanoparticles as discussed in Chapter 3. However, no SERS enhancement effect was observed from the available laser (488 nm) at Newcastle University (described further in Section 4.3.7). Further preliminary work with AgNPs found that very strong and intense SERS enhancements were obtained, however, attempts to encapsulate AgNPs within polymer nanoparticles were unsuccessful due to difficulties in modifying their surfaces. The advantages of the strong SERS enhancement of AgNPs and ease of surface chemistry of AuNPs can be captured with Au-Ag nanoalloys, which are of high interest because they combine characteristics of pure Au and Ag. Work by the group of El-Sayed[1] showed that Au-Ag alloys nanoparticles can be produced, possessing a single SPR band. Therefore, nanoalloys of Au and Ag were synthesized[1] by co-reduction of chlorauric acid ($HAuCl_4$) and silver nitrate ($AgNO_3$) with sodium citrate in boiling aqueous solution. The Au-Ag alloy nanoparticles were prepared by substituting a predetermined number of moles of gold atoms by the equivalent number of moles of silver atoms in the form of $AgNO_3$. In this

work, mixed particles with gold mole fractions (χ_{Au}) of 0.5 were synthesized in order to produce Au-Ag alloy particles possessing a 1:1 molar ratio of Au to Ag.

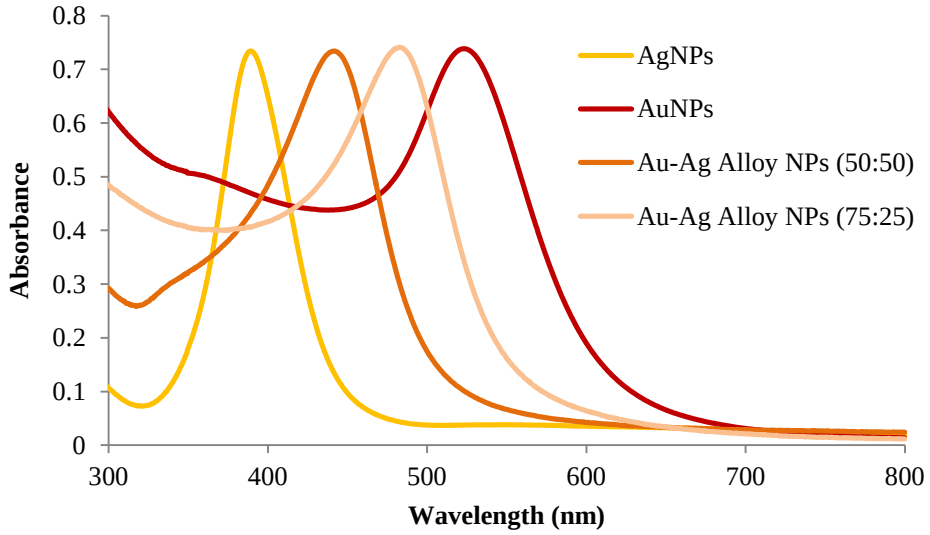

Figure 4.1 UV-Vis absorption spectra of aqueous dispersions of AgNPs, AuNPs and Au-Ag alloy nanoparticles.

The Au-Ag alloy nanoparticles (Au-Ag NPs) obtained possessed average diameters of approximately 30.0 ± 3.9 nm and a polydispersity index of 0.18 ± 0.02, as determined by DLS. From the UV-Vis absorption spectra (Figure 4.1), the surface plasmon resonance (SPR) bands of pure AgNPs and AuNPs are around 395 nm and 525 nm, respectively. The SPR peak for the Au-Ag alloy NPs was observed at 448 nm, intermediate between pure Ag and Au nanoparticles. The fact that a single plasmon peak was observed from the Au-Ag NPs confirms the formation of alloy nanoparticles rather than a core shell system, which would be expected to display peaks for both Au and Ag[25] whose relative intensities depend upon the thickness of the shell obtained.[1, 26] The presence of a single peak in the absorption spectra maybe attributable to a change in dielectric functions when different metal atoms are mixed. Ag presents approximately free electron behaviour in the visible range, showing a sharp absorption band. In contrast, other metals including Au, do not show free-electron behaviour and exhibit a broad absorption band.[27] Furthermore, a control sample of Au-rich aqueous Au-Ag NPs possessing an Au:Ag ratio of 75:25 was also synthesized, and it was found that the plasmon band is further red-shifted (490 nm) when the amount of gold is increased. A comparison in terms of their SERS enhancement effect will be further explained in Section of 4.3.7.

4.3.2 Surface Modification of Aqueous Au-Ag Alloy Nanoparticles for Surface Enhance Raman Scattering (SERS) Effect

As discussed in Chapter 3, one of the most important requirements in the preparation of inorganic/polymer composite nanoparticles by miniemulsion polymerization is the formation of a good dispersion of the inorganic species within the hydrophobic organic monomer. Surface modification of the hydrophilic inorganic nanoparticles is a prerequisite to improve the hydrophobicity of inorganic species, ensuring their dispersability in the monomer phase. The surface functionalization of Au-Ag NPs was accomplished using a modification of the procedure described by Merican *et al.*[28] The surfaces of Au-Ag NPs were first encoded with SERS active molecules in order to demonstrate that the modified Au-Ag nanoparticles (Au-Ag@SERS) possessed the ability to be effective in SERS. Then, thiol-terminated PS (**P2**) was grafted onto the Au-Ag alloy NPs via the "grafting-to" approach[28] in order to improve nanoparticle hydrophobicity (Scheme 4.1).

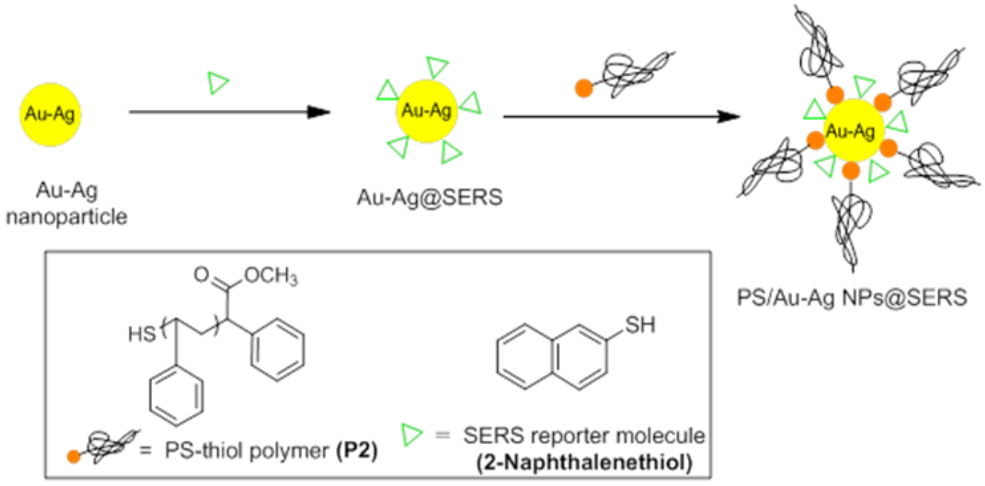

Scheme 4.1: Cartoon scheme representation of the formation of RAFT polymer-stabilized Au-Ag NPs encoded with SERS reporter molecules (PS/Au-Ag@SERS).

SERS Reporter molecules should possess a strong, distinctive SERS spectrum, and sulphur-containing functional groups such as thiols, thiocyanate or isothiocyanate to allow their conjugation to the nanoparticle surface. In this particular work, 2-naphthalenethiol was chosen as the SERS active molecule on account of its strong sharp Raman signals as observed from confocal Raman microspectroscopy (Figure 4.2).

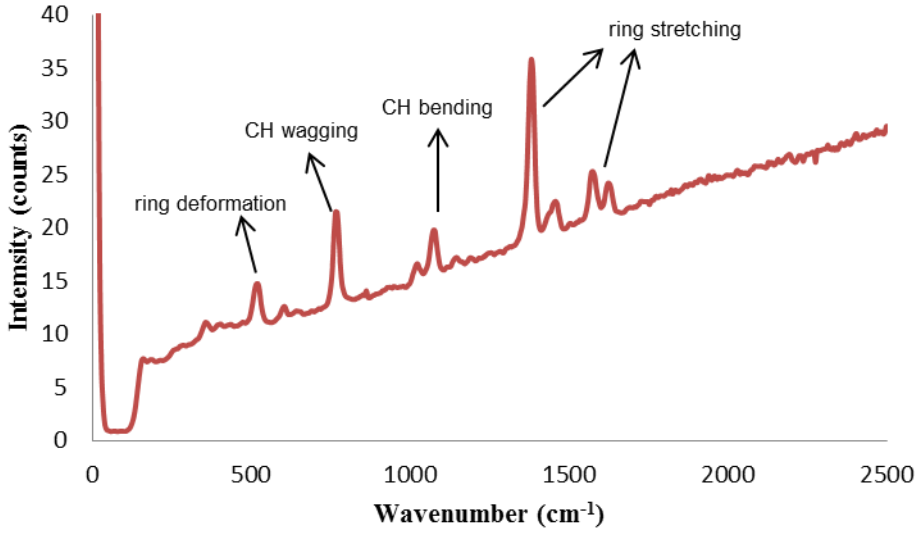

Figure 4.2 Average Raman spectra of 2-naphthalenethiol. The higher intensity peak at 0 cm^{-1} is attributed to elastically scattered laser light (excitation wavelength λ = 488 nm and with a grating of 600 lines per mm). Raman signals of 2-naphthalenethiol were labelled according to the literature.[29]

In the synthetic method employed here, the surfaces of the metal nanoparticles are first encoded with SERS reporter molecules followed by conjugation of thiol-terminated PS (**P2**) (synthesis discussed in page 129) *via* the "grafting-to" method, in which the order of functionalization is different to a previously reported procedure.[28] As the grafting of the thiol-terminated PS proceeds, there is partial displacement of the Raman-active molecules. As depicted in Scheme 4.1, after the addition of **P2** to the solution of the 2-naphthalenethiol encoded Au-Ag alloy NPs, the solution changed from yellow to light brown in colour, indicating the successful grafting of **P2** onto the nanoparticle surfaces. The PS-grafted Au-Ag alloy NPs encoded with 2-naphthalenethiol (abbreviated as PS/Au-Ag@SERS) was isolated by its extraction into $CHCl_3$, an organic solvent in which the polymer is soluble. It was observed that the $CHCl_3$ turned light brown, suggesting that modified Au-Ag alloy NPs were successfully dispersed in the organic phase and that the polymer layer coating the Au-Ag alloy NPs and had indeed improved hydrophobicity. The UV-Vis spectra (Figure 4.3) indicates the SPR band of PS/Au-Ag@SERS in THF is slightly red shifted (480 nm) relative to the citrate-stabilized Au-Ag alloy NPs (448 nm) dispersed in water. This red shifting is expected on account of the different refractive indices of the surrounding media of the metal nanoparticles.[28] The particle size of PS/Au-Ag@SERS was measured by DLS to be 32.6 ± 0.4 nm, which is slightly larger than the aqueous Au-Ag alloy NPs, and suggests the presence of the polymer coating surrounding the metal nanoparticles.

Gratifyingly, these nanoparticles were found to form a good dispersion in the organic monomer system (as described on the following page).

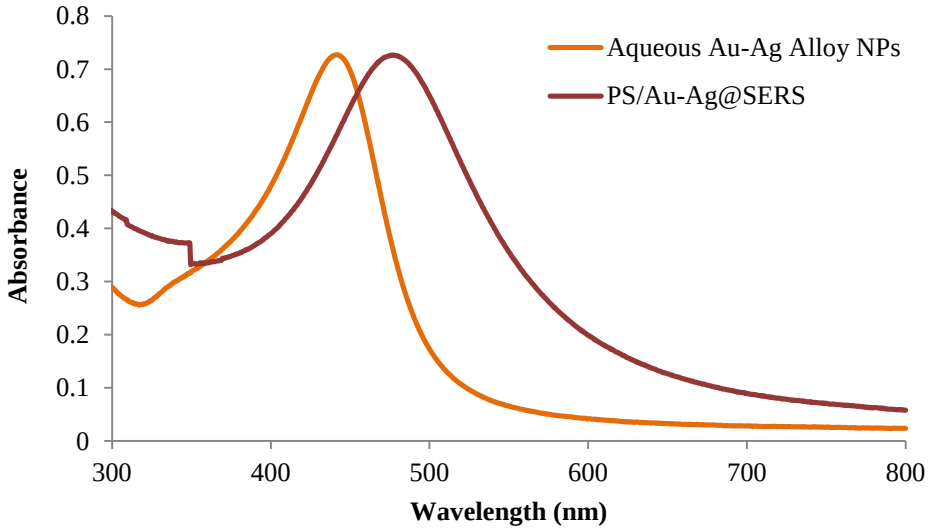

Figure 4.3 Comparison of UV-Vis absorption spectra of aqueous Au-Ag alloy NPs and PS/Au-Ag@SERS in THF.

A second approach towards the surface modification of Au-Ag NPs was also investigated in order to produce hydrophobic Au-Ag NPs endowed with active Raman units. This approach also utilized the "grafting to" method, where it was hypothesized that by employing a thiol-terminated poly(vinyl naphthalene) the Raman signals of naphthalene units close to the surface of the Au-Ag NPs would be enhanced.

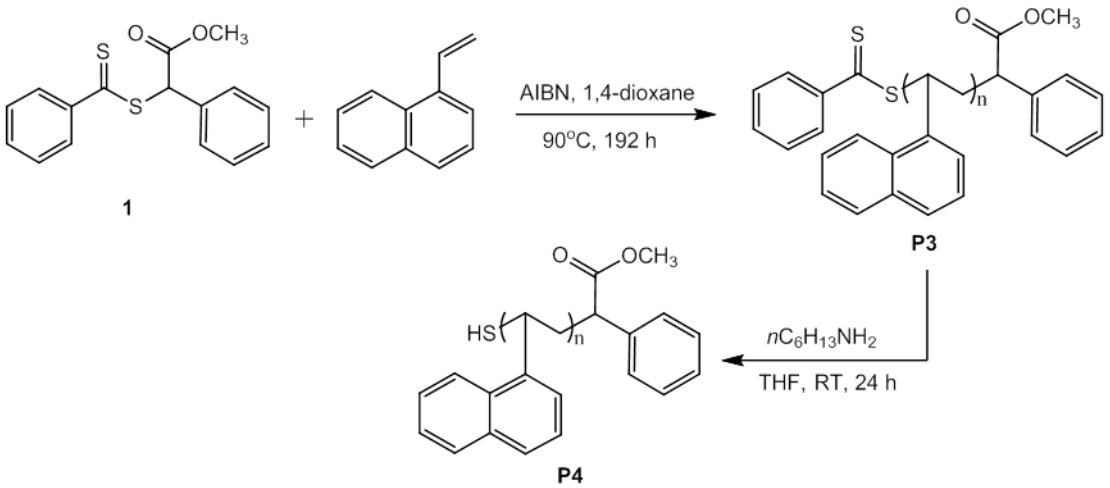

Scheme 4.2 Synthesis of poly(vinyl naphthalene) (**P3**) and thiol-terminated poly(vinyl naphthalene) (**P4**) by RAFT polymerization.

Poly(vinyl naphthalene) (**P3**) was prepared[30] by the polymerization of 1-vinyl naphthalene mediated by the RAFT CTA (**1**) at 90 °C in 1,4-dioxane for one week to

afford **P3** after purification *via* precipitation in cold methanol (Scheme 4.2). The dithioester end group of **P3** was then cleaved by aminolysis with hexylamine at room temperature for 24 h to afford thiol-terminated poly(vinyl naphthalene) (**P4**) (Scheme 4.2). Polymers **P3** and **P4** were characterized by ^{1}H NMR spectroscopy and gel permeation chromatography (GPC). The ^{1}H NMR spectrum of **P3** (Figure 4.4) showed very broad signals attributed to the aromatic groups (δ 5.50 – 8.00) (H_a) and the methylene and methine units (δ 1.10 – 3.20) (H_b) of the polymer backbone. The signal for the aromatic end group of **P3**, which would be expected at δ 8.35, is not observed as a consequence of overlap by the broad aromatic signals of the aromatic units. The methoxy end group was observed at δ 3.49 (H_d). The ^{1}H NMR spectrum of **P4** (not shown) was very similar to that of **P3.** GPC Analysis of **P3** and **P4** indicated monomodal molecular weight distributions and acceptable polydispersities in both cases (Table 4.1, Figure 4.5). The appearance of additional peaks at retention time ~ 34 min was attributed to traces of solvent present in the polymer sample. The thiol-terminated poly(vinyl naphthalene) (**P4**) was then grafted onto the surface of the Au-Ag alloy NPs. However, work on this approach was discontinued due to time limitations, and future directions of this aspect of the work will be discussed in Chapter 5.

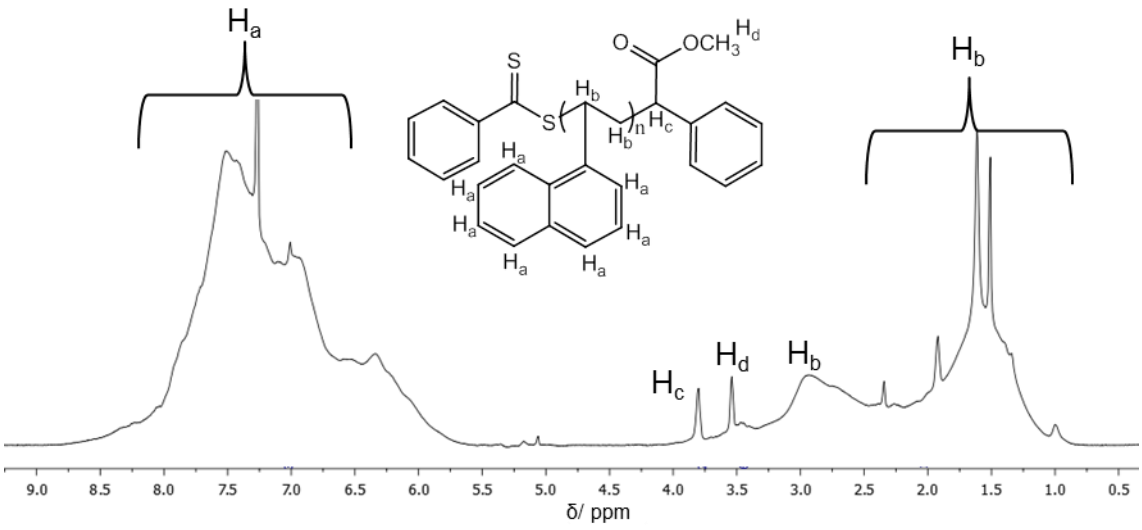

Figure 4.4 ^{1}H NMR spectrum (400 MHz, $CDCl_3$) of poly(vinylnaphthalene) (**P3**).

Polymer	M_n (g mol^{-1})	M_w (g mol^{-1})	PDI (M_w/M_n)
P3	8 700	14 100	1.63
P4	8 600	14 400	1.68

Table 4.1 Characterization of polymers **P3** and **P4** by GPC in DMF/LiBr (1 gL^{-1}) (0.6 mL min^{-1}) calibrated against polystyrene standards.

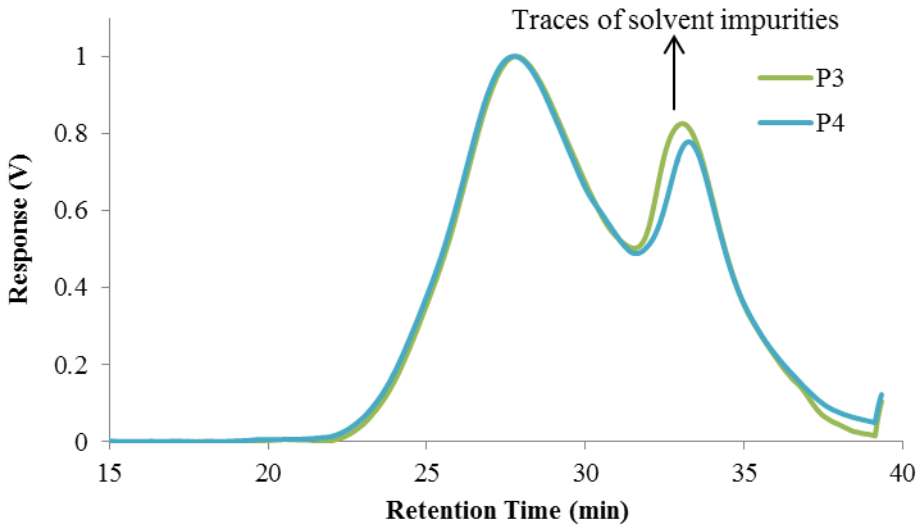

Figure 4.5 Gel permeation chromatography (GPC) traces for **P3** and **P4**.

4.3.3 The Co-Encapsulation of PS/Au-Ag@SERS and SiQDs within Poly(divinylbenzene) Nanoparticles by Miniemulsion Polymerization

Multicomponent polymer composite nanoparticles co-encapsulating both SiQDs and PS/Au-Ag@SERS were prepared via miniemulsion polymerization according to a modification of the procedure described[30] by Hawker *et al*. (Scheme 4.3). Poly(divinylbenzene) was selected as the polymer matrix based on our previous success with this polymer.[31] The strategy employed requires the preparation of stable aqueous miniemulsions of monomer droplets into which organic-capped inorganic species can migrate. Initiation of polymerization within the monomer droplets then results in an aqueous emulsion of the inorganic/polymer composite nanoparticles in which the final morphological characteristics of the polymer composite nanoparticles depend on the polymerization conditions and abilities of the inorganic species to disperse within the monomer droplets.

To determine if the PS/Au-Ag@SERS were suitable for encapsulation, a control experiment which involved their encapsulation within polymer nanoparticles was performed. It was found, however, that inhomogeneous emulsions were observed during the polymerization process. The emulsion tended to separate into two layers and a dark precipitate was detected in the organic layer, which was assumed to arise from metal nanoparticles which were not well-encapsulated within the polymer matrix. This assumption was further strengthened from the observation of broad particle size distributions within the resultant polymer composite nanoparticles. The poor stability of

the emulsion may occur on account of the larger particle size of PS/Au-Ag@SERS, which leads to their incomplete encapsulation within the polymeric nanoparticles. Consequently, the polymerization conditions were optimized by adjusting the composition of the polymerization in order to obtain a stable emulsion of polymer composite nanoparticles (as discussed further in Section 4.3.4).

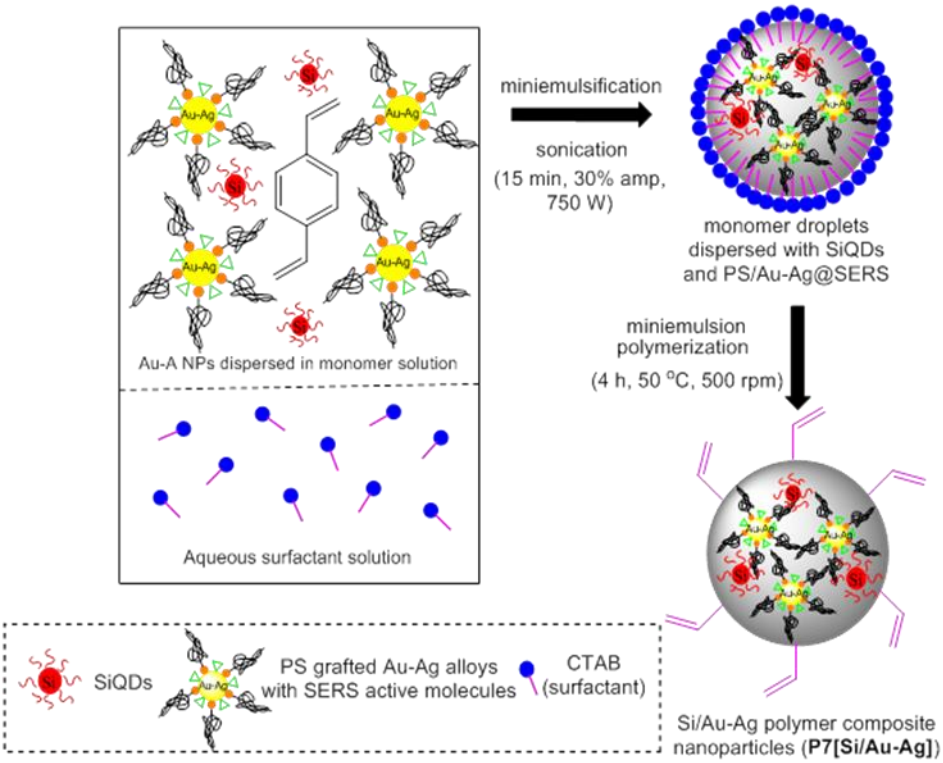

Scheme 4.3 Synthetic scheme for the miniemulsion polymerization of Si/Au-Ag polymer composite nanoparticles (**P7[Si/Au-Ag]**).

Thus, miniemulsion polymerization to prepare poly(divinylbenzene) nanoparticles encapsulating both SiQDs and PS/Au-Ag@SERS was performed as depicted in Scheme 4.3, where the mixture of monomer and inorganic species were mixed in aqueous surfactant solution (CTAB) with water soluble initiator (V-50). The mixture was miniemulsified by vigorous stirring for 1 h prior to high power ultrasonication, and the polymerization was performed at 50 $^{\circ}$C. It worth noting that the emulsion of polymer composite nanoparticles obtained was pale brown, and this colour most likely originates from the dark brown colour of the PS/Au-Ag@SERS.

4.3.4 Characterization of Particle Sizes and Size Distributions

As mentioned in the previous section, on account of the difficulties in obtaining homogenous dispersions of the alloy-containing polymer composite nanoparticles,

attempts were made to optimize the composition of the miniemulsion polymerization. Table 4.2 presents the particle sizes and size distributions of the monomer droplets and the polymer composite nanoparticles obtained under different polymerization conditions. It should be noted that a constant amount of PS/Au-Ag@SERS (around 12 mg) and a low volume of aqueous dispersion (~ 2 mL) was used in each polymerization. Furthermore, the previous work suggested[31] that this amount of metal nanoparticle is the optimum level for efficient metal encapsulation.

Entry	Polymer composite NPs	CTAB (mg)	V-50 (mg)	Au-Ag NPs[b] (mg)	Droplet and Particle Sizes Characterization[a]			
					Droplets		Purified Latex	
					D_h (nm)	PDI	D_h (nm)	PDI
1	**P1[Au-Ag]**	1.3	7.5	11	276.2 ± 5.2	0.68 ± 0.11	250.4 ± 4.3	0.63 ± 0.19
2	**P2[Au-Ag]**[c]	1.3	7.5	12	245.5 ± 3.6	1.00	233.3 ± 3.1	1.00
3	**P3[Au-Ag]**	2.6	15	12	207.2 ± 2.4	1.00	213.5 ± 2.3	0.67 ± 0.15
4	**P4[Au-Ag]**	0.65	7.5	11	302.3 ± 6.4	1.00	316.2 ± 7.1	1.00
5	**P5[Au-Ag]**	1.5	7.5	12	225.7 ± 2.5	0.42 ± 0.12	232.6 ± 3.1	0.38 ± 0.12
6	**P6[Au-Ag]**	1.5	7.5	9	219.8 ± 3.7	0.32 ± 0.05	221.4 ± 2.5	0.30 ± 0.06
7	**P7[Si/Au-Ag]**	1.5	7.5	9	206.3 ± 2.9	0.29 ± 0.08	205.8 ± 1.3	0.17 ± 0.01

Table 4.2 Particle sizes and particle size distributions (PDI) for a series of Au-Ag polymer composite nanoparticles (**P1[Au-Ag]**–**P6[Au-Ag]**) and Si/Au-Ag polymer composite nanoparticles (**P7[Si/Au-Ag]**). [a] As determined by DLS. [b] Total mass of PS/Au-Ag@SERS used in the miniemulsion protocol. [c] Addition of 2.3 mg of hexadecane (costabilizer) in the miniemulsion reaction. V-50 (2,2'-Azobis-(2-amidinopropane) dihydrochloride) is water soluble initiator.

Samples **P1[Au-Ag]** – **P6[Au-Ag]** were prepared to investigate the encapsulation of the alloy nanoparticles. The resulting particles sizes were found to be 200 nm – 300 nm in diameter, with relatively broad PDIs as determined by DLS. Sample **P1[Au-Ag]** was prepared according to the protocol reported by Hawker *et. al.*[30] However, a broad PDI and inhomogeneous emulsion dispersion were observed for this sample (Table 4.2, Entry 1), probably as a consequence of the relatively large size of PS/Au-Ag@SERS, which makes its complete encapsulation of PS/Au-Ag@SERS within the polymer nanoparticles difficult. This observation therefore has important

implications in developing an improved composition for miniemulsion polymerization of Au-Ag polymer composite nanoparticles. Initial attempts (Table 4.2, Entry 2) involved addition of small amounts of the ostabilizer hexadecane, a typical miniemulsion ingredient, which was added in order to help stabilize the emulsion droplets against coalescence and Ostwald ripening.[32] Disappointingly, no differences were found in the PDI of both monomer droplets and resultant polymer composite nanoparticles. Similar observations were also noted for the PDIs of the monomer droplets and polymer nanoparticles of **P3[Au-Ag]** and **P4[Au-Ag]**, where the amount of CTAB was increased/decreased by a factor of two (Table 4.2, Entries 3 and 4). However, by reducing the amount of surfactant used in the miniemulsion process, slightly larger particle sizes of the monomer droplets and polymer nanoparticles were achieved (**P4[Au-Ag]**).[33, 34]

When the amount of surfactant was slightly increased (Table 4.2, Entry 5), the PDIs of both monomer droplets and polymer composite nanoparticles became narrower. This result may be explained by the fact that surfactant acts to retard droplet coalescence caused by collisions between monomer droplets and hence can stabilize the droplets from aggregation during miniemulsion polymerization.[35] Taking advantage of this observation, two control samples were prepared (**P5[Au-Ag]** and **P6[Au-Ag]**) at different loadings of PS/Au-Ag@SERS. The average hydrodynamic diameter and PDI for **P5[Au-Ag]** was slightly larger and broader than **P6[Au-Ag]**, which possessed fewer Au-Ag NPs (Table 4.2, Entry 5) in the miniemulsion formulation. The broader PDI of **P5[Au-Ag]** may be attributed to the larger amount of Au-Ag NPs used, resulting in larger monomer droplets and the possibility of some droplet aggregation. The relatively large particle sizes of the PS/Au-Ag@SERS may result in the formation of an inhomogenous dispersion caused by strong interactions between metal NPs, and therefore broadening the size distribution of **P5[Au-Ag]**. By reducing the amount of PS/Au-Ag@SERS (**P6[Au-Ag]**), a slight improvement in PDI of the polymer composite nanoparticles was observed with no significant change in particle size (Table 4.2, Entry 6). Confident that this formulation was effective, the miniemulsion polymerization to encapsulate both SiQDs and PS/Au-Ag@SERS was accomplished using 9 mg of PS/Au-Ag@SERS. On account of the low mass of SiQDs produced by the electrochemical etching method, the exact amount of SiQDs used in the polymerization cannot be precisely measured. However, in each polymerization, four batches of SiQDs which contained 24 Si chips were prepared, and it was estimated that the total amount of SiQDs obtained is less than 0.1 mg per chip. Interestingly, the PDI of the obtained

Si/Au-Ag polymer composite nanoparticles (**P7[Si/Au-Ag])** shows a narrow particle size distribution in comparison to the control sample (**P6[Au-Ag]**). This observation is in agreement with the findings reported in Chapter 2 and Chapter 3, where it was found that polymer composite nanoparticles composed of SiQDs have low PDI values. This phenomenon maybe attributable to the presence of SiQDs which most likely acts as a costabilizer to improve the stability of polymer composite nanoparticles, as reflected in the improved PDI values.

4.3.5 UV-Visible Spectroscopy Characterization

The plasmon resonance band of the polymer composite nanoparticles **P7[Si/Au-Ag]** was characterized by UV-Vis spectroscopy. As reported previously,[31] the red shifting of the SPR of **P7[Si/Au-Ag]** is expected as a consequence of small changes in dielectric environments and the capping layer surrounding the PS/Au-Ag@SERS. It is well-known[11] that the increase in the refractive index of the surrounding medium and the decrease in the inter-particle distance between neighbouring metal nanoparticles influences the spectral features of samples containing dispersed metal nanoparticles.

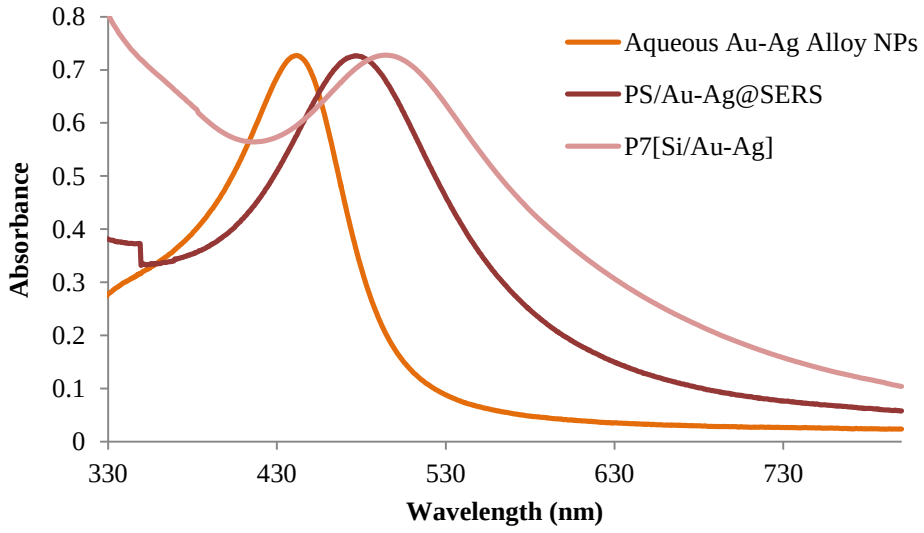

Figure 4.6 Comparison of the UV-Vis spectra of aqueous Au-Ag alloy NPs, PS/Au-Ag@SERS (in THF) and **P7[Si/Au-Ag]**.

As depicted in Figure 4.6, the absorption peak for **P7[Si/Au-Ag]** shows a bathochromic shift ($\Delta\lambda$ = 18 nm) in comparison to the SPR band of the PS/Au-Ag@SERS. Furthermore, differences in colour were observed for aqueous Au-Ag alloy NPs, PS/Au-Ag@SERS and Si/Au-Ag polymer composite nanoparticles (**P7[Si/Au-**

Ag]). Aqueous Au-Ag NPs afforded a yellow coloured dispersion whilst the PS/Au-Ag@SERS afforded a brown-coloured dispersion. The Si/Au-Ag polymer composite nanoparticles gave light brown-coloured emulsions which are due to the long wavelength tail observed from Figure 4.6 indicating aggregation inside the polymer nanoparticles. The colour observed most likely depends upon the collective oscillation of the electrons in the conduction band identified as the surface plasmon oscillation, and the plasmon resonance of Au-Ag alloy NPs frequently appears in the visible region giving rise to strong surface plasmon resonance absorption.[36]

4.3.6 Characterization by Transmission Electron Microscopy

The size and morphology of the polymer composite nanoparticles was investigated by TEM. Representative images of aqueous Au-Ag alloy NPs, PS/Au-Ag@SERS and **P7[Si/Au-Ag]** polymer composite nanoparticles are presented in Figure 4.7.

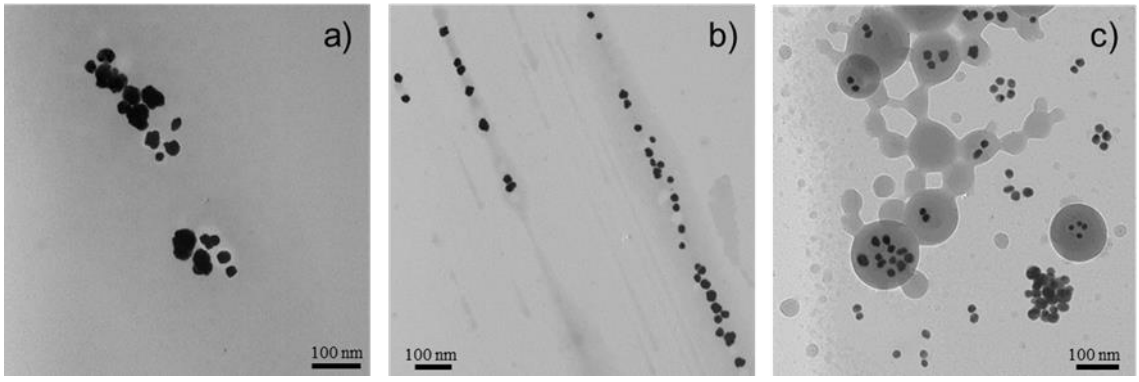

Figure 4.7 Transmission electron microscopy (TEM) images of (a) aqueous Au-Ag alloy NPs (64 000x magnification) (b) PS/Au-Ag@SERS in THF (64 000x magnification) (c) **P7[Si/Au-Ag NPs]** (92 000x magnification). Because of the low scattering factor of Si, TEM cannot confirm the presence or absence of SiQDs within the polymer matrix.

Figure 4.7a indicates a typical TEM micrograph of citrate-stabilized Au-Ag alloy NPs dispersed in H_2O cast onto a carbon coated TEM grid. The average particle diameter was observed to be 30 – 40 nm, which agrees well with DLS measurements. It should be noted that most of the aqueous Au-Ag alloy NPs tend to aggregate during sample preparation on the carbon coated grid. PS/Au-Ag@SERS, which were encoded with 2-naphthalenethiol and stabilized with polystyrene, showed a more uniform distribution on the TEM grid (Figure 4.7b), an observation which suggests the polymer coating surrounding the surface of the Au-Ag alloy NPs prevents aggregation. Both

observations obtained from aqueous Au-Ag alloy NPs and PS/Au-Ag@SERS are consistent with work reported in Chapter 3.

The TEM image of **P7[Si/Au-Ag]** (Figure 4.7c) reveals the average diameter of the polymer composite nanoparticles to be approximately 100 – 250 nm, in good agreement with results obtained from DLS measurements. The encapsulated PS/Au-Ag@SERS are clearly evident as visible spheres of high TEM contrast (black), distributed evenly within the lower contrast poly(divinylbenzene) matrix (grey). Furthermore, the existence of unencapsulated PS/Au-Ag@SERS and "empty" polymer nanoparticles was also observed. These two features have been prevalent in previous reports of polymer composite nanoparticles formed by miniemulsion polymerization.[37, 38] As highlighted in the previous chapters, because of the low scattering factor of SiQDs, TEM cannot confirm the existence or absence of SiQDs within the polymer nanoparticles.

4.3.7 Evaluation of Fluorescence Enhancement and Surface Enhanced Raman Scattering (SERS) Effects of Si/Au-Ag Alloy Polymer Composite Nanoparticles by Confocal Microspectroscopy

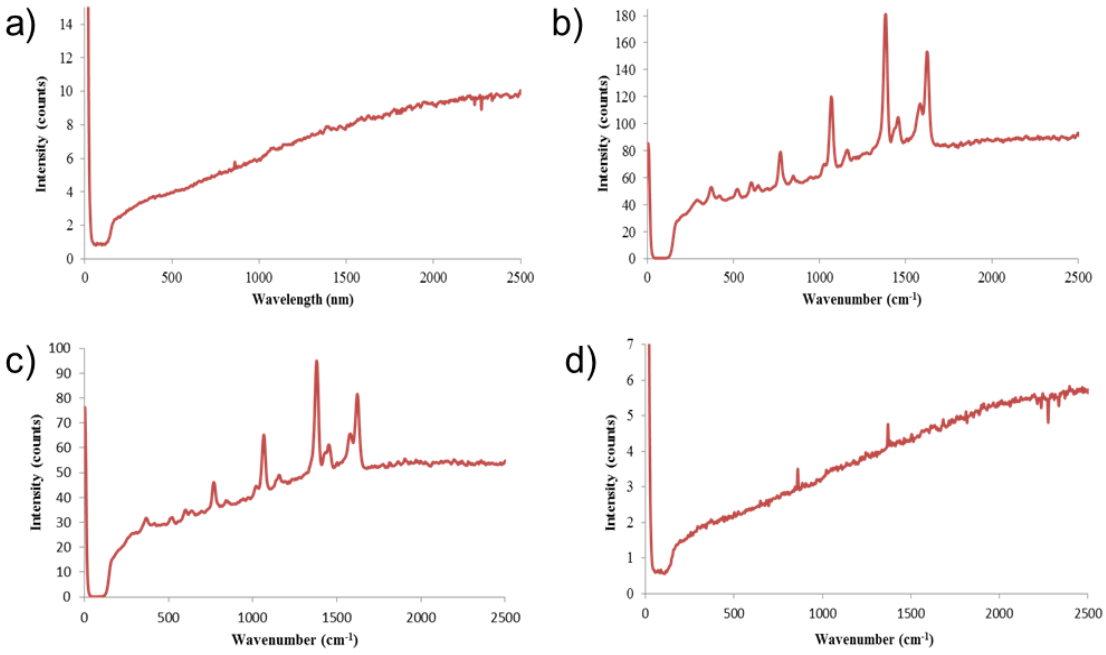

Figure 4.8 Average Raman spectra of (a) AuNPs (b) AgNPs (c) Au-Ag alloy NPs (50:50) and (d) Au-Ag alloy NPs (75:25). All the samples contained 2-naphthalenethiol (10 mg/mL). The higher intensity peak at 0 cm^{-1} is the elastically scattered laser light. The excitation wavelength, λ = 488 nm and with a grating of 600 lines per mm.

Au-Ag alloy NPs possessing equimolar ratios of Au and Ag have been utilized throughout this study. It is known that the magnitude of the SERS effect can be affected by the wavelength of the laser used and the SPR wavelength of the metal nanoparticles, and thus matching of the laser wavelength with the metal compositions is desirable.[39] Wavelength-scanned SERS experiments by McFarland *et al.*[40] have shown that for a fixed Raman shift the surface plasmon wavelength should be halfway between the incident laser wavelength and the Stokes shifted wavelength. They found that the SERS enhancement factor increases as the LSPR and laser wavelength are simultaneously shifted toward the red (up to a maximum wavelength of 785 nm). Our data show a somewhat different behaviour: AuNPs are ineffective at the laser wavelength (488 nm), but AgNPs with a higher energy plasmon band (Figure 4.1) are highly effective. The Au-Ag nanoalloys are intermediate, although too high an Au mole fraction reduces the SERS enhancement.

A series of control experiments were conducted involving different metals encoded with Raman reporter molecules. Initial attempts employing AuNPs as metal components modified with 2-naphthalenethiol as a SERS reporter were found to be unsuccessful in producing SERS enhancement effects (Figure 4.8a). In contrast, when AgNPs encoded with 2-naphthalenethiol were utilized, intense SERS enhancements were observed (Figure 4.8b). A similar observation was also made for the Au-Ag alloy NPs (Figure 4.8c). Contrary to expectations, when increased ratios of Au:Ag (75:25) were used, no SERS enhancement effect was observed (Figure 4.8d). The possible explanation for this observation may on account of the presence of inter-band transitions near the green region of the spectrum for Au, and thus, it can only be efficiently excited from the red onward. In contrast, Ag can be effectively excited at the green and the blue regions.[41] Therefore, the use of shorter laser wavelength (488 nm) may account for the lack of success in obtaining SERS effects using AuNPs and Au-Ag alloy nanoparticles which possess a rich composition of Au. On account of this limitation, Au-Ag alloy NPs possessing a 1:1 ratio of the two elements were utilized throughout this study.

Raman and luminescence spectra of Au-Ag@SERS, PS/Au-Ag@SERS, and polymer composite nanoparticles **P6[Au-Ag]** and **P7[Si/Au-Ag]** were investigated by confocal microspectroscopy. All samples were evaluated at an excitation wavelength of 488 nm using an Ar ion laser, and the scattered/emitted light was dispersed on a grating of 150 lines per mm to display both Raman and luminescence spectra. The reflected light and confocal luminescence images of **P7[Si/Au-Ag]** drop-casted onto a glass cover

slip are depicted in Figure 4.9. The bright regions obtained from the confocal luminescence image of **P7[Si/Au-Ag]** confirms the existence of SiQDs which are encapsulated inside or associated onto the surface of polymer nanoparticles. On the contrary, no luminescence was monitored for the Au-Ag polymer composite nanoparticle absent in SiQDs (**P6[Au-Ag]**).

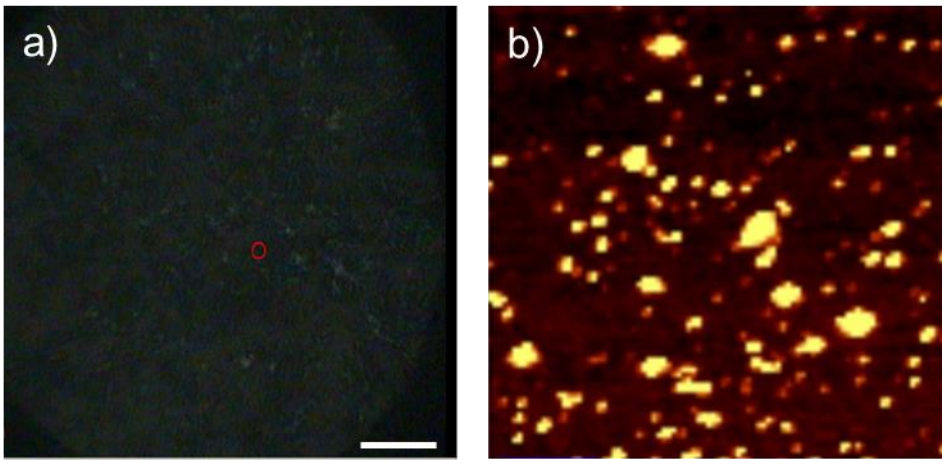

Figure 4.9 (a) Dark field image and (b) confocal luminescence spectrum image of **P7[Si/Au-Ag].** In both cases the colour scale represents the integral of the spectral intensity from a Raman shift of 200 cm^{-1} to 7000 cm^{-1}, which corresponds to a mixture of luminescence and Raman signals which are analysed below. Scale bar on the reflected image = 10 µm and scan size of luminescence images = 50 x 50 µm.

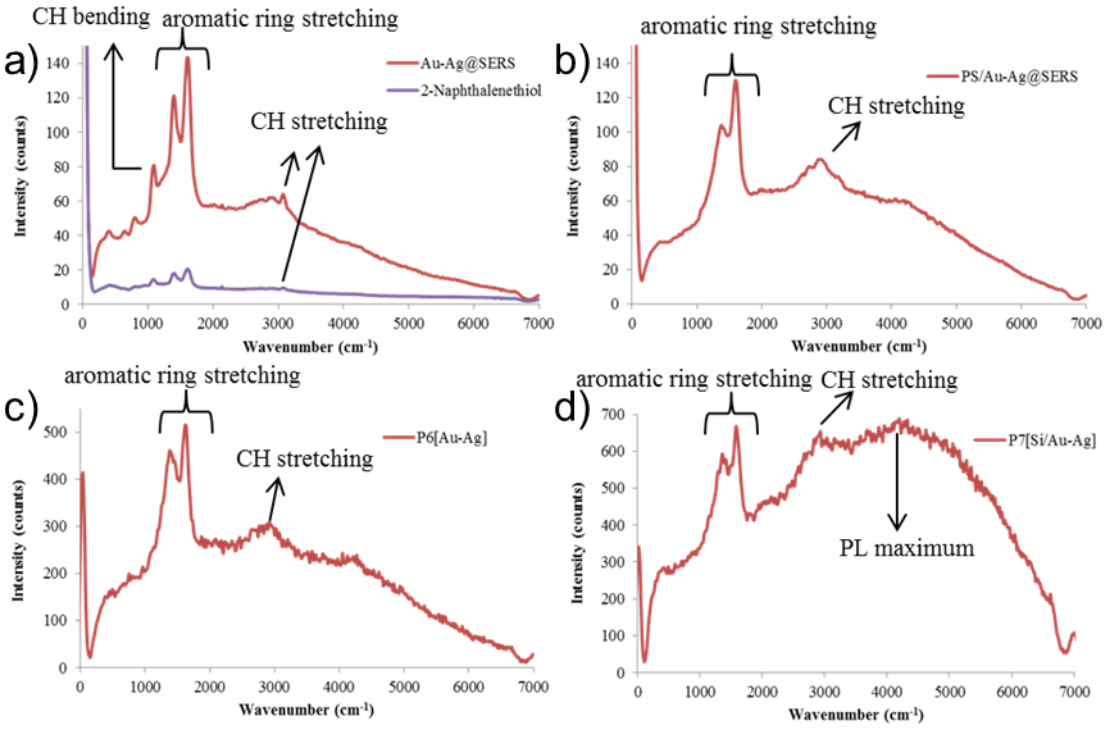

Figure 4.10 Average luminescence/Raman spectra of (a) Au-Ag@SERS and 2-naphthalenethiol (b) PS/Au-Ag@SERS (c) **P6[Au-Ag]** and (d) **P7[Si/Au-Ag]**. The higher intensity peak at 0 cm^{-1} is the elastically scattered laser light. The excitation wavelength, λ = 488 nm and with a grating of 150 lines per mm.

To evaluate the SERS and luminescence enhancement behaviour of modified Au-Ag NPs and **P7[Si/Au-Ag]**, the average luminescence/Raman spectra were obtained by averaging the luminescence confocal images of each sample (Figure 4.10). The obvious changes of SERS in comparison to the conventional Raman spectrum of 2-naphthalenethiol (Figure 4.2) can be observed in the differences in relative intensities of the most intense bands, and the simplification of the SERS spectrum where several bands are either not detected or exhibit a very low intensity.[11]

The mean luminescence/Raman spectra of Au-Ag@SERS (Figure 4.10a) shows significant SERS peaks at 1392 – 1578 cm^{-1} which are attributed to the aromatic ring stretching mode of the 2-naphthalenethiol unit. A SERS enhancement up to 7 times higher was observed for the Au-Ag@SERS in comparison to the intensity of the conventional Raman spectra of 2-naphthalenethiol; we cannot quote a precise enhancement factor because of the differences in the amount of 2-naphthalenethiol, although the enhancement is relatively small, well-defined spectra were obtained which are sufficient for our purpose. Additionally, small signals at 1069 cm^{-1}, 773 cm^{-1} and 356 cm^{-1} were also observed which correspond to the C–H bending, C–H wagging and ring deformation respectively. A weak and small SERS signal at 3059 cm^{-1} refers to the CH stretching of 2-naphthalenethiol. It should be noted that the observed SERS spectra may be quite different from the normal Raman scattering spectra of the same molecule due to factors such as light polarization at the metal surface, orientation of the chemisorbed species, and other factors such as photo-dissociation or photochemistry at the metal interface.[29, 42] The major SERS bands observed for Au-Ag@SERS were also observed for the PS/Au-Ag@SERS (Figure 4.10b). The fact that the SERS effect can be observed for PS/Au-Ag@SERS is expected because surface modification of PS/Au-Ag@SERS via the "grafting to" approach results in less dense packing of polymer chains onto the Au-Ag NPs surfaces, allowing sufficient space to bind SERS reporter molecules.[28] However, minor differences in the spectra were observed, including the disappearance of small peaks around 300 – 1100 cm^{-1} and the broadening of the peak at ~ 3000 cm^{-1}. This phenomenon maybe a consequence of the presence of polymer chains at the surface which overlap with the small Raman peaks, and also to a slight change in band shapes (heterogeneous broadening).

The average luminescence/Raman spectrum of **P6[Au-Ag]** (Figure 4.10c) shows a significant SERS effect as evidenced from the four-fold increase in intensity of the most intense band (aromatic stretching band) in comparison to PS/Au-Ag@SERS. Presumably, the increase in SERS signal intensities can be attributed to the enhanced

polarizability of the coupled plasmons present in Au-Ag alloy NPs, when two or more metal nanoparticles are located within a distance less than their own diameters. This phenomenon results in the near field of one nanoparticle influencing the plasmon oscillation of other nanoparticles.[9] By co-encapsulating both PS/Au-Ag@SERS and SiQDs within polymer nanoparticles (**P7[Si/Au-Ag]**), a five-fold increase in SERS intensity was observed relative to the PS/Au-Ag@SERS (Figure 4.10d). Furthermore, a broad signal around 1900 – 7000 cm^{-1} was attributed to the luminescence peak of SiQDs, where significant luminescence enhancement was obtained as the SiQDs are in close proximity with PS/Au-Ag@SERS within the polymer nanoparticles. It is difficult to directly compare the SERS enhancement obtained in this study with those reported in the literature[11, 18, 23] because the degree of nanoparticle aggregation and the concentration of SERS reporter molecules are often not reported. However, in comparison to the previous work,[31] the resulting luminescence enhancement of **P7[Si/Au-Ag]** correlates with the Au/Si polymer composite nanoparticles (as discussed in Chapter 3), and thus it can be assumed that the SERS enhancement effect obtained for **P7[Si/Au-Ag]** is acceptable. It is worth pointing that, unlike what happens in pure rough silver electrodes, where massive SERS enhancement signals up to 10^6 can be achieved, this study involved a composite whose main component is polymer, which is a SERS inactive substrate. The enhanced intensity of SERS bands, together with the intense broad luminescence enhancement signals of SiQDs, indicates that the co-encapsulation of PS/Au-Ag@SERS leads to a significant and simultaneous increase in both SERS and luminescence characteristics of the species co-encapsulated within polymer nanoparticles.

4.4 Conclusion

A new approach to enhance both SERS and fluorescence simultaneously was developed in which Au-Ag alloy NPs encoded with Raman reporter molecules and SiQDs are co-encapsulated inside polymer nanoparticles using miniemulsion polymerization techniques. Au-Ag alloy nanoparticles were utilized as plasmonic metal nanoparticles due to a strong SERS effect observed when excited at the wavelength of laser light available at Newcastle University, supporting the idea that a good match between SPR absorption of metal and laser wavelength is a crucial experimental requirement in SERS. The surfaces of Au-Ag alloy NPs were modified by encoding with the Raman reporter molecule, 2-naphthalenethiol, followed by grafting with thiol-terminated polystyrene

chains to afford PS/Au-Ag@SERS, which are sufficiently hydrophobic to be dispersed in the organic monomer. The successful modification of PS/Au-Ag@SERS was confirmed by the red shifting of the surface plasmon resonance band of Au-Ag relative to the aqueous Au-Ag NPs, and the presence of SERS effect as observed by confocal Raman microspectroscopy. The encapsulation of both PS/Au-Ag@SERS and SiQDs was confirmed by UV-Visible spectroscopy, where further red shifting was observed. The formation of Si/Au-Ag polymer composite nanoparticles was investigated by TEM characterization, where the black spheres of PS/Au-Ag@SERS were evenly distributed within the poly(divinylbenzene) matrix. Co-encapsulation of PS/Au-Ag@SERS and SiQDs inside polymer nanoparticles was found to simultaneously enhance the luminescence of SiQDs and SERS up to five-fold. This phenomenon probably arises on account of the close proximity of PS/Au-Ag@SERS with SiQDs within the polymer nanoparticles, allowing the intense field of the Au-Ag alloy NPs surface to couple strongly to the SiQDs. Noteworthy to highlight that the simultaneous intense SERS-fluorescence enhancement is possible only because of the large Stokes shift of SiQDs. This study suggests that the distinct and strong optical signals of metal-enhanced fluorescence and SERS can be simultaneously achieved by co-encapsulation of PS/Au-Ag@SERS and SiQDs within polymer nanoparticles. These multifunctional polymer composite nanoparticles possess the potential to be utilized as SERS-based probes in numerous applications, especially in biological labelling and anti-counterfeiting.

4.5 Experimental

All chemicals were purchased from Sigma Aldrich or Alfa Aesar and were used as received without purification. Water was deionized before use (nominal resistivity 18 MΩ cm, Nanopure™ purification system, Barnstead). Divinylbenzene and 1-vinyl naphthalene were refrigerated and used without purification. Membranes for purification by dialysis of polymer composite nanoparticles were obtained from Spectrum Laboratories (Spectra/Por® Dialysis Membrane Tubing, molecular weight cut-off: 3500 Da, width: 18 mm and diameter: 11.5 mm). Toluene was dried over sodium and distilled as required.

Preparation of silicon quantum dots (SiQDs)

SiQDs were prepared by the procedure reported in Chapter 2, page 71.

Preparation of citrate stabilized Au-Ag NPs

Aqueous Au-Ag alloy nanoparticles were prepared using the citrate reduction method described by El Sayed *et al.*[1] Au-Ag Alloy nanoparticles with gold mole fractions of 0.5 and 0.75 were prepared by substituting a predetermined number of moles of gold atoms by the equivalent number of moles of silver atoms in the form of $AgNO_3$. To boiling distilled water (95 mL) was added $HAuCl_4 \bullet 3H_2O$ and $AgNO_3$ to afford a cloudy solution. A solution of 1% sodium citrate was added and the colour changed yellow. The solution was further boiled for 30 min and then left to cool to room temperature. The resultant aqueous dispersion of Au-Ag alloy NPs was used without any purification. The average diameters of the resulting aqueous Au-Ag NPs were determined by TEM and DLS (Section 4.3).

Preparation of citrate stabilized AuNPs

Refer to Chapter 3, page 100.

Preparation of citrate stabilized AgNPs

Citrate stabilized AgNPs were prepared according to the method described by Hawker *et al.*[30] An aqueous solution of $AgNO_3$ (0.1 M, 1.2 mL) and sodium citrate (0.2 M, 1.5 mL) was added to 600 mL of water then heated to 60 $^{\circ}$C. Aqueous sodium borohydride solution (1 M, 0.6 mL) was added which resulted in the immediate formation of an intense yellow-orange colour, and the solution was further heated for 2 h. The resultant aqueous dispersion of AgNPs was used without any purification. The average diameter of the resulting AgNPs was 15 – 20 nm as measured by DLS and TEM.

Preparation of polymer-stabilized Au-Ag NPs encoded with SERS reporter molecules (PS/Au-Ag@SERS)

PS/Au-Ag@SERS were synthesised using a modification of a literature method.[28] A solution of 2-naphthalenethiol (2.5 µL, 1.6 mM) in THF was added to an aqueous solution of Au-Ag alloy NPs (Au-Ag@SERS). Thiol-terminated polystyrene (5 mg) was dissolved in inhibitor free THF (50 mL) and mixed with an aqueous solution of encoded Au-Ag alloy NPs (50 mL) in a separating funnel, resulting in a colour change from yellow to brown. $CHCl_3$ (25 mL) was added and the organic and aqueous layers separated. The organic layer was collected and evaporated to dryness to afford a brown film. This film was re-dissolved in a small volume of inhibitor free THF and the desired

grafted nanoparticles isolated by using centrifugation (7000 rpm for 30 min) as a brown solid.

*Synthesis of thiol-terminated poly(vinyl naphthalene)(**P4**) by RAFT polymerization*

Thiol-terminated poly(vinyl naphthalene) was prepared by RAFT polymerization of 1-vinyl naphthalene followed by aminolysis to convert the dithioester end group into a thiol. The RAFT CTA (*S*-methoxycarbonylphenylmethyl dithiobenzoate**)** (0.022 g, 1 eq relative to 1-vinyl naphthalene), azobisisobutyronitrile (1.05 mg, 0.09 eq), 1,4-dioxane (3 mL) and a magnetic stirrer bar were added to a Schlenk flask which was then sealed. The reaction mixture was degassed by three freeze–pump–thaw cycles, and then heated with stirring at 90 $^{\circ}$C for one week under an atmosphere of N_2. The product was precipitated into cold MeOH, filtered and dried under vacuum to afford the desired polymer (**P3**) as a pink powder (0.26 g, 54%). ^{1}H NMR (400 MHz, $CDCl_3$): δ 1.10 – 3.20 (br, $CHCH_2$, polymer backbone), δ 3.49 (br, OCH_3, of the chain terminus), δ 3.75 (br, R–CH–CO_2Me, δ 5.50 – 8.00 (br, Ar, polymer backbone). GPC analysis: M_n = 8700, M_w = 14100, PDI = 1.63. A solution of poly(vinyl naphthalene) (0.2 g) in THF (20 mL) was subjected to five freeze–pump–thaw cycles. Hexylamine (3.5 eq.) was then added using a N_2-purged syringe, and the reaction mixture was heated at 60 $^{\circ}$C for 30 min, and then stirred under an atmosphere of N_2 at room temperature for 20 h. The resulting thiol-terminated poly(vinyl naphthalene) (**P4**) was purified by precipitation in cold MeOH to afford a white powder (0.1 g, 50%). ^{1}H NMR (400 MHz, $CDCl_3$): δ 1.10 – 3.20 (br, $CHCH_2$, polymer backbone), δ 3.49 (br, OCH_3, of the chain terminus), δ 3.75 (br, R–CH–CO_2Me, δ 5.50 – 8.00 (br, Ar, polymer backbone). GPC analysis: M_n = 8600, M_w = 14400, PDI = 1.68.

General procedure for miniemulsion polymerization

Polymer composite nanoparticles were prepared according to a modification of the route described by Hawker *et al.*[30] 2,2'-Azobis-(2-amidinopropane) dihydrochloride (V-50) (7.5 mg) and cetyltrimethylammonium bromide (CTAB) (1.5 mg) were dissolved in 2 mL of deionized water. Polymer-stabilized Au-Ag NPs encoded with SERS reporter molecules (PS/Au-Ag@SERS) were dispersed in the monomer phase (55 mg of divinylbenzene containing dispersed SiQDs), and the resulting mixture was added into the aqueous solution and emulsified by stirring vigorously (600 rpm) for 30 min. The emulsion mixture was then subjected to sonication over an ice bath for 15 min using a

high intensity ultrasonic processor at 30% amplitude (VC750220, Fisher Scientific, tapered microtips, power: 750 W). The reaction vessel was fitted with a condenser inlet and the polymerization was performed at 50 $^{\circ}$C under an atmosphere of N_2 with continuous stirring for 4 h. The resulting polymer nanocomposites were purified by dialysis against deionized water (overnight) and the purified polymer composites were stored as dispersions in aqueous solution.

Characterization of Polymer Composite Nanoparticles

Gel permeation chromatography

Gel permeation chromatography (GPC) was performed using DMF/LiBr (1 gL^{-1}) as solvent at a flow rate of 0.6 mL min^{-1} on a Varian ProStar instrument (Varian Inc.) equipped with a Varian 325 UV-vis dual wavelength detector (254 nm), a Dawn Heleos II multiangle laser light scattering detector (Wyatt Technology Corp.), a Viscotek 3580 differential RI detector and a pair of PL gel 5 μm Mixed D 300 x 7.5 mm columns with guard column (Polymer Laboratories Inc.) in series. Near monodisperse polystyrene standards (Polymer Laboratories) were used for calibration. Data analysis was achieved with Galaxie software (Varian Inc.) and chromatograms characterized with the Cirrus software (Varian Inc.) and Astra Software (Wyatt Technology Corp.).

Dynamic light scattering

Refer to Chapter 2, page 72.

UV-Visible spectroscopy

UV-Visible absorption spectra of the aqueous Au-Ag NPs, PS/Au-Ag@SERS, Au-Ag polymer composite nanoparticles and Si/Au-Ag polymer composite nanoparticles were obtained using a Cary 100 Bio UV-visible spectrophotometer with 1 cm path length quartz cuvettes.

Transmission electron microscopy

Refer to Chapter 3, page 104.

Confocal microspectroscopy (luminescence and Raman)

Luminescence and Raman spectra were obtained using a confocal Raman microscope (WiTec model CRM200, Ulm, Germany). A high intensity argon ion laser (Melles-Griot) with output power 35 mW at a wavelength of 488 nm was used as the excitation source. The collected light was analysed by a spectrograph equipped with a CCD detector; a grating with 150 lines per mm was chosen in order to capture the full spectrum including all Raman and luminescence bands of interest. Raman spectra were obtained by using a grating with 600 lines per mm. All experiments were performed at scan size of 50 x 50 μm with 100 lines at 100 pixels per line and an integration time of 0.2 s per pixel. An emulsion solution of polymer composite nanoparticles dispersed in aqueous solution was drop cast onto glass cover slips for observation by confocal microspectroscopy.

4.6 References

1. S. Link, Z. L. Wang and M. A. El-Sayed, *The Journal of Physical Chemistry B*, 1999, **103**, 3529-3533.
2. L. Polavarapu, K. K. Manga, K. Yu, P. K. Ang, H. D. Cao, J. Balapanuru, K. P. Loh and Q.-H. Xu, *Nanoscale*, 2011, **3**, 2268-2274.
3. M. Wang, J. Fu, D. Huang, C. Zhang and Q. Xu, *Nanoscale*, 2013, **5**, 7913-7919.
4. A. J. Haes, S. Zou, G. C. Schatz and R. P. Van Duyne, *The Journal of Physical Chemistry B*, 2003, **108**, 109-116.
5. R. Bardhan, N. K. Grady, J. R. Cole, A. Joshi and N. J. Halas, *ACS Nano*, 2009, **3**, 744-752.
6. X. Huang, I. H. El-Sayed, W. Qian and M. A. El-Sayed, *Journal of the American Chemical Society*, 2006, **128**, 2115-2120.
7. Z.-Q. Tian, B. Ren and D. Y. Wu, *The Journal of Physical Chemistry B*, 2002, **106**, 9463-9483.
8. M. Fleischmann, P. J. Hendra and A. J. McQuillan, *Chemical Physics Letters*, 1974, **26**, 163-166.
9. I. Freitag, U. Neugebauer, A. Csaki, W. Fritzsche, C. Krafft and J. Popp, *Vibrational Spectroscopy*, 2012, **60**, 79-84.
10. G. Baker and D. Moore, *Analytical and Bioanalytical Chemistry*, 2005, **382**, 1751-1770.
11. S. Fateixa, A. V. Girao, H. I. S. Nogueira and T. Trindade, *Journal of Materials Chemistry*, 2011, **21**, 15629-15636.
12. K. Willets, *Analytical and Bioanalytical Chemistry*, 2009, **394**, 85-94.
13. Y. C. Liu, C. C. Yu and T. C. Hsu, *Electrochemistry Communications*, 2007, **9**, 639-644.
14. R. J. Chimentão, I. Cota, A. Dafinov, F. Medina, J. E. Sueiras, J. L. G. de la Fuente, J. L. G. Fierro, Y. Cesteros and P. Salagre, *Journal of Materials Research*, 2006, **21**, 105-111.
15. A. Q. Wang, J. H. Liu, S. D. Lin, T. S. Lin and C. Y. Mou, *Journal of Catalysis*, 2005, **233**, 186-197.
16. J. Liu, G. Qin, P. Raveendran and Y. Ikushima, *Chemistry – A European Journal*, 2006, **12**, 2131-2138.

17. K.I. Okazaki, T. Kiyama, K. Hirahara, N. Tanaka, S. Kuwabata and T. Torimoto, *Chemical Communications*, 2008, 691-693.
18. M. Yang, T. Chen, W. S. Lau, Y. Wang, Q. Tang, Y. Yang and H. Chen, *Small*, 2009, **5**, 198-202.
19. D. Craig, J. Simpson, K. Faulds and D. Graham, *Chemical Communications*, 2013, **49**, 30-32.
20. L. Sun, K. B. Sung, C. Dentinger, B. Lutz, L. Nguyen, J. Zhang, H. Qin, M. Yamakawa, M. Cao, Y. Lu, A. J. Chmura, J. Zhu, X. Su, A. A. Berlin, S. Chan and B. Knudsen, *Nano Letters*, 2007, **7**, 351-356.
21. X. Qian, X. H. Peng, D. O. Ansari, Q. Yin-Goen, G. Z. Chen, D. M. Shin, L. Yang, A. N. Young, M. D. Wang and S. Nie, *Nature Biotechnology*, 2008, **26**, 83-90.
22. W. E. Doering and S. Nie, *Analytical Chemistry*, 2003, **75**, 6171-6176.
23. S. Fateixa, P. C. Pinheiro, H. I. S. Nogueira and T. Trindade, *Spectrochimica Acta Part A: Molecular and Biomolecular Spectroscopy*, 2013, **113**, 100-106.
24. W. Lin, *Applied Physics A*, 2011, **102**, 121-125.
25. Y. Shin, A. Dohnalkova and Y. Lin, *The Journal of Physical Chemistry C*, 2010, **114**, 5985-5989.
26. M. P. Mallin and C. J. Murphy, *Nano Letters*, 2002, **2**, 1235-1237.
27. H. G. Boyen, G. Kästle, F. Weigl, B. Koslowski, C. Dietrich, P. Ziemann, J. P. Spatz, S. Riethmüller, C. Hartmann, M. Möller, G. Schmid, M. G. Garnier and P. Oelhafen, *Science*, 2002, **297**, 1533-1536.
28. Z. Merican, T. L. Schiller, C. J. Hawker, P. M. Fredericks and I. Blakey, *Langmuir*, 2007, **23**, 10539-10545.
29. R. A. Alvarez-Puebla, D. S. Dos Santos Jr and R. F. Aroca, *Analyst*, 2004, **129**, 1251-1256.
30. K. Y. van Berkel and C. J. Hawker, *Journal of Polymer Science Part A: Polymer Chemistry*, 2010, **48**, 1594-1606.
31. N. A. Harun, M. J. Benning, B. R. Horrocks and D. A. Fulton, *Nanoscale*, 2013, **5**, 3817-3827.
32. D. Crespy and K. Landfester, *Soft Matter*, 2011, **7**, 11054-11064.
33. K. Landfester, N. Bechthold, F. Tiarks and M. Antonietti, *Macromolecules*, 1999, **32**, 5222-5228.
34. K. Landfester, N. Bechthold, F. Tiarks and M. Antonietti, *Macromolecules*, 1999, **32**, 2679-2683.
35. J. M. Asua, *Progress in Polymer Science*, 2002, **27**, 1283-1346.
36. L. Nguyen Ngoc, V. Le Van, K. Chu Dinh, D. Sai Cong, N. Cao Thi, H. Pham Thi, T. Nguyen Duy and Q. Luu Manh, *Journal of Physics: Conference Series*, 2009, **187**, 012026.
37. N. Joumaa, P. Toussay, M. Lansalot and A. Elaissari, *Journal of Polymer Science Part A: Polymer Chemistry*, 2008, **46**, 327-340.
38. F. Tiarks, K. Landfester and M. Antonietti, *Macromolecular Chemistry and Physics*, 2001, **202**, 51-60.
39. S. E. Hunyadi and C. J. Murphy, *Journal of Materials Chemistry*, 2006, **16**, 3929-3935.
40. A. D. McFarland, M. A. Young, J. A. Dieringer and R. P. Van Duyne, *The Journal of Physical Chemistry B*, 2005, **109**, 11279-11285.
41. R. A. Álvarez-Puebla, *The Journal of Physical Chemistry Letters*, 2012, **3**, 857-866.
42. F. René, *Reports on Progress in Physics*, 1998, **61**, 691.

.

Chapter 5

Conclusions and Future Work

5.1 Conclusions and Future Work

Inorganic–polymer composite nanoparticles have been synthesized successfully using miniemulsion polymerization, demonstrating that this technique is a robust and versatile approach to fully encapsulate hydrophobic inorganic materials within the interior of polymer nanoparticles.

The successful encapsulation of SiQDs within a series of polymer nanoparticles composed of the monomers styrene or 4-vinylbenzaldehyde has been accomplished. Future attention should be focused on the development of polymer nanoparticles with improved hydrophilicity, which could be utilized as fluorescent probes in biological imaging and labelling. It is well known hydrophilic polymer nanoparticles can be produced by inverse miniemulsion.[1] For instance, copolymerizing the hydrophilic co-monomer methacrylic acid with styrene can afford hydrophilic polymer nanoparticles which are also suitable for the encapsulation of hydrophobic substances.[2] Holzapfel *et al.* synthesized[3] a series of polystyrene nanoparticles functionalized on their surfaces with carboxyl and amino groups by miniemulsion polymerization. A fluorescent dye was incorporated into the copolymer nanoparticles and the fluorescent particles were utilized as markers for cell uptake in HeLa cells. This synthetic strategy could afford polymer composite nanoparticles of high aqueous compatibility which have potential to be used in biological applications.

Further research was performed to investigate the metal-enhanced fluorescence properties of SiQDs by co-encapsulating them with Au nanoparticles. The resulting polymer composite nanoparticles showed luminescence enhancement up to 15 fold at an optimum loading of AuNPs. Since luminescence enhancements depend upon the spacing between the metal nanoparticles and the fluorophores,[4, 5] further work could explore how different molecular weight of the polystyrene layer surrounding the AuNPs, which would vary the spacing of AuNPs and SiQDs, upon the luminescence enhancement properties.

Polymer composite nanoparticles which offer simultaneous dual optical properties of surface-enhanced Raman scattering (SERS) and metal-enhanced fluorescence effects were investigated by co-encapsulation of Raman-active Au-Ag NPs and SiQDs. Further work could explore the possibility of using poly(vinyl naphthalene-thiol) as a thiolated polymer in the surface modification of metal nanoparticles, as it is hypothesized that a Raman signal could be obtained from the naphthalene units within

the poly(vinyl naphthalene-thiol) polymer. Furthermore, attention should be focused on improving the SERS and metal-enhanced fluorescence by using different metals, for example, 'pure' AuNPs or AgNPs. This might be accomplished by using a longer wavelength of laser light for AuNPs, and improving the surface modification of AgNPs to achieve their good encapsulation within polymer nanoparticles. Additionally, more optimization should be performed to achieve a better composition of ingredients for miniemulsion polymerization, where a more monodisperse distribution of polymer composite nanoparticles could be obtained.

From the broader perspective, the possibilities for further study described here should eventually lead to new classes of polymer composite nanoparticles which combine the ease of processability of an organic polymer with the unique optical properties of inorganic nanoparticles. Inorganic-polymer composite nanoparticles are a creative way to design new materials for academic research, where their improved and unusual features will most likely result in the development of future commercial application opportunities ranging from information technology and communications, biotechnology and medicine, photonics, electronics and sensor, fuel and solar cells to environment and catalysis. The rapid growth in nanoscience research is evidence from the development of sophisticated instrumentation to probe small length scales such as scanning force, laser scanning fluorescence and electron microscopies, which allow research aimed at probing the influence of particle size and shape of polymer composite nanoparticle. A challenge for future studies is to seek processing techniques in producing polymer nanocomposites in a large-scale which are effective on the nanoscale yet are applicable to macroscopic processing and offer beneficial outputs to society goals. This issue will generate more fascinating research in the future.

5.1 References

1. D. Crespy and K. Landfester, *Beilstein Journal of Organic Chemistry*, 2010, **6**, 1132-1148.
2. Y. Luo and X. Zhou, *Journal of Polymer Science Part A: Polymer Chemistry*, 2004, **42**, 2145-2154.
3. V. Holzapfel, A. Musyanovych, K. Landfester, M. R. Lorenz and V. Mailänder, *Macromolecular Chemistry and Physics*, 2005, **206**, 2440-2449.
4. O. Kulakovich, N. Strekal, A. Yaroshevich, S. Maskevich, S. Gaponenko, I. Nabiev, U. Woggon and M. Artemyev, *Nano Letters*, 2002, **2**, 1449-1452.
5. I. M. Soganci, S. Nizamoglu, E. Mutlugun, O. Akin and H. V. Demir, *Optics Express*, 2007, **15**, 14289-14298.

The end